THERMAL AND MECHANICAL PROPERTIES OF A FERROELECTRIC COPOLYMER P(VDF/TrFE)

SUBMITTED BY

HUI NGAI MAN

FOR THE DEGREE OF

MASTER OF PHILOSOPHY
IN APPLIED PHYSICS

AT

THE HONG KONG POLYTECHNIC UNIVERSITY

IN SEPTEMBER, 1999

ACKNOWLEDGMENTS

I would like to thank my chief supervisor, Dr. Y.W. Wong, and co-supervisor, Prof. C.L. Choy, for their constant encouragement, support, precious advice and invaluable direction throughout the whole research work.

I would also like to express my warm appreciation to Prof. H.L.W. Chan and Prof. F.G. Shin for their helpful discussions, suggestions and comments.

Apart from these, I owe a debt of appreciation to many people for that friendly helping hands in dealing with the practical details. I am thankful to the technical staff of our department for technical support.

Last but not least, I gratefully acknowledge the financial support of the research grant from the Hong Kong Polytechnic University.

ABSTRACT

Ferroelectric copolymer samples of Poly(vinylidene/trifluoroethylene) [P(VDF/TrFE)] of two VDF mole fractions were prepared using the hot-press method. Samples of different crystallinities were made by controlled heat treatment.

Thermal and mechanical properties of the samples were investigated as a function of temperature. These properties exhibit a drastic change near the ferroelectric phase transition temperature. The results also show that both kinds of properties were dependent on the degree of crystallinity.

Thermal expansivity and specific heat of the copolymer samples generally increase with temperature, peaking at the Curie temperature. On the other hand, the density decreases with temperature and drops abruptly at around the Curie temperature. The thermal diffusivities were determined by the laser flash radiometry method. The results show that they decrease with temperature and drop rapidly during ferroelectric phase transition. As a result, the thermal conductivities increase with temperature, exhibiting a peak at the Curie temperature, and then drop to similar values as those obtained before the ferroelectric phase transition.

The mechanical properties of the copolymer as revealed by the elastic moduli were determined by the ultrasonic method. The elastic stiffness constants calculated from the longitudinal and transverse ultrasonic velocities show a decreasing trend with increasing temperature and drop with a great magnitude at the phase transition. Since the Young's, shear and bulk moduli are all related to the stiffness constants, they decrease in a similar manner with temperature.

The measured properties display the thermal hysteresis effect to differing extents. Samples with higher VDF content have a more profound shift to lower temperature at the phase transition during the cooling measurements. This result is consistent with the investigations found in the literature.

TABLE OF CONTENTS

Appendices

LIST OF FIGURE CAPTIONS

LIST OF TABLE CAPTIONS

CHAPTER 1

INTRODUCTION

1.1 BACKGROUND

In the past two decades, the fluoro-polymers vinylidene fluoride (VDF) and its copolymer with trifluoroethylene VDF/TrFE have been widely studied by many researchers. These two types of polymeric materials, particularly the latter, exhibit ferroelectric properties [Furukawa, 1984b; Furukawa, 1989; Marcus, 1984; Lovinger, 1983c] which make them suitable for a number of new applications, such as in piezoelectric sensors and actuators. The copolymer has been proposed to be used in integrated pyroelectric sensor arrays due to their low thermal conductivity [Lando, 1988]. Therefore, in order to assess the effectiveness of the copolymer as a pyroelectric or piezoelectric transducer material, it is necessary to evaluate its thermal and mechanical properties.

1.2 LITERATURE REVIEW

1.2.1 Ferroelectric Polymers

Most of the popular ferroelectric materials are ceramics: Lead Zirconate Titanate (PZT) and Triglycine sulphate (TGS) are well-known examples. In the 1970s, poly(vinylidene fluoride) (PVDF) has been identified to possess ferroelectric properties. PVDF is also chemically stable and weather resistant. It is the simplest fluorocarbon polymer, and its chemical formula is $-(-CH_2-CF_2-)-_n$ or can be written as

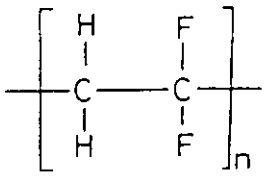

PVDF

PVDF is semi-crystalline in nature. The molecular chains fold in lamellar form of 10nm thick and 100nm in width, and the lamellar crystals grow radially from nucleation centres and form spherulites. The spherulites are embedded in an amorphous region of the polymer. The interlamellar region is non-crystalline, which may occupy more than half of the total volume and exhibit the properties of the amorphous polymer [Abkovitz, 1975].

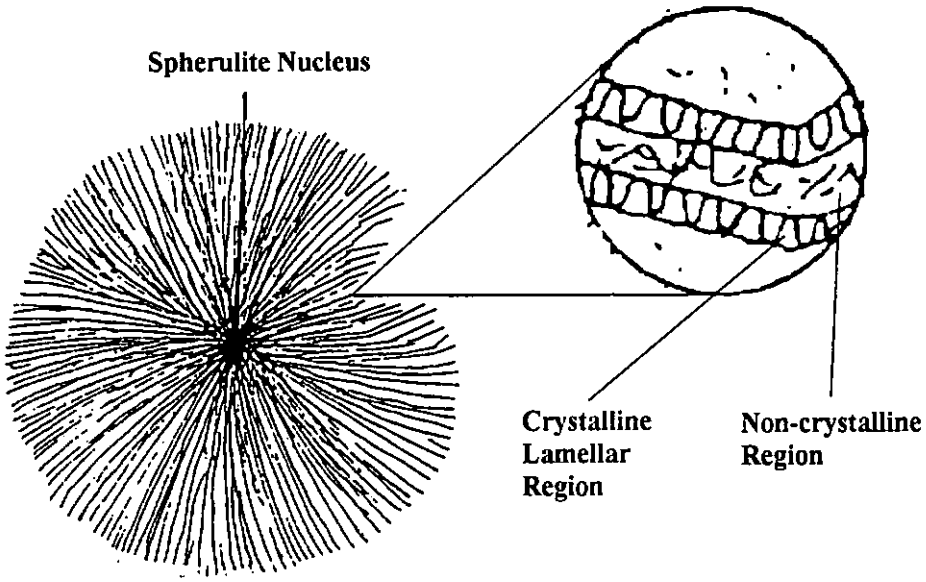

Figure 1.1 **Schematic diagram of the spherulitic structure of the semi-crystalline PVDF polymer showing the radial growth of lamellar crystals from the nucleus and the location of non-crystalline components between the crystalline lamellar regions.**

PVDF consists of polar molecular chains having permanent dipoles in the direction perpendicular to the chain axis as shown in Figure 1.2. The all-trans conformation and parallel packing produce the spontaneous polarization. A 180° rotation of individual molecules about its chain axis is responsible for the polarization reversal. Conformational disorder at above a critical temperature causes a phase transition from the ferroelectric phase to the paraelectric phase. This critical temperature is called the Curie temperature T_c [Furukawa, 1984a].

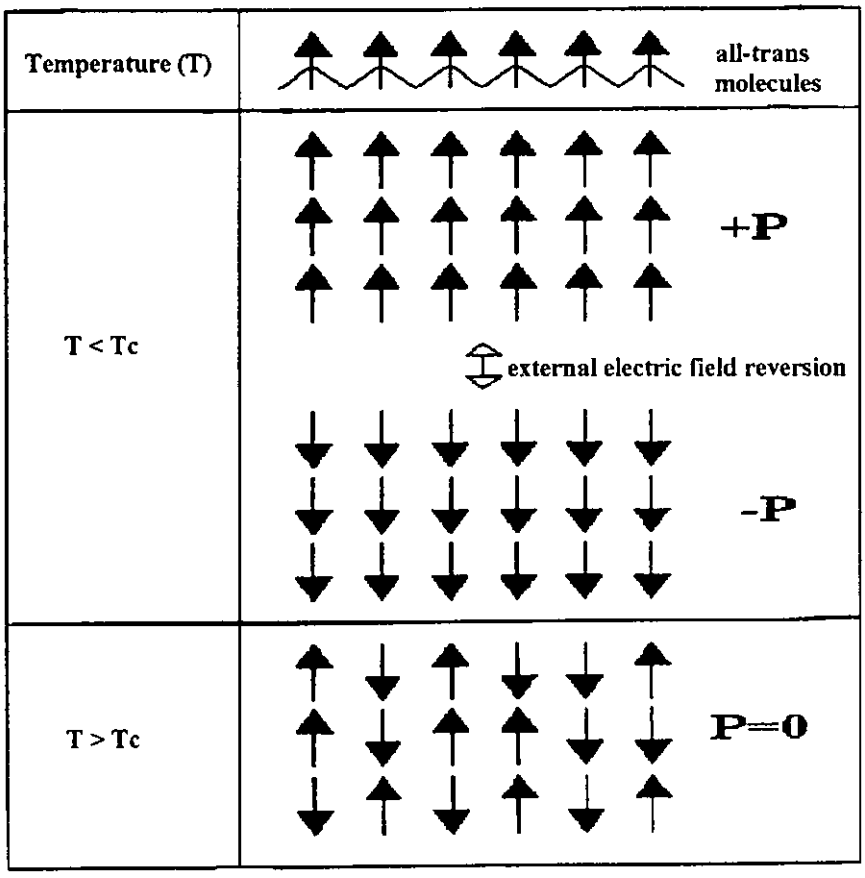

Figure 1.2 Schematic illustration of the polarization change of PVDF below T_c and above T_c, the arrows represent the dipole moments.

PVDF consists of a repeat unit CH_2-CF_2 which exhibits a vacuum dipole moment of about $7x10^{-30}$ C-m [Wen, 1984] associated with the positively charged hydrogen (H) ions and negatively charged fluorine (F) ions. Since such dipoles are rigidly attached to the main chain carbons, their orientation is subjected to molecular conformation and packing [Furukawa, 1984a]. These monomer units tend to polymerize predominantly "head to tail", i.e., -CH_2-CF_2-CH_2-CF_2- , and thus the polymer chain exhibits a large net dipole moment [Tasaka, 1985] in the all-trans conformation.

PVDF is polymorphic. The predominate phase of PVDF is the α-phase. The crystal structure of the α-phase is monoclinic which has lattice constants of a = 4.96 Å, b = 9.64 Å, c = 4.62 Å and β = 90° [Hasegawa, 1972]. As shown in Figure 1.3 (a), the unit cell of the lattice of α-PVDF consists of two chains in the $TGT\overline{G}$ conformation, whose dipole components normal to the chain axes are anti-parallel thus neutralizing each other.

An analogous polar structure is called the δ-phase which is similar to the α-phase [Hasegawa, 1972]. It can be obtained by application of a high electric field to the polymorphic film; in effect, this involves rotation of every second chain by 180° about its axis, so that molecules are now packed with the transverse components of their dipole moments pointing in the same direction as shown in Figure 1.3 (b).

The ferroelectric β-phase is obtained by uniaxial drawing of melt-crystallized α-PVDF. The β-phase has an orthorhombic structure with lattice constants a = 8.58 Å, b = 4.91 Å, c = 2.56 Å [Hasegawa, 1972]. The unit cell consists of two all-trans chains packed with their dipoles pointing in the same direction as shown in Figure 1.3 (c). Packing of chains in β-PVDF is such that F and H atoms of neighboring chains are approximately at the same level parallel to the a-axis of the unit cell.

Chains of the $TTTG\overline{T}\overline{T}\overline{T}\overline{G}$ conformation are packed in a polar fashion to yield the γ-phase. The lattice constants of its monoclinic structure are a = 4.96 Å, b = 9.58 Å, c = 9.23 Å and β = 92.9°. A solid-state transformation from the α-PVDF to the thermodynamically more stable γ-phase can occur readily at high temperatures (~ 160 °C) solely through limited intermolecular motions. A non-polar analog of γ-PVDF with monoclinic cell has also been reported but may exist only within a mixture of phases obtained at very high temperatures. This wealth of crystalline phases for PVDF is very unusual among polymers (where one or two polymorphs are common) and is another reflection of its unique molecular structure [Koga, 1986].

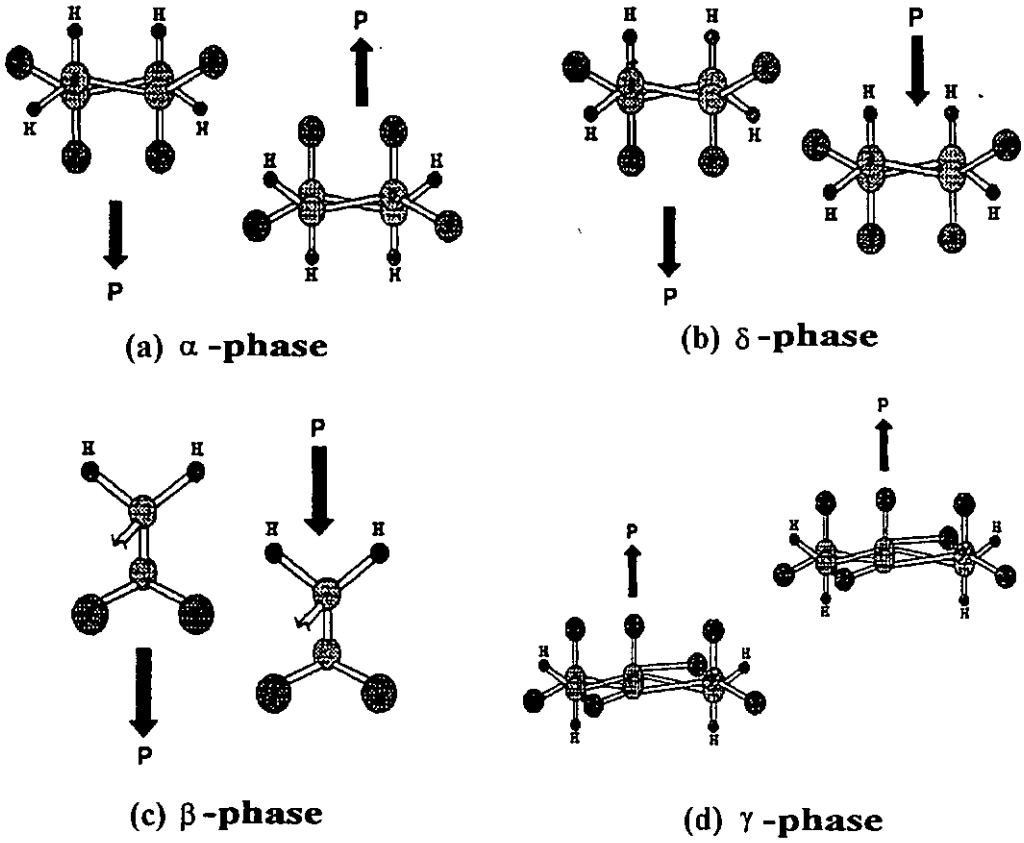

Figure 1.3 Molecular arrangement in unit cells of (a) the α-phase, (b) the δ-phase, (c) the β-phase and (d) the γ- phase of PVDF shown in projection parallel to the chain axes. Arrows indicate dipole directions normal to the molecular axes [Koga, 1986].

PVDF polymer can be fabricated into large-area film of uniform thickness, which is suitable for use in pyroelectric detectors with a large-area sensitive element. However, it has to be drawn to transform to the ferroelectric β phase, which is inconvenient for the production and applications. P(VDF/TrFE) copolymer, reported by Yagi et al. [Lovinger, 1983d] in 1979, has the ferroelectric characteristic without prior mechanical stretching.

1.2.2 Ferroelectric Copolymers

Recently, random copolymers of vinylidene fluoride and trifluoroethylene P(VDF/TrFE) have been introduced as a new class of ferroelectric polymeric materials. They have strong piezoelectric and pyroelectric responses [Yagi, 1980b]. Vinylidene fluoride (VDF: CH_2CF_2) copolymerizes readily with trifluoroethylene (TrFE: $CHFCF_2$), as shown in Figure 1.4, providing copolymers with randomly distorted comonomer units in the molecular chains.

Copolymers with a wide range of comonomer content have been studied by T. Yagi et al. [Yagi, 1979a; Yagi, 1979b; Yagi, 1980c]. It is found that the hydrogen atoms of adjacent VDF units are replaced by large fluoride atoms, thus restricting the formation of $TGT\overline{G}$ polymer chain conformation and enhancing the all-trans β-phase [Lando, 1968]. Hence the P(VDF/TrFE) copolymers need not be drawn as they crystallize directly from the solution or melt into analogous β-phase

when the VDF content (m) is within the range 0.6 - 0.82 [Furukawa, 1984b; Wen, 1984; Tasaka, 1985; Koga, 1986]. This fact renders P(VDF/TrFE) much more attractive than PVDF from a technological standpoint which needs an extra stretching operation. Apart from the fact that P(VDF/TrFE) has an obvious Curie temperature and ferroelectric behavior without being stretched, P(VDF/TrFE) copolymer is very similar to PVDF in many aspects because of their similar structures [Ikeda, 1990].

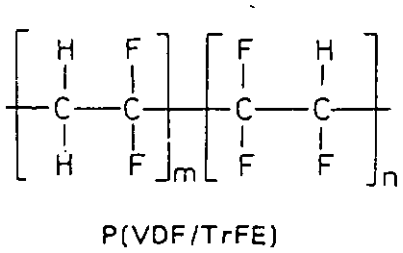

Figure 1.4 The chemical formula of P(VDF/TrFE).

P(VDF/TrFE) copolymers exhibit ferroelectric to paraelectric phase transition at the Curie temperature [Lovinger, 1983d]. The Curie temperature of these copolymers increases almost linearly with increasing vinylidene fluoride content. In effect, it allows one to extrapolate the VDF content to the PVDF homopolymer to obtain the Curie temperature of the homopolymer for which no Curie transition has been observed [Lovinger, 1983d]. It is found that the Curie temperature of PVDF is close to its melting temperature [Yagi, 1980b].

According to Koizumi [Koizumi, 1994], the Curie transition T_c, melting temperature T_m and crystallization temperature T_{crys} can be obtained from DSC (Differential Scanning Calorimetry) method and the results are listed in Table 1.1 for reference.

Table 1.1 Temperatures of fusion T_m, crystallization T_{crys}, and transition T_c in VDF/TrFE copolymers.

VDF content /mol%	Heating		Cooling	
	T_c / K	T_m / K	T_{crys} / K	T_c / K
0 (PTrFE)	--	463	446	--
52.8	333	425	415	335
64.6	343	423	410	337
73	389	418	406	348
75	393	416	405	350
78	402	418	406	358
100 (PVDF)	--	426	412	--

Ikeda et al. have measured the degree of crystallinity of the ferroelectric copolymers by X-ray analysis. It was found that the ferroelectricity of the copolymers belongs to the crystalline state. The ferroelectric phase transition, therefore, should occur in the crystal region of the copolymer. On the basis of the two-phase model, which is well established in polymer physics, the crystallization process, which occurs in the amorphous part, should be independent of the ferroelectric phase transition.

On the other hand, Tashiro et al. [Tashiro et al., 1991] have measured the temperature dependence of the ultrasonic velocity for a series of P(VDF/TrFE) copolymers of various VDF contents. The trans-gauche conformational transitions were observed and the ultrasonic modulus was found to exhibit an unusual minimum in the Curie transition region. An obvious thermal hysteresis was found in the heating and cooling measurements of the temperature dependence of ultrasonic velocity.

In general, polymers have lower thermal conductivity compared with ceramics because of their loose molecular packing. For this reason special considerations should be given to applications such as in pyroelectric transducers where heat conduction is important. The thermal conductivity of PVDF has been measured by Choy et al. On the other hand, the thermal conductivity of the copolymers P(VDF/TrFE) have not yet been fully investigated. Hence it will be useful as well as interesting to study the thermal conductivity of the copolymers and evaluate their behavior at the phase transition temperature.

Furthermore, since both thermal and mechanical properties of a polymer are dependent on its molecular structure as well as its crystallinity, a comparison of these two kinds of properties may give a more thorough understanding of this interesting copolymer.

1.3 THESIS OUTLINE

This thesis will first describe the preparation of P(VDF/TrFE) 56/44 and 70/30 copolymer samples. Then results of the investigation of the samples' thermal and mechanical properties will be given. The thesis is divided into five chapters.

The preparation method of the copolymer films for this work is the subject of Chapter 2. The determination of their crystallinity by X-ray diffraction is also given. Density measurement by the flotating method is presented at the end of the chapter.

Chapter 3 starts with the principles of the laser flash method for measuring the thermal diffusivity. This laser flash radiometry method was applied to the copolymers to evaluate their thermal properties. Differential scanning calorimetry (DSC) was used to determine the samples' specific heat and transition temperature. The temperature dependence of density is evaluated based on thermal expansion coefficient measurement.

Chapter 4 reports the behavior of elastic stiffnesses and moduli of the copolymers. They are determined by the ultrasonic immersion method. The thermal hysteresis of these properties will also be presented.

Finally, some conclusions about the thermal and mechanical properties of the copolymers are given in the last chapter.

CHAPTER 2
SAMPLE PREPARATION AND CHARACTERISTICS

The material to be investigated in this thesis is polyvinylidene fluoride and trifluoroethylene P(VDF/TrFE) copolymer. This chapter deals with sample preparation and the determination of sample characteristics such as crystallinity and density of the as-prepared samples. Basically, the samples were produced by the hot-press method (Section 2.1), the degree of crystallinity of the samples were determined by X-ray diffraction method (Section 2.2) and the density of the samples were obtained by the flotation method (Section 2.3).

2.1 P(VDF/TrFE) COPOLYMERS

In this project, two kinds of P(VDF/TrFE) copolymers were used. One of which consists of 56 mol% of VDF and 44 mol% TrFE, and the other one consists of

70 mol% VDF and 30 mol% TrFE. They will be referred to in short as 56/44 and 70/30 copolymers respectively in this thesis. The copolymers were supplied by Piezotech of France in pellet form.

2.1.1 Sample Preparation and Dimensions

Copolymer samples were prepared by hot-press moulding. The hot-press is shown schematically in Figure 2.1. Copolymer pellets were put in the mould and kept at 190°C for 1 hour, then a pressure of about 83 kg/cm^2 was applied. Thickness of the samples was controlled by the spacer of the mould. After keeping the temperature and pressure for 5 minutes, the samples were either quenched in iced water or allowed to cool down slowly (naturally) in the press under the same pressure after melt. Samples of other crystallinities were prepared by annealing the quenched films for four hours at 100, 120, 130 or 140°C. Dimensions of the samples used for the various measurements are shown in Table 2.1.

Table 2.1 Dimensions of samples for various measurements.

Samples	Dimensions (mm) (length x width x thickness)		
	Ultrasonic Measurements	***Thermal Diffusivity Measurements***	***Thermal Expansivity Measurements***
Quenched P(VDF/TrFE) 56/44	20mm x 15mm x 770μm	8mm x 8mm x 100μm	3mm x 1mm x 1.804mm
Slow-cooled P(VDF/TrFE) 56/44	20mm x 15mm x 583μm	8mm x 8mm x 113μm	3mm x 2mm x 1.431mm
Quenched P(VDF/TrFE) 70/30	20mm x 15mm x 470μm	8mm x 8mm x 146μm	3mm x 1mm x 1.724mm
Slow-cooled P(VDF/TrFE) 70/30	20mm x 15mm x 634μm	8mm x 8mm x 105μm	3mm x 1.5mm x 1.537mm

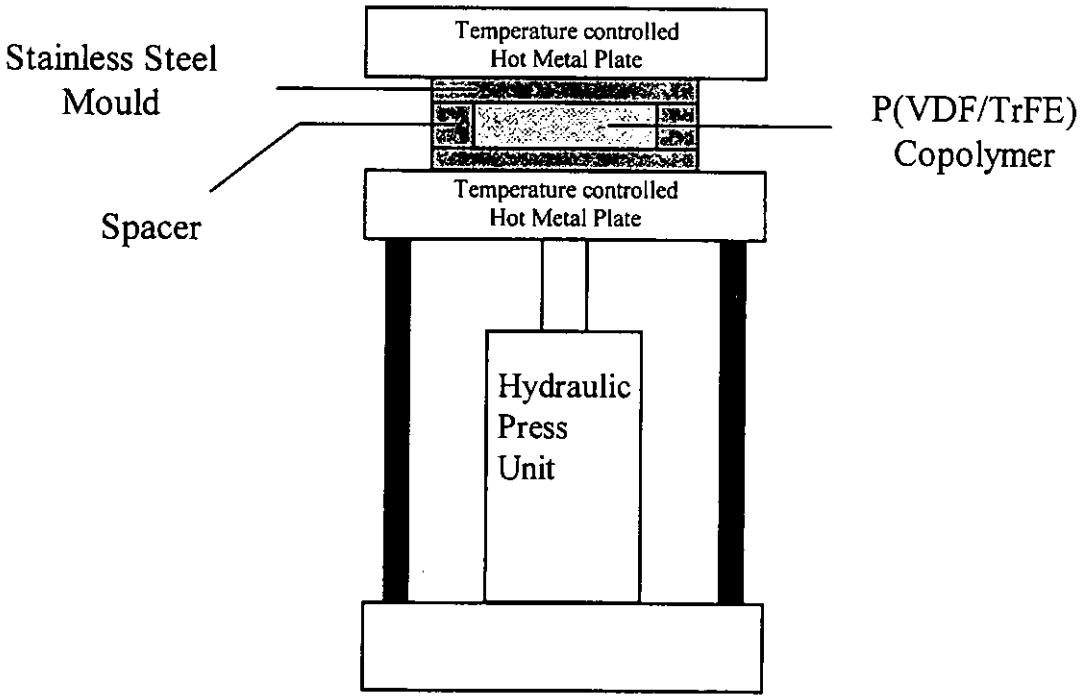

Figure 2.1 Schematic diagram of the hot-press.

2.2 CRYSTALLINITY OF COPOLYMER SAMPLES

It is envisaged that the properties of the vinylidene fluoride and trifluoroethylene copolymer samples prepared under the various conditions will depend quite heavily on the degree of crystallinity of the samples. The degree of crystallinity of a sample may be measured by X-ray diffractometry (XRD) techniques. The model of XRD is Philips Xpert Diffractometer.

2.2.1. Principles of XRD

A beam of X-rays incident on a material is partly absorbed and partly scattered, and the rest is transmitted. The scattering of X-rays occurs as a result of interaction with the crystal lattice in the materials. The X-rays scattered from different lattice planes interfere with each other (Figure 2.2) and produce a diffraction pattern. Constructive peaks in the pattern will appear when Bragg's law is satisfied, that is, when

$$2d_{hkl}\sin\theta_{hkl} = n\lambda \qquad (2.1)$$

where d_{hkl} is the interplanar spacing of the set of lattice planes with Miller indices $\{hkl\}$, θ_{hkl} is the incident angle made with the lattice plane, n is the integer order of the diffracted peak and λ is the wavelength of the X-ray. For semi-crystalline polymers, although the amorphous phase has no definite ordered structure, it would

have contribution to the diffraction pattern in the form of a broad diffraction peak or so-called halo. Since the intensities of the diffraction peaks reflect the quantities of the corresponding phases in the sample, one can work backward using the peak intensity to determine the phase quantity.

The degree of crystallinity X of a semi-crystalline polymer can be expressed in terms of the X-ray diffraction intensity ratio of the crystalline phase to the total diffraction intensity:

$$X = \int I_c(\theta)d\theta / \left(\int I_c(\theta)d\theta + \int I_a(\theta)d\theta\right), \qquad (2.2)$$

where $I_c(\theta)$ and $I_a(\theta)$ are the diffraction intensity of the crystal phase and amorphous phase respectively [Fernandez et al., 1987]. Since most crystal diffraction peaks and the amorphous halo would appear at similar diffraction angles, deconvolution of the two types of peaks are necessary. Gaussian distribution profiles will be used to obtain best fit.

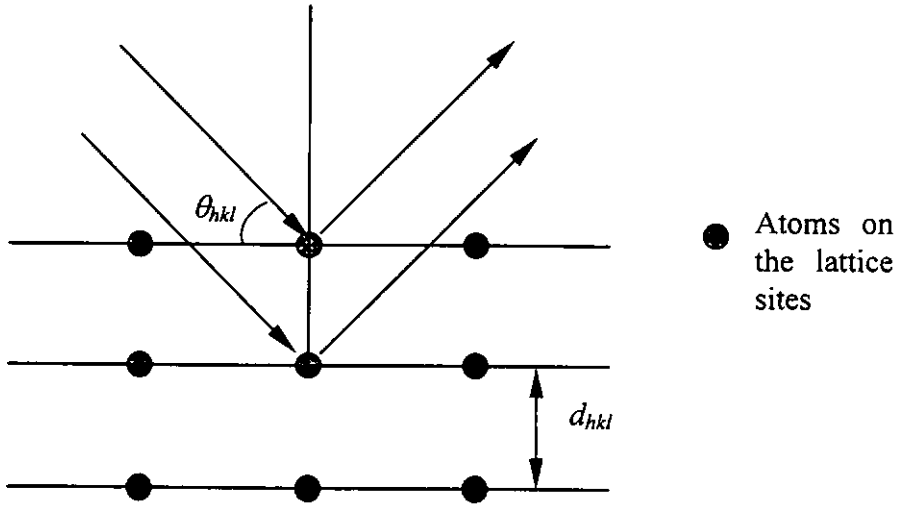

Figure 2.2 X-ray diffraction by atomic lattice planes.

2.2.2. Determination of Degree of Crystallinity

It has been widely shown that annealing a P(VDF/TrFE) copolymer at a temperature between T_c and T_m results in a significant increase in the piezoelectric and pyroelectric activities due probably to an increase in the crystallinity. We have undertaken X-ray diffraction measurements using the wide angle X-ray diffraction (WAXD) technique to determine the degrees of crystallinity of quenched and slow-cooled samples and those annealed at various temperatures after quenching. WAXD

patterns of these samples were obtained by a 2θ - θ scan method. The patterns were fitted by Gaussian functions as shown below:

$$Y = C_c \exp\left\{-(1/2)\left[(\chi - \mu_c)/\sigma_c\right]^2\right\} + C_a \exp\left\{-(1/2)\left[(\chi_a - \mu_a)/\sigma_a\right]^2\right\} \quad (2.3)$$

The first term and the second term of equation 2.3 represent the diffraction intensities coming from the crystalline phase and the amorphous phase of the sample respectively. C is an adjustable parameter corresponding to the height of the diffraction peak. χ is the scattering angle 2θ, and σ is the dispersion of the intensity distribution around μ. Subscripts c and a specify the crystalline and amorphous phases, respectively. The fitted pattern can be deconvoluted to the crystal and amorphous terms of equation 2.3. The crystallinity of the sample can then be obtained by integrating the deconvoluted profile according to equation 2.2.

2.3 FLOTATION METHOD

The flotation method was applied to determine the densities of the samples at room temperature.

In conducting the measurement, two clear miscible liquids were chosen, one of which was dibromomethane of density 2.4770 g/cm^3 and the other was ethanol of density 0.791 g/cm^3 at room temperature. They were then mixed in various proportions such that the copolymer samples can be floated freely inside the well-mixed liquid. The density of the liquid was then determined by the density bottle method.

The measured densities of the copolymer samples were tabulated in Appendix A. They were also used to calibrate the copolymer densities as a function of temperature which were determined by the thermal expansivity method to be reported in the next chapter.

2.4 RESULTS AND DISCUSSION

Figures 2.3 and 2.4 show the WAXD profiles of the 56/44 and 70/30 samples. The peaks at $2\theta \cong 19^{\circ}$ in both sets of figures are the (110) reflections of the β phase of the copolymers. The diffraction profile of quenched samples also exhibits a strong halo at around 19° that may be assigned to the amorphous phase. As the sample annealing temperature increases, this halo becomes weaker.

Figure 2.5 shows the deconvolution results of WAXD patterns of quenched and slow-cooled 56/44 samples. The background of the profiles has been removed before the fitting process. Similar procedures were applied to all other samples. The crystallinities thus obtained are tabulated in Table 2.2.

Table 2.2 **Crystallinity of copolymer samples to be used in thermal properties and elastic moduli studies.**

P(VDF/TrFE) 56/44 COPOLYMER	
SAMPLES	χ
Quenched	0.45
Annealed at 100 °C	0.49
Annealed at 120 °C	0.58
Annealed at 130 °C	0.63
Slow-Cooled	0.65
Annealed at 140 °C	0.72

P(VDF/TrFE) 70/30 COPOLYMER	
SAMPLES	χ
Quenched	0.55
Annealed at 100 °C	0.58
Annealed at 120 °C	0.71
Annealed at 130 °C	0.78
Slow-Cooled	0.80
Annealed at 140 °C	0.85

From the tabulated results, it is evident that even the quenched samples have over 40% crystal phase. The amorphous phase converts to the all-trans β-phase as a result of increasing annealing temperature. It has been shown that annealing a P(VDF/TrFE) copolymer at a temperature between T_c and T_m results in a significant increase in the piezoelectric and pyroelectric activities, due probably to an increase in the crystallinity [Ohigashi, 1983]. Crystallization takes place at the interface between the crystalline and the amorphous phases. That is, the crystallization process is dominated by the growth of the crystallites. In the case of the P(VDF/TrFE) copolymer, the free energies of the paraelectric crystals are lower than that of the amorphous phase. As the annealing temperature is above T_c, the copolymer will re-crystallize to the paraelectric phase by consumption of the amorphous phase [Tashiro, 1984b].

According to M. Hikosaka (1987), the copolymer molecules in the crystal can move parallel to the molecular chain direction under circumstances determined by temperature. This results in hexagonal packing of the chain molecules. The molecular chains in the P(VDF/TrFE) copolymers are packed in the two-dimensional hexagonal lattice in the paraelectric phase, thus facilitating an increase in the degree of crystallinity in the P(VDF/TrFE) copolymer around T_c, as particularly noted in the 70/30 copolymer (Table 2.1).

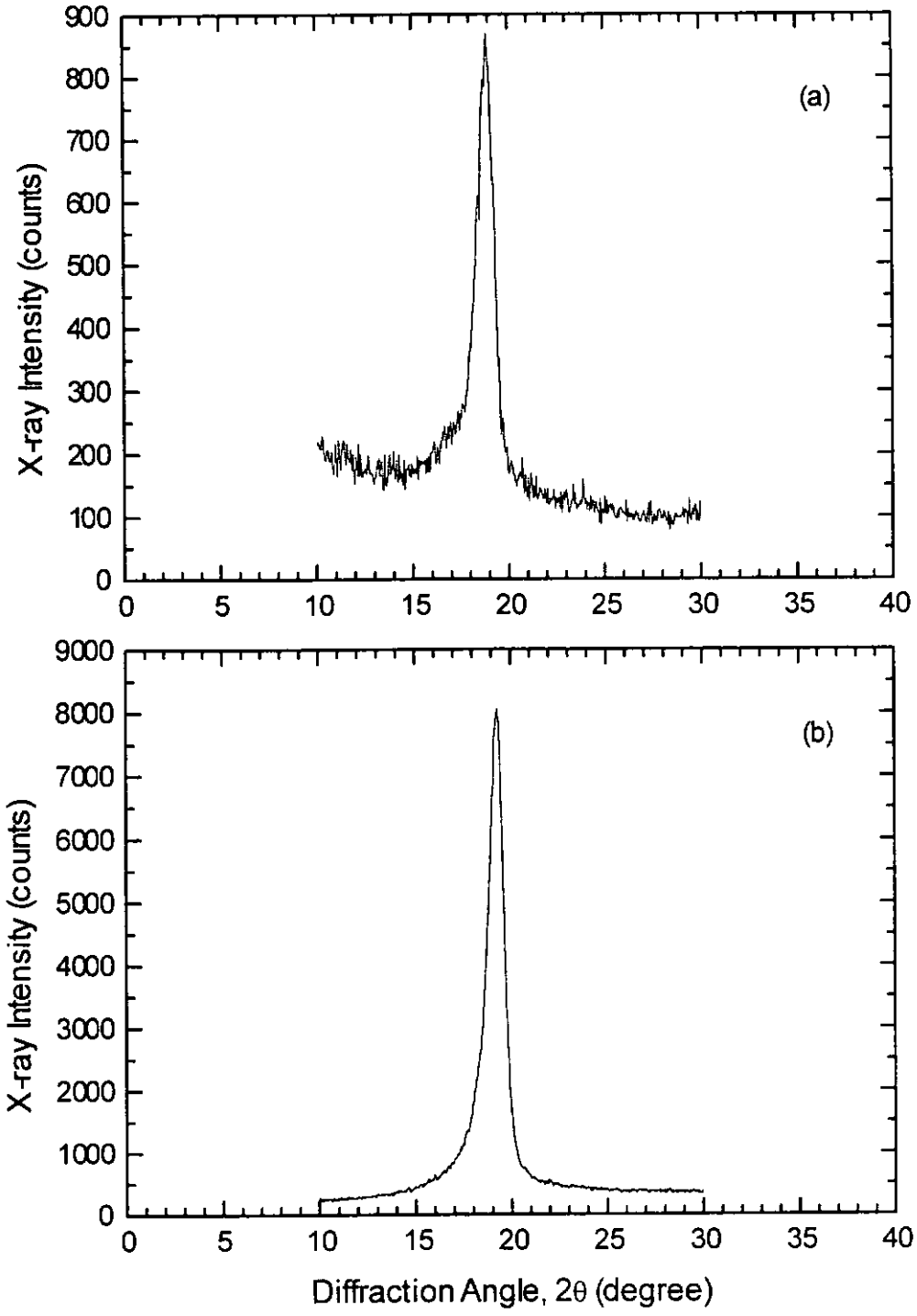

Figure 2.3 **X-ray diffraction profiles of the quenched (a) 56/44 and (b) 70/30 copolymer samples.**

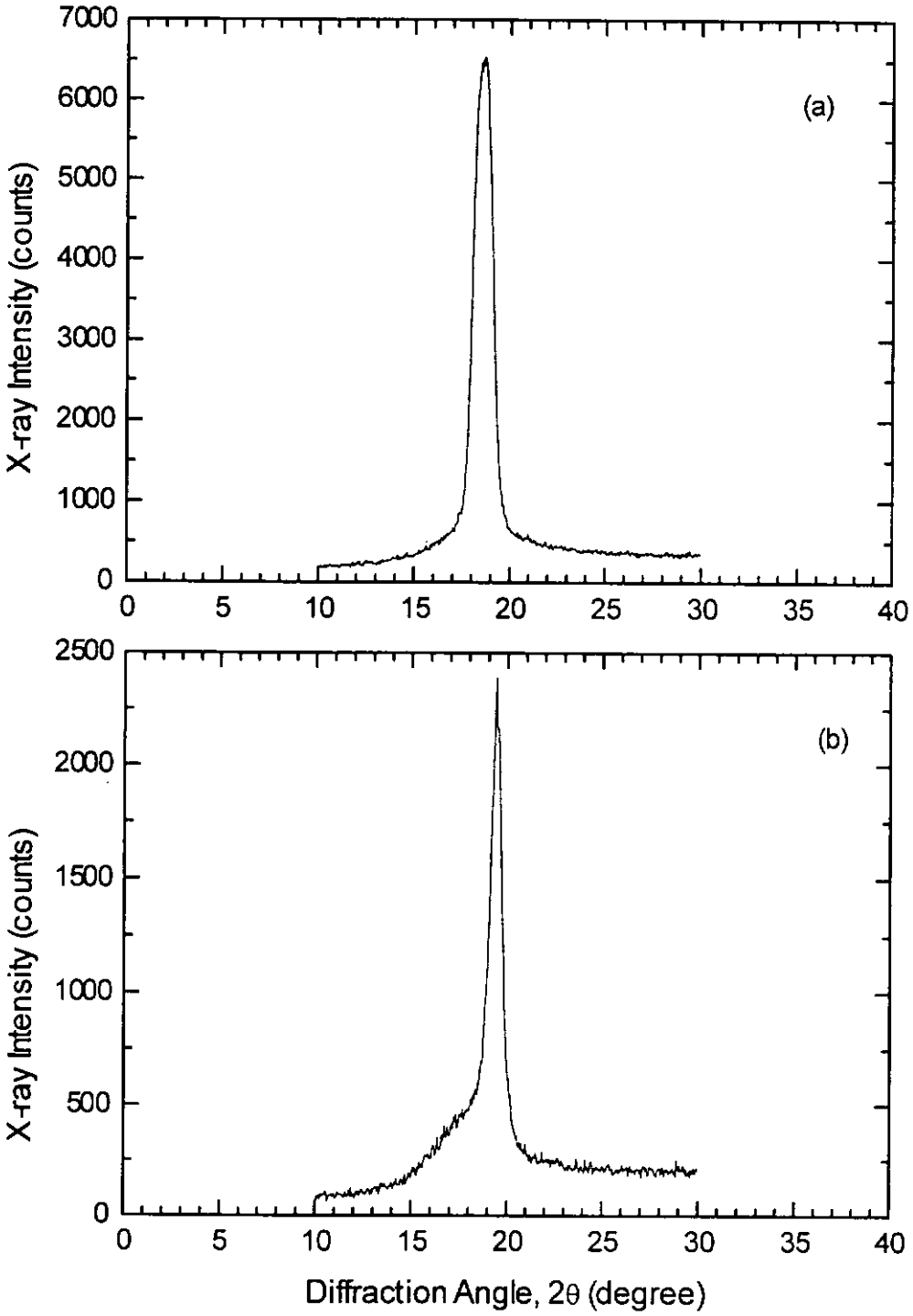

Figure 2.4 **X-ray intensity diffraction profiles of the slow-cooled (a) 56/44 and (b) 70/30 copolymer samples.**

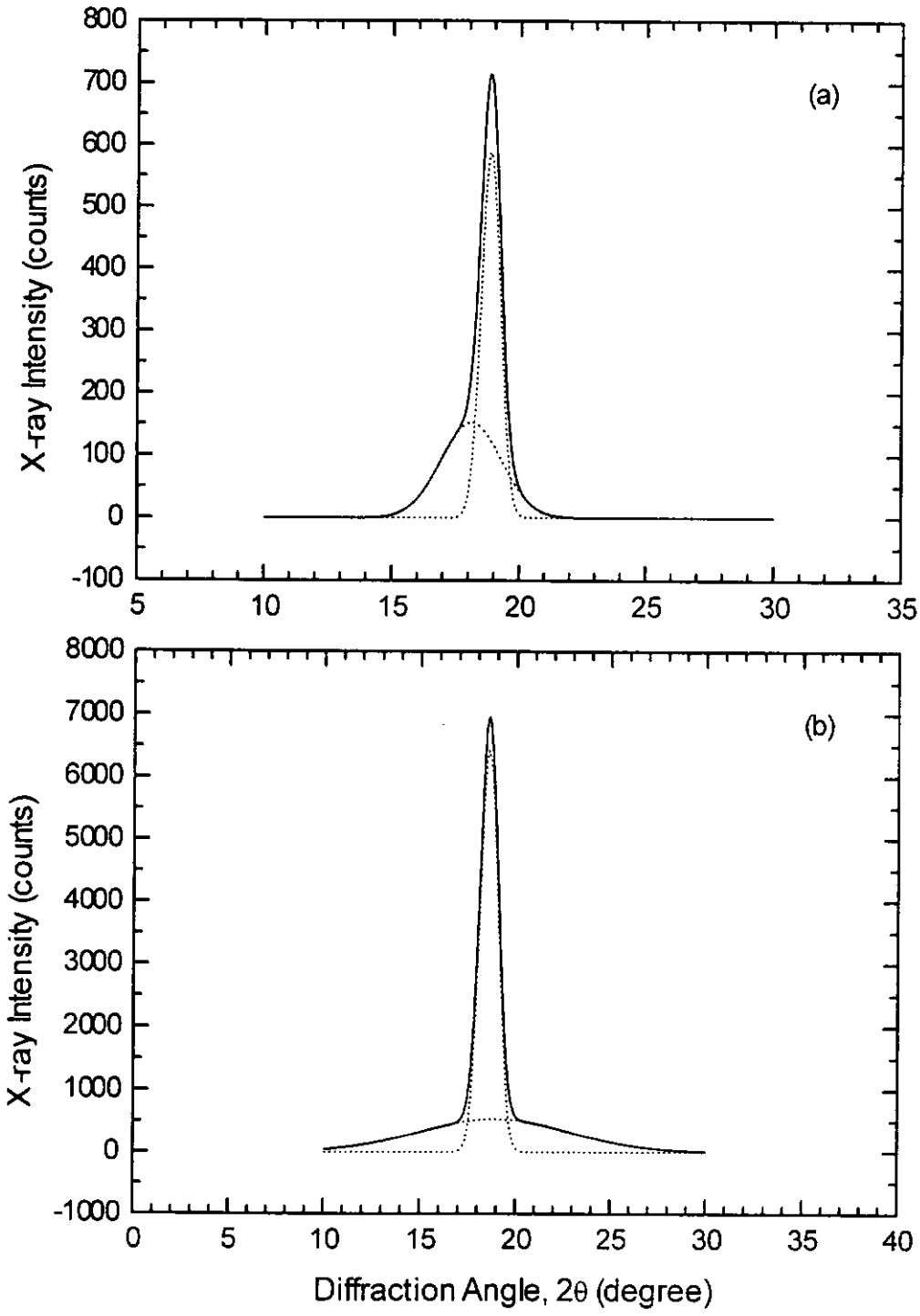

Figure 2.5 **Deconvoluted X-ray intensity profiles for the 56/44 copolymers : (a) Quenched, (b) Slow-cooled.**

CHAPTER 3

THERMAL PROPERTIES

In this chapter, three kinds of thermal properties of the copolymer will be described, viz. the thermal expansivity, specific heat and thermal conductivity, to illucidate the thermal behavior of the material.

3.1 THERMAL EXPANSIVITY

In fact, among many crystalline polymers, the vinylidene fluoride-trifluoroethylene (VDF/TrFE) copolymers exhibit special structural change in the ferroelectric phase transition. This structural change is characterized by the large conformational change of the molecular chain between the extended all-trans form (below the transition temperature T_c) and the contracted trans-gauche form (above T_c) [Tashiro, 1981; Tashiro, 1984a; Tashiro, 1984b; Lovinger, 1982; Lovinger, 1983a]. Such a conformational change induces a large dimensional change of the samples.

Therefore, the study of the thermal expansion of the copolymers will provide more detailed information of the structural change.

3.1.1 Thermal Expansivity Measurement

The samples used for expansivity studies were quenched and slow-cooled 56/44 and 70/30 copolymers. In order to increase the accuracy of the measurement, samples were made to about 1.5 mm thick.

Thermal expansion measurements were conducted on a Perkin-Elmer TMA 7 thermal mechanical analyzer. The block diagram of TMA 7 is shown in Figure 3.1. The sample was attached to a linear variable differential transformer (LVDT) through a quartz rod. The sensitivity of the LVDT is about 4 nm. The whole sample was put in a temperature controlled oven set at a heating rate of 2 K/min. The setup is computer controlled. The temperature and the displacement of the LVDT are displayed and the data may be stored for future analysis.

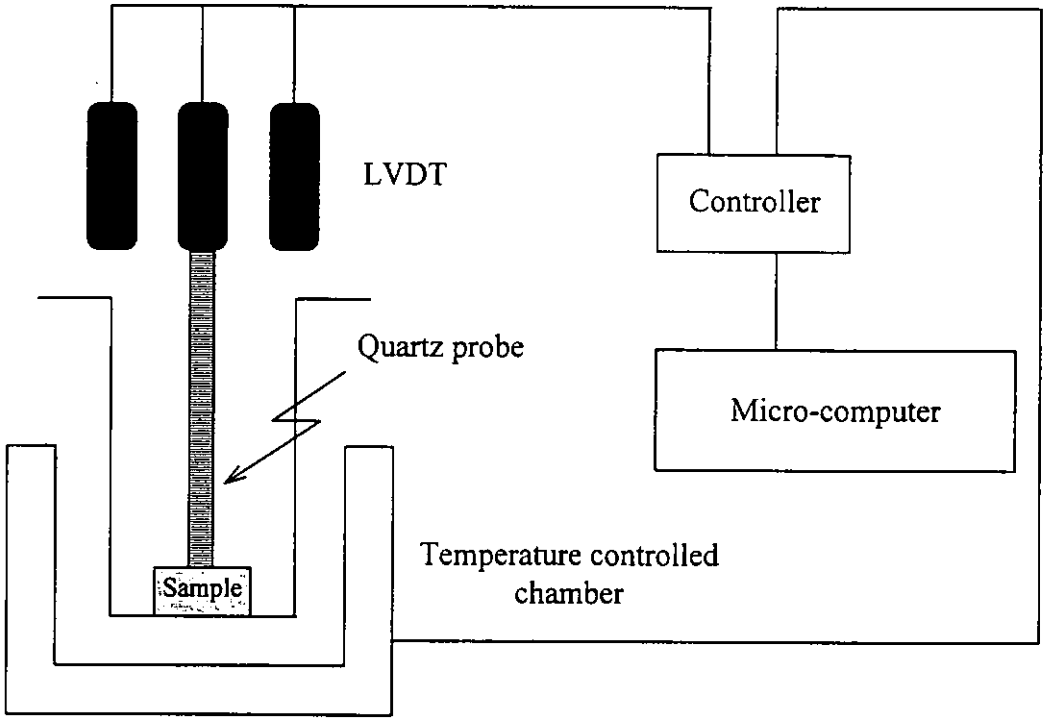

Figure 3.1 Schematic set-up of TMA 7 Thermal Mechanical Analyzer system for the thermal expansion measurements.

3.1.2 Results of the Measurement

The Curie transition T_c in P(VDF/TrFE) copolymers is well reflected in the thermal expansion measurements. The expansion (fractional change in linear dimension) curve of the quenched 56/44 sample is shown in Figure 3.2 (a), and the linear expansion coefficient as a function of temperature is shown in Figure 3.2 (b). Similar curves of slow-cooled 56/44 are given in Figures 3.3 (a) and (b). An abrupt change in thermal expansion for both samples occurs at about 65 °C which is also reflected in the expansion coefficient peaks in Figures 3.2 (b) and 3.3 (b). There is a slight shift of the curves in the cooling runs with respect to the heating curves and the peaks occur at about 60 °C. The 70/30 samples of higher VDF content had been similarly measured. Results of the quenched and slow-cooled samples are shown in Figures 3.4 and 3.5, respectively. The abrupt change in thermal expansion occurs at a higher temperature of about 105 °C for heating runs and at 60 °C for cooling runs. It is obvious that the copolymer samples with higher VDF content displays thermal hysteresis more definitely compared with the 56/44 samples.

To a first approximation, it can be assumed that the volume expansion coefficients of the isotropic copolymers are simply three times the linear expansion coefficients. Therefore, the volume change as a function of temperature of the samples can be obtained and hence the density change. By making use of the room temperature densities of the samples determined by the flotation method as mentioned in section

2.3, the samples' densities at various temperatures can be calculated. These results are tabulated in Appendix D.

Figures 3.6 and 3.7 show the temperature dependence of density of the quenched and slow-cooled 56/44 and 70/30 copolymers, respectively. From the graphs, it can be seen that the density decreases as the temperature rises, and the thermal hysteresis effect is quite obvious for the 70/30 samples. There is almost a 10 % decrease in density for both 56/44 and 70/30 copolymers from the room temperature ferroelectric phase to the high temperature paraelectric phase.

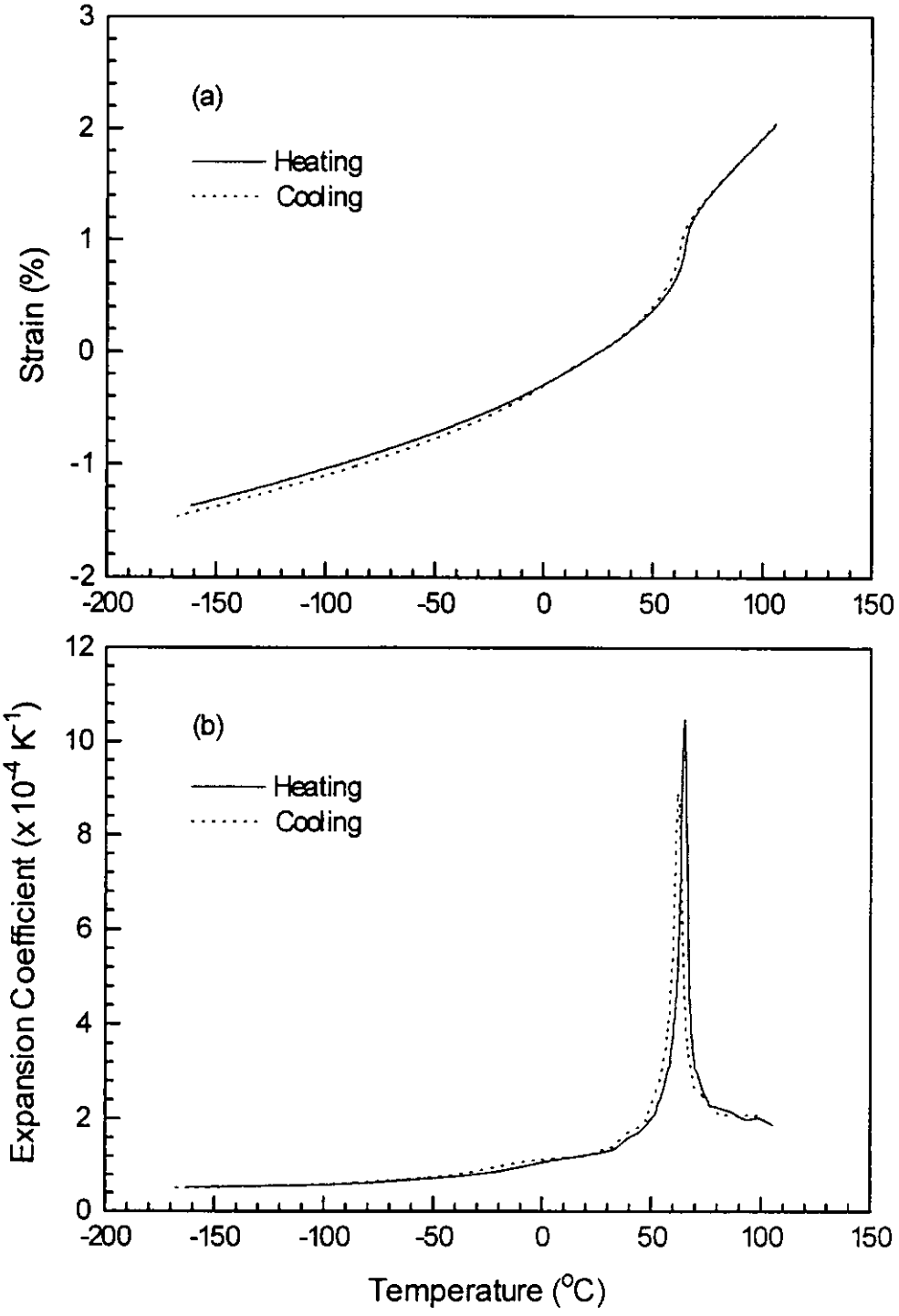

Figure 3.2 **(a) Thermal expansion and (b) expansion coefficient curves measured for the quenched 56/44 sample in heating and cooling runs.**

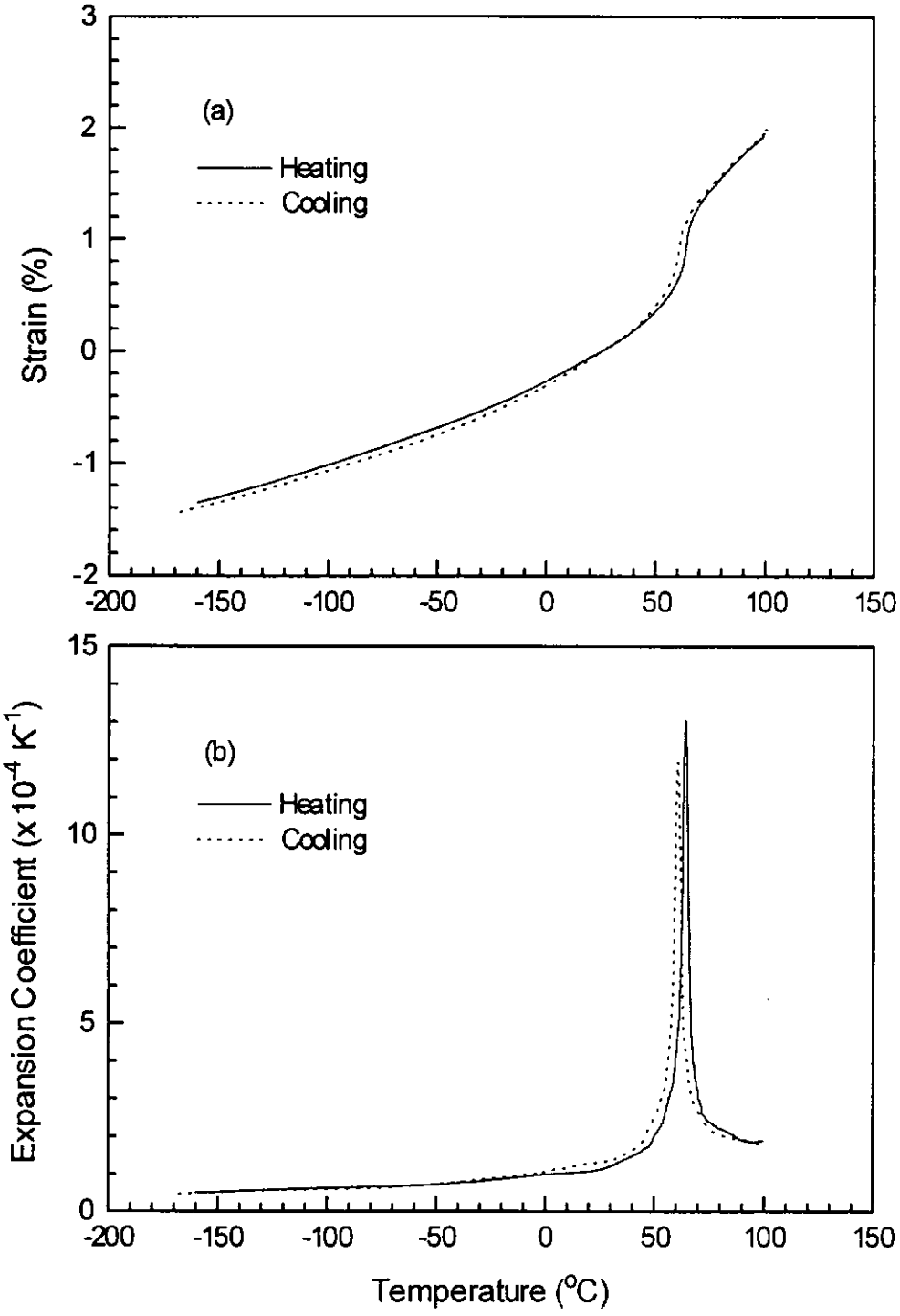

Figure 3.3 **(a) Thermal expansion and (b) expansion coefficient curves measured for the slow-cooled 56/44 sample in heating and cooling runs.**

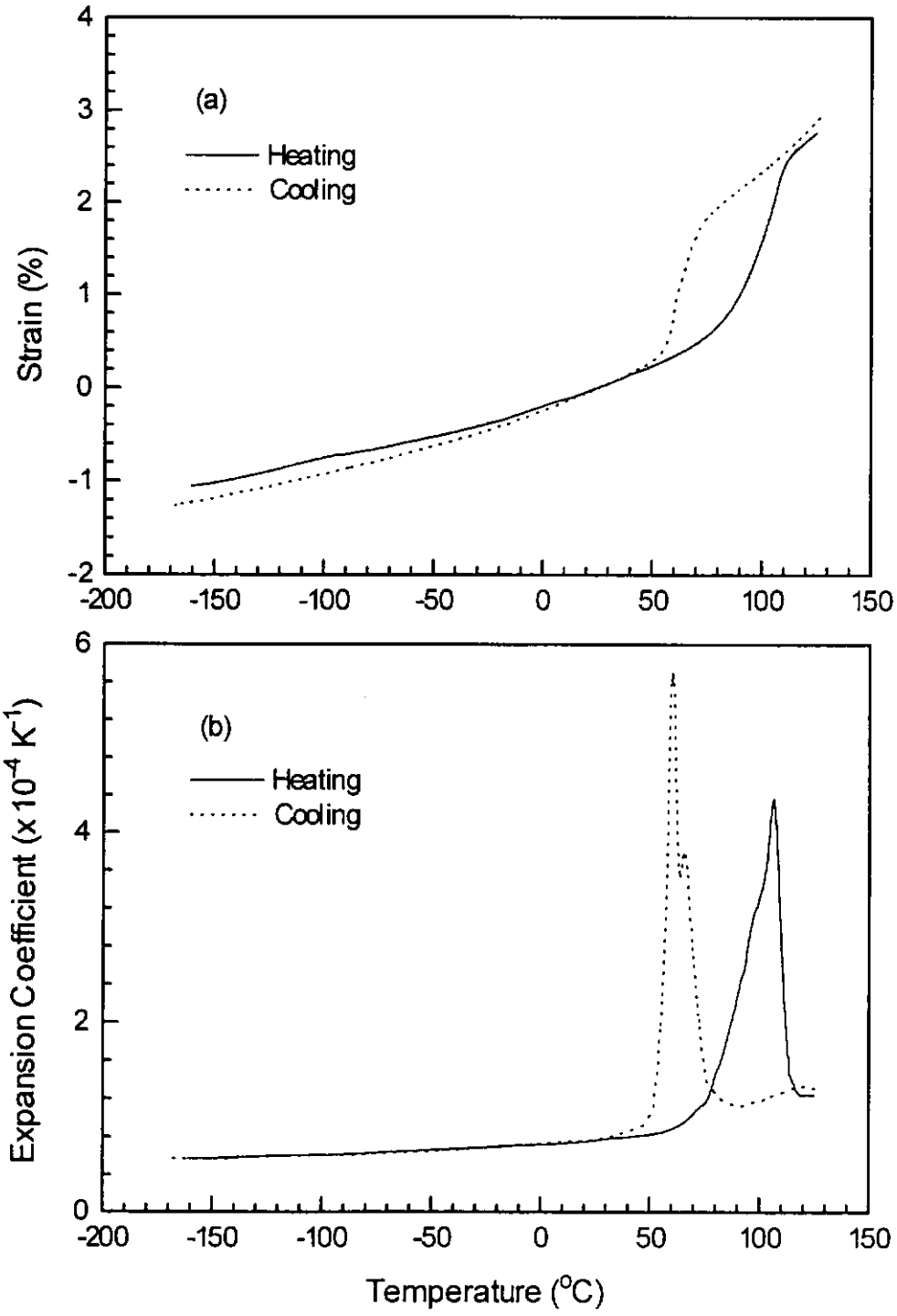

Figure 3.4 **(a) Thermal expansion and (b) expansion coefficient curves measured for the quenched 70/30 sample in heating and cooling runs.**

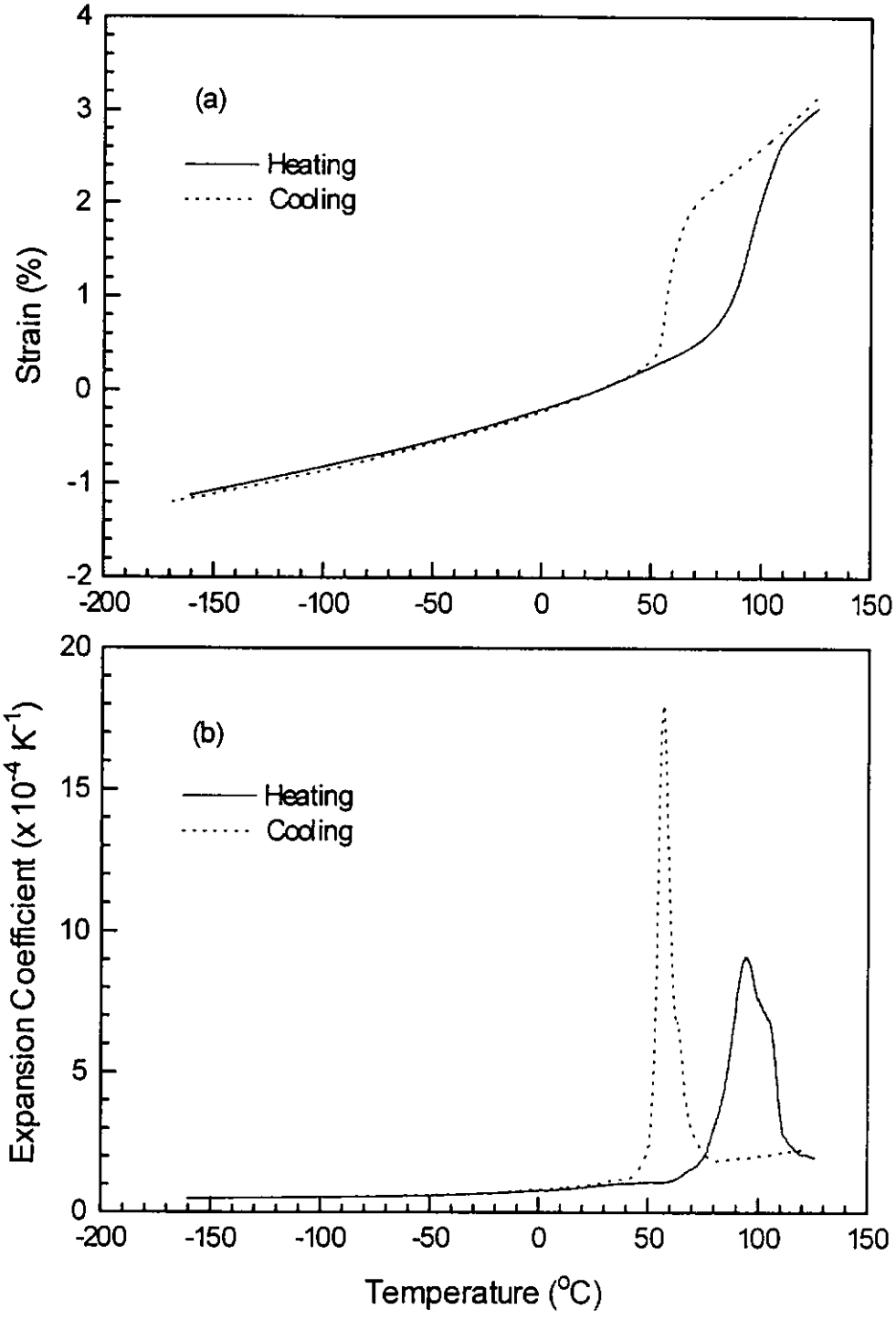

Figure 3.5 **(a) Thermal expansion and (b) expansion coefficient curves measured for the slow-cooled 70/30 sample in heating and cooling runs.**

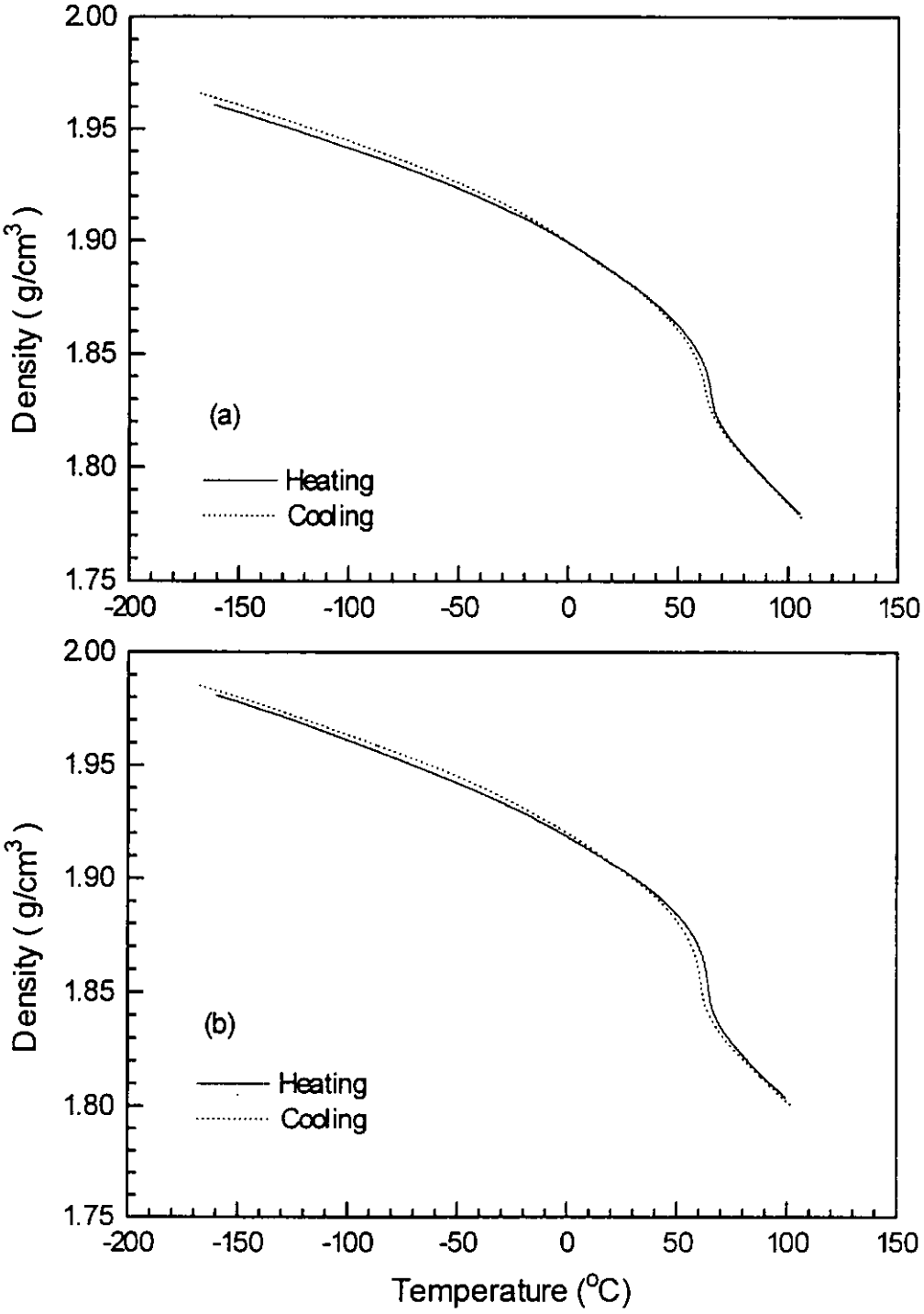

Figure 3.6 **Density of 56/44 P(VDF/TrFE) measured in heating and cooling runs. (a) Quenched, (b) Slow-cooled.**

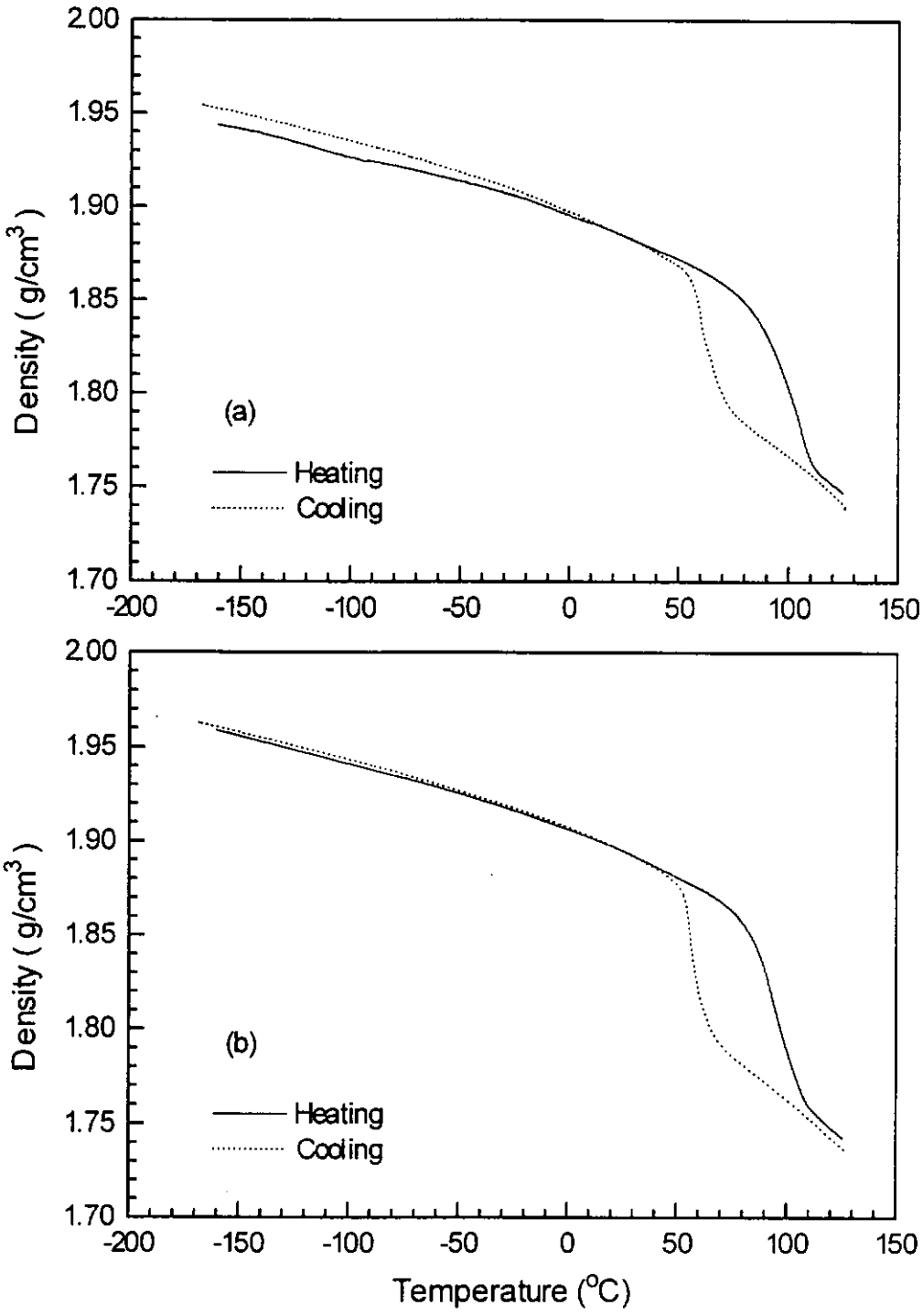

Figure 3.7 **Density of 70/30 P(VDF/TrFE) measured in heating and cooling runs. (a) Quenched, (b) Slow-cooled.**

3.2 DETERMINATION OF SPECIFIC HEAT

One of the important thermal properties of polymers is their specific heat. The phase transitions in most materials can be revealed from studying the temperature dependence of the specific heat. In our present study, the specific heat of the copolymer samples were determined by the Differential Scanning Calorimetry method.

3.2.1 Differential Scanning Calorimeter (DSC)

The DSC is based on heating (or cooling) a sample and a reference at a preset rate. In order to keep their temperatures the same, the compensating heat flux that is needed for the sample is measured. Eventually, a DSC curve is obtained from plotting the heat flow against the temperature. In conducting DSC experiment, the reference side usually is an empty sample pan. For the determination of specific heat, the mass of the sample should be known.

In our experiment, the Perkin-Elmer DSC-7 was used. The mass of the copolymer sample for each test was about 10 mg. A heating rate or cooling rate of 10°C/min was chosed. The DSC-7 would be able to provide an accuracy of about 1 to 2 %.

3.2.2 Specific Heat and Enthalpy Change

The specific heats of the copolymers were found in the temperature range -120 °C to 120 °C in heating runs and from 120 °C to room temperature in cooling.

Figure 3.8 shows the specific heat of quenched and slow-cooled 56/44 as a function of temperature in heating and cooling runs. Figure 3.9 shows similar results for the 70/30 copolymer. It is noteworthy to mention that 70/30 exhibits obvious thermal hysteresis as in thermal expansion.

For the slow-cooled P(VDF/TrFE) 70/30 copolymer as shown in Figure 3.9 (b), two peaks were observed in the ferroelectric transition region. These are probably due to the coexistence of the two kinds of ferrorelectric phases.

The melting temperature and the Curie temperature of the copolymers can also be determined by enthalpy curves as shown in Figure 3.10. These curves run from room temperature to 180 °C which is higher than the melting point of the copolymers. There are two main endothermic peaks in each heating curve which indicate the melting temperature (T_m) and the Curie temperature (T_c) of the samples. Exothermic peaks indicating the crystallization temperature (T_{cry}) and the ferroelectric transition temperature (T_c) are also observed in cooling runs. The corresponding transition temperatures are in good agreement with those observed in thermal expansion studies. T_c, T_m and T_{cry} of the copolymer samples are listed in Table 3.1 for reference.

Table 3.1 **Curie temperature T_c, melting temperature T_m and crystallization temperature T_{cry} of P(VDF/TrFE).**

Sample		Heating		Cooling	
		T_c/°C	T_m/°C	T_c/°C	T_{cry}/°C
Quenched	56/44	65.1	156.2	59.5	141.6
	70/30	106.3	153.2	67.5	138.9
Slow-cooled	56/44	64.7	159.2	60.1	140.5
	70/30	105.5	156.3	66.3	137.5

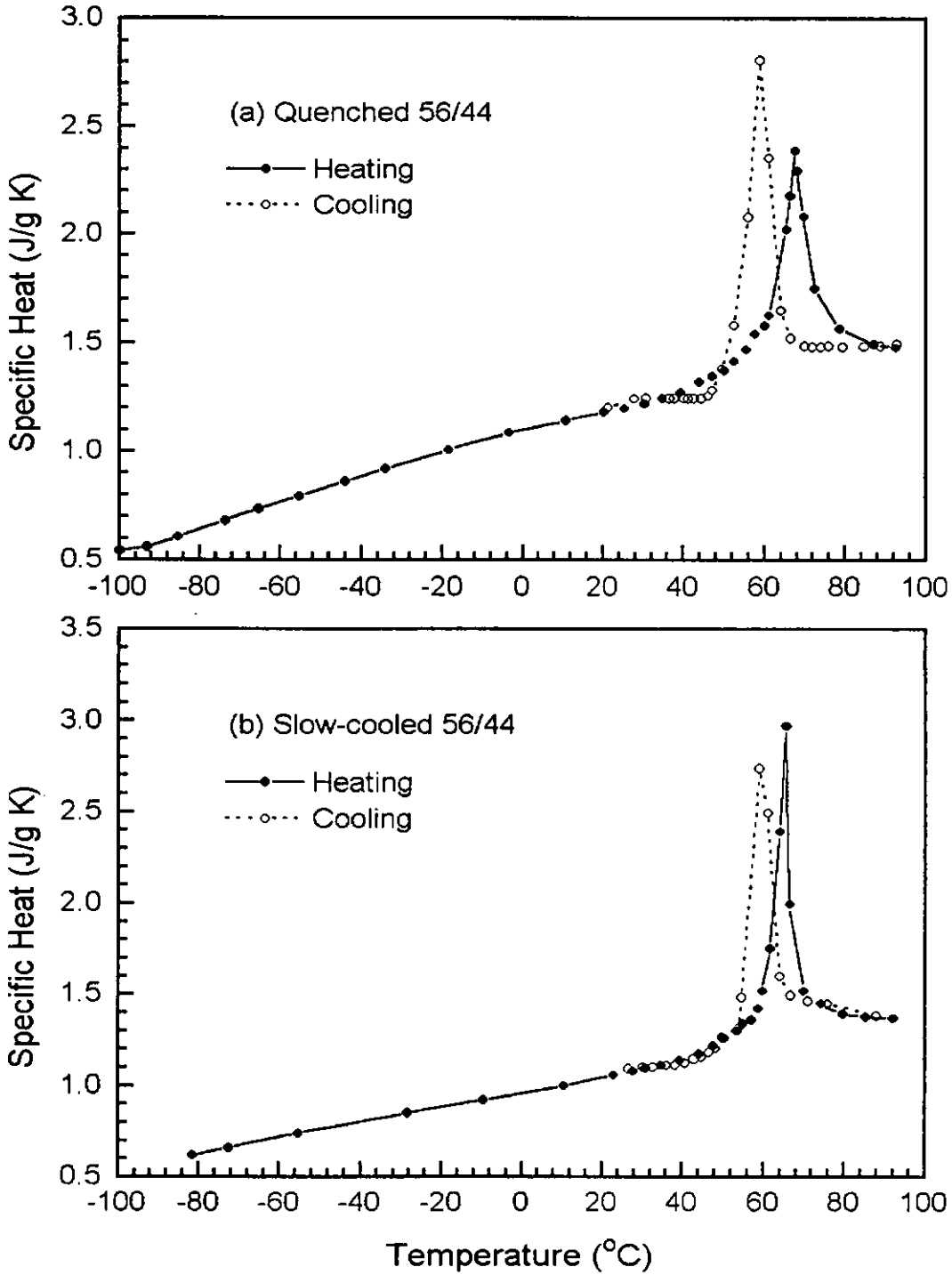

Figure 3.8 **(a) Specific heat of quenched P(VDF/TrFE) 56/44 copolymer as a function of temperature upon heating and cooling. (b) Specific heat of slow-cooled P(VDF/TrFE) 56/44 copolymer as a function of temperature upon heating and cooling.**

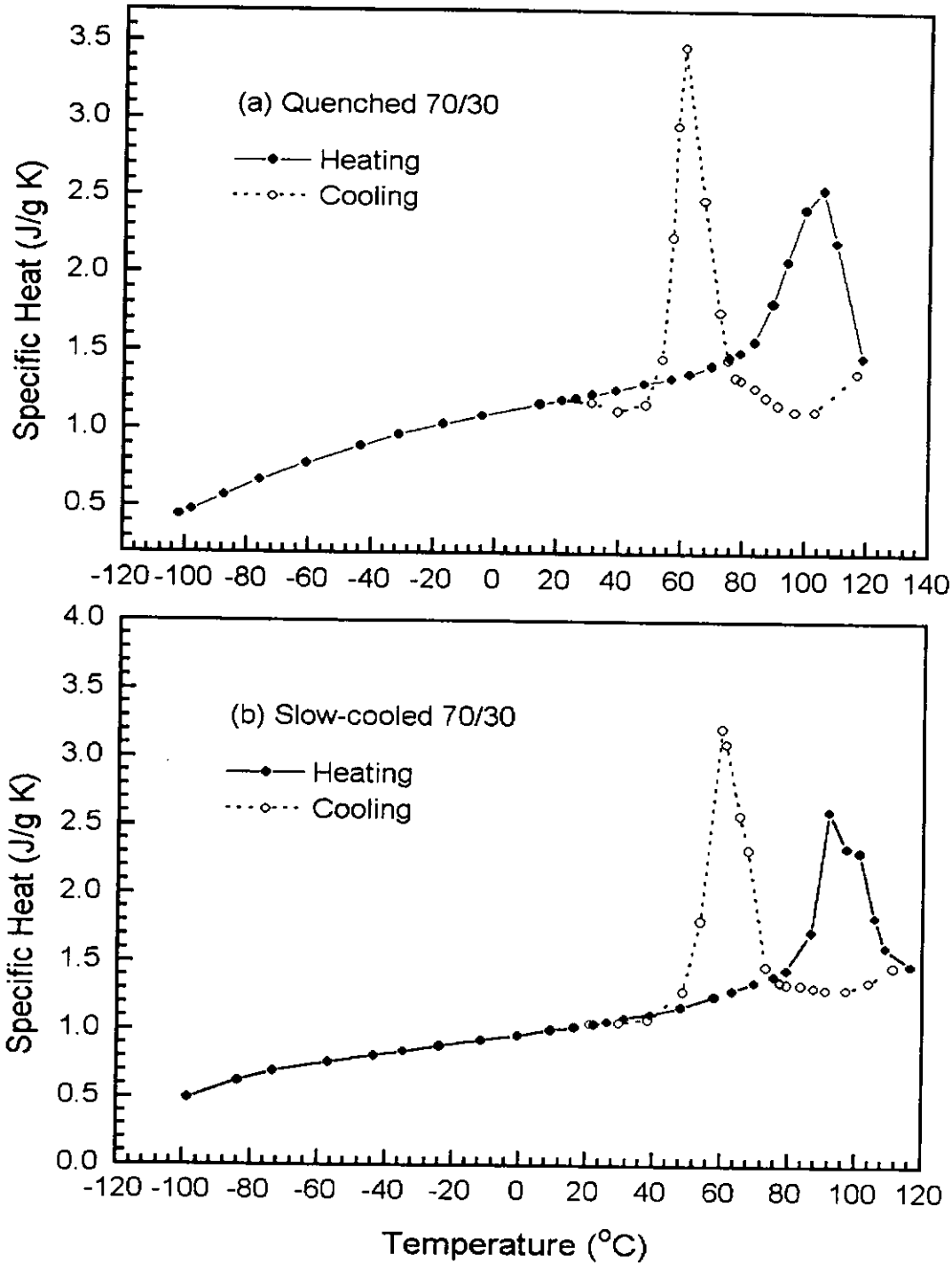

Figure 3.9 **(a) Specific heat of quenched P(VDF/TrFE) 70/30 copolymer as a function of temperature upon heating and cooling. (b) Specific heat of slow-cooled P(VDF/TrFE) 70/30 copolymer as a function of temperature upon heating cooling.**

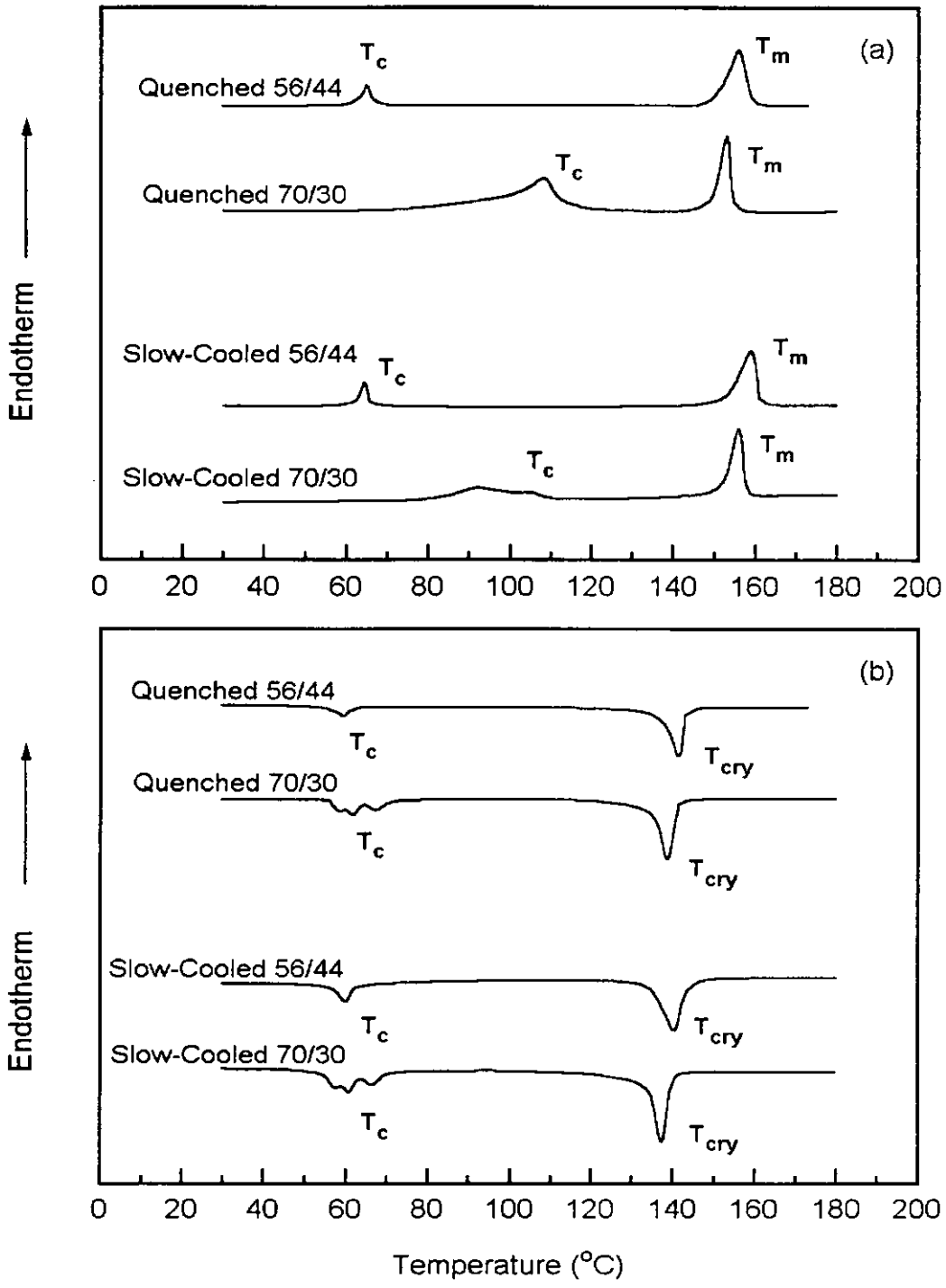

Figure 3.10 **The DSC heat flow curves of the P(VDF/TrFE) copolymer samples: (a) Heating, (b) Cooling.**

3.3 LASER FLASH RADIOMETRY MEASUREMENT

The laser flash radiometry method is used to measure the thermal diffusivity of solid film materials. The transmission technique of this method utilizes an intense light pulse to heat up the front surface of the sample, then the transient temperature rise at the rear surface is measured by an IR detector as a function of time. By using this transient transmission measurement method, the effect arising from radiation loss can be neglected and hence can be used to measure the thermal diffusivity of insulating materials. Furthermore, the use of a light pulse as the thermal energy input and an IR detector as the temperature sensor allows the use of a relatively small sample and avoids physical contact with the sample. This greatly simplifies the problem of correction for systematic errors.

3.3.1 Principles of Laser Flash Radiometry

The flash radiometry method for measuring the thermal diffusivity of solid materials has been in use for decades. An intense light pulse is used to heat up the front surface of the sample, and the transient temperature rise at the rear surface is measured by an infrared detector as a function of time. The following discussion is based on an one dimensional heat flow model. This assumption is valid as long as the thickness of the sample is at least 10 times smaller than the lateral dimensions of the area illuminated by the light pulse. Besides, since the temperature diffusion time is far less than the time for the sample to reach thermal equilibrium, the heat loss due to convection and radiation at the sample surfaces may be negelected [Leung, 1984a].

Consider a short laser pulse impinging onto the front surface of a thin sample of thickness L. Let $T(x,t)$ be the temperature distribution (above ambient temperature T_o) in the sample at time t. The x direction is along the sample thickness. The diffusion of the absorbed heat energy through the sample of thermal diffusivity D is governed by the one dimensional heat diffusion equation:

$$\frac{\partial T}{\partial t} = D\frac{\partial^2 T}{\partial x^2} \qquad (3.1)$$

subject to the adiabatic boundary condition:

$$\frac{\partial T(x,t)}{\partial x} = 0 \qquad (3.2)$$

at the front surface. The solution of heat diffusion under adiabatic boundary condition for thin samples has been given by Carslaw and Jaeger [Carlsaw, 1959]. If the initial temperature distribution inside the sample is $T(x,0)$, the temperature at a distance x from the irradiated surface of a sample of thickness L at time t is :

$$T(x,t) = \frac{1}{L}\int_0^L T(x,0)dx + \frac{2}{L}\sum_{n=1}^{\infty} exp\left(\frac{-n^2\pi^2 Dt}{L^2}\right) \times cos\frac{n\pi x}{t}\int_0^L T(x,0)cos\frac{n\pi x}{L}dx \qquad (3.3)$$

If α is the absorption coefficient of the sample at the excitation wavelength, the initial temperature distribution $T(x,0)$ can be expressed as follows:

$$T(x,0) = A\alpha e^{-\alpha x} \qquad (3.4)$$

where A is a constant depending on the pulse energy and the heat capacity of the sample. With this initial condition, equation 3.3 becomes:

$$T(x,t)=\frac{A}{L}\left[\left(1-e^{-\alpha L}\right)+2\sum_{n=1}^{\infty}\exp\left(\frac{-n^2\pi^2 Dt}{L^2}\right)\times\cos\frac{n\pi x}{L}\left(\frac{1-(-1)^n e^{-\alpha L}}{1+\frac{n^2\pi^2}{\alpha^2 L^2}}\right)\right] \tag{3.5}$$

According to the Stefan-Boltzmann law, the total energy density radiated from the surface of a blackbody is proportional to the fourth power of its temperature, thus the radiometry signal $S_R(t)$ monitored by the infrared detector behind the rear surface of the sample can be written as [Leung, 1984a]:

$$S_R(t)=K'\alpha'\int_0^L\left\{\left[T_0+T(x,t)\right]^4-T_0^4\right\}e^{-\alpha'(L-x)}dx \tag{3.6}$$

where $K' = G\varepsilon\sigma_0$ is a constant, in which G is a geometrical factor, ε is emissivity averaged over the detection spectral bandwidth and σ_0 is the Stefan-Boltzmann constant; α' is the infrared absorption coefficient of the sample over the detection spectral bandwidth.

Provided that $T(x,t)$ is small compared to T_0, the radiometry signal $S_R(t)$ received by the infrared detector at the rear face can be deduced by substitution of equation 3.5 into 3.6. The result is shown in the following equation [Leung, 1984a]:

$$S_R(t) = P\left[\left(1-e^{-\alpha L}\right)\left(1-e^{-\alpha' L}\right) - 2e^{-\alpha' L}\sum_{n=1}^{\infty}\left(\frac{1-(-1)^n e^{-\alpha L}}{1+\frac{n^2\pi^2}{\alpha^2 L^2}}\right)\left(\frac{1-(-1)^n e^{-\alpha' L}}{1+\frac{n^2\pi^2}{\alpha'^2 L^2}}\right) e^{-n^2 t/\tau_L}\right] \tag{3.7}$$

where

$P = 4AK'T_0^3/L$

τ_L = the thermal diffusion time constant, which is related to the thermal diffusivity D by

$$\tau_L = \frac{L^2}{\pi^2 D} \tag{3.8}$$

Since the peak wavelength of the radiation emitted from a black body at room temperature is around 10 μm, an infrared detector can be used to record the flash radiometry signal. By fitting equation 3.7 to the detected signal, the thermal diffusivity D can be deduced.

Then, the thermal conductivity K is calculated through the relation

$$K = \rho C_p D \tag{3.9}$$

where ρ and C_p are the density and specific heat of the sample, respectively.

3.3.2 Experimental Method

As shown in Figure 3.11, the experimental laser flash radiometry set-up includes a Q-switched Nd^{+}:YAG pulsed laser used as the pulsed radiation source. Its fundamental wavelength is 1064 nm, while shorter wavelength radiation can be generated by inserting the KD*P frequency doubling crystal into its beam path. Thus the laser system can provide laser pulses of wavelengths 1064, 532, 355 and 266 nm. The third harmonic, ultra-violet radiation of wavelength 355 nm, with pulse duration of about 10 ns is employed as the heat source in our experiment. The laser beam spot size is approximately 6 mm in diameter.

Aluminium plates of thickness 1mm with appropriate aperture are placed at both sides of the sample, leaving air gaps between the plates and sample to prevent heat loss to the plates by conduction. The apertures help to ensure uniform illumination flashing on the front surface of the sample. The size of the aperture is adjusted according to the diameter of the sample used.

The sample is placed at a distance of 8 cm before a meniscus Ge lens which has a focal length of 4 cm, thus the rear surface of the sample is imaged at 8 cm behind a germanium lens onto a liquid nitrogen cooled HgCdTe infrared detector (Infrared Associates, Inc.). The active area of the detector is 0.25 x 0.25 mm and is sensitive to 8 - 12 μm infrared radiation. The rise time of this photo-conductive type detector is about 120 ns.

The signal from the infrared detector is then boosted by a pre-amplifier, the output of which is connected to a HP54510B digitizing storage oscilloscope (DSO). The bandwidth of the DSO is 350 MHz and the fastest digitizing rate is 1 Gsa/sec. The sample is irradiated at intervals of 10 seconds to allow the temperature to decay to ambient before firing the next pulse. The experiment is performed by averaging the signals obtained in 30-50 laser shots.

The averaged and digitized signals are then transferred to a microcomputer and stored for further analysis. The thermal diffusivity D is deduced from a recursive fitting program to the digitized data based on the equation 3.7.

In our experiment, ultraviolet radiation of wavelength 355 nm is used because it is strongly absorbed by the copolymers. The sample, of size about 10 mm x 10 mm x 100 μm, is clamped on its edge to the copper sample holder. The sample holder is in contact with a liquid nitrogen chamber and a heater. The temperature of the sample can be changed from –150 °C to 200 °C with a precision of ± 0.5°C.

For the flash radiometry measurement at room temperature, the polymer sample thickness L was kept below 250 μm to avoid the necessity for correction of radiative and air conduction effects, and the laser beam radius r was adjusted to give $r/L > 10$, thus eliminating the need to consider radial heat flow. On the other hand, for measurement over a wide temperature range up to 200 °C, a thinner sample (100 - 150 μm) was used since the radiative heat loss became more serious at high temperature. In order to enhance the laser absorption, a carbon-black film (about 2 μm thick) was painted on the front surface. The laser pulse energy was adjusted to give a temperature rise of about 2K.

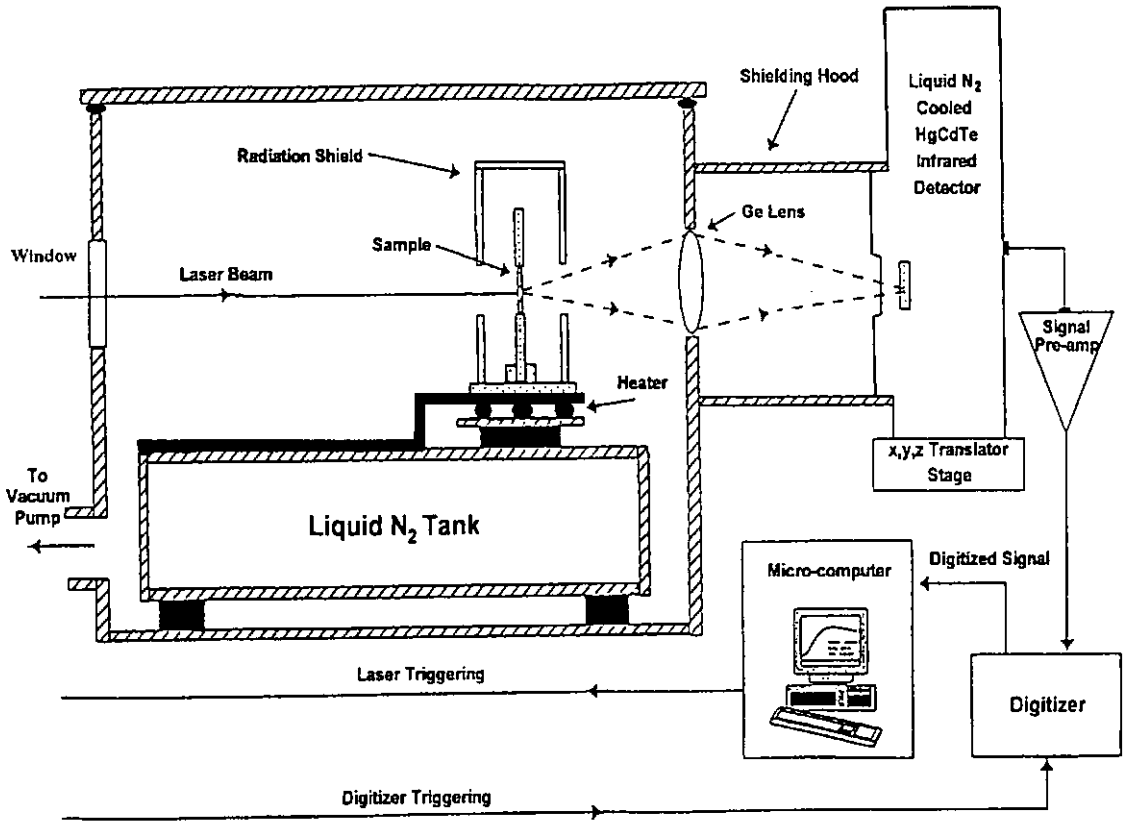

Figure 3.11 Schematic diagram of the apparatus for the laser flash radiometry measurement.

3.3.3 Results and Discussion

Appendix F shows the radiometry signal profile and mathematically simulated radiometry signal obtained through "Laser Flash Radiometry", respectively.

The thermal diffusivity D, the thermal conductivity K and the degree of crystallinity χ of the 56/44 and 70/30 copolymers at room temperature are given in Table 3.2.

Table 3.2 Room temperature thermal diffusivity D, thermal conductivity K and crystallinity χ of the quenched and slow-cooled P(VDF/TrFE) copolymer samples.

	P(VDF/TrFE) 56/44 samples		P(VDF/TrFE) 70/30 samples	
	Quenched	Slow-cooled	Quenched	Slow-cooled
Thickness (μm)	100	113	146	105
Density ρ (g/cm^3)	1.885	1.907	1.886	1.911
Specific Heat C (J/g K)	1.20	1.04	1.19	1.04
Diffusivity D (x 10^{-3} cm^2/s)	0.730	1.06	0.745	1.08
Conductivity K (mW/cm K)	1.64	2.11	1.67	2.16
Crystallinity χ	0.45	0.72	0.55	0.80

From the table, we find that the thermal diffusivity D and thermal conductivity K of both 56/44 and 70/30 samples increase with the crystallinity. This is understandable because the thermal conductivity of the crystalline phase is normally higher than that of the amorphous phase.

The temperature dependence of the thermal diffusivity D of the quenched and slow-cooled 56/44 samples were measured from -100 °C to 100 °C upon heating and cooling. The results are shown in Figure 3.12 (b) and Figure 3.13 (b). Also, the temperature dependence of the thermal diffusivity D of the quenched and slow-cooled 70/30 samples were measured from -120 °C to 120 °C upon heating and cooling. The results are depicted in Figure 3.14 (b) and Figure 3.15 (b). There are common features that can be found from these graphs. The diffusivities gradually decrease with increasing temperature, which is typical of semi-crystalline polymers. Near the phase transition temperature, the decline in diffusivity becomes slow, followed by a sudden drop in a heating process; the reverse is true in a cooling process.

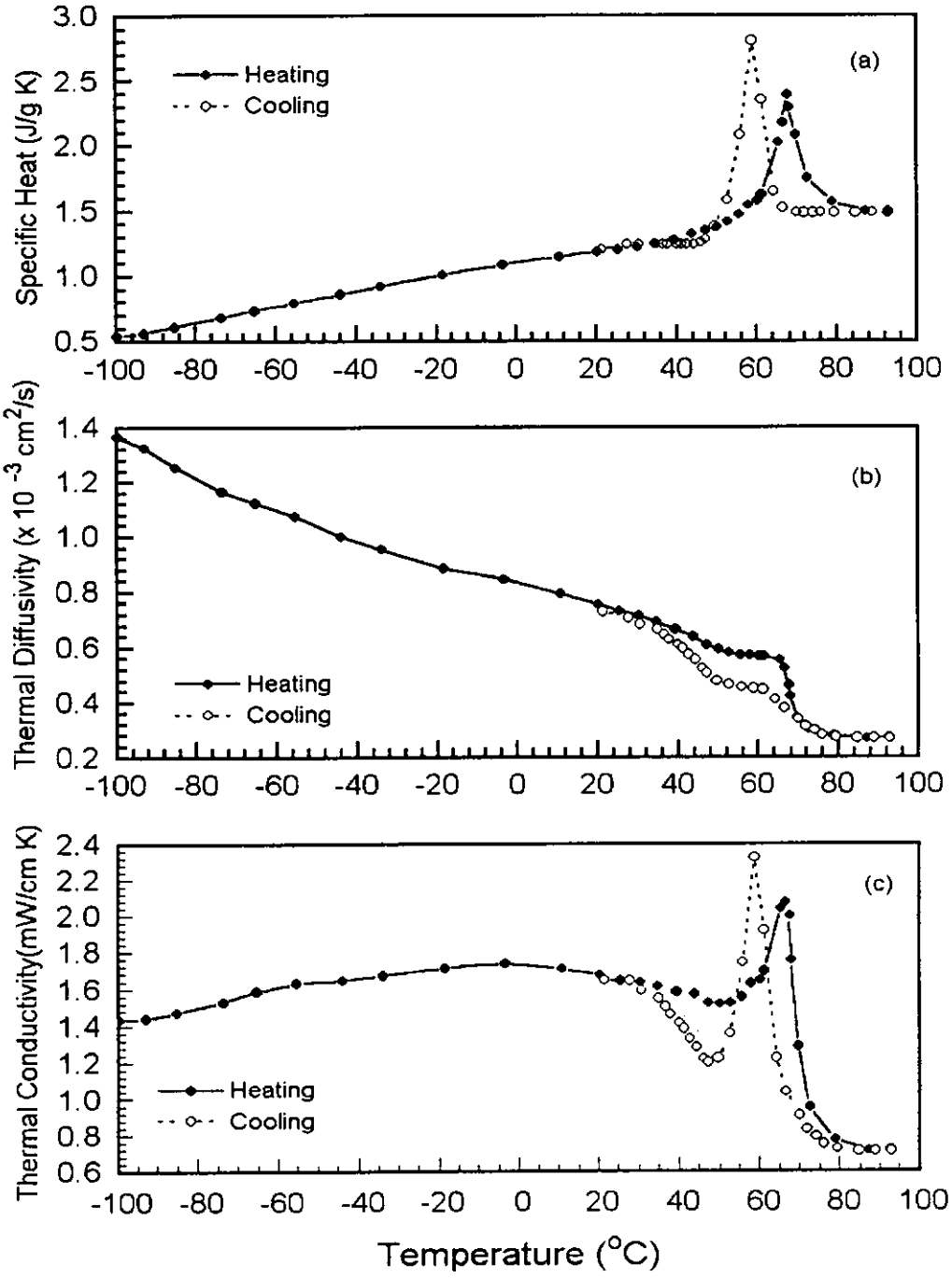

Figure 3.12 **Temperature dependence of the (a) specific heat, (b) thermal diffusivity and (c) thermal conductivity of quenched P(VDF/TrFE) 56/44 copolymer against temperature upon heating and cooling runs.**

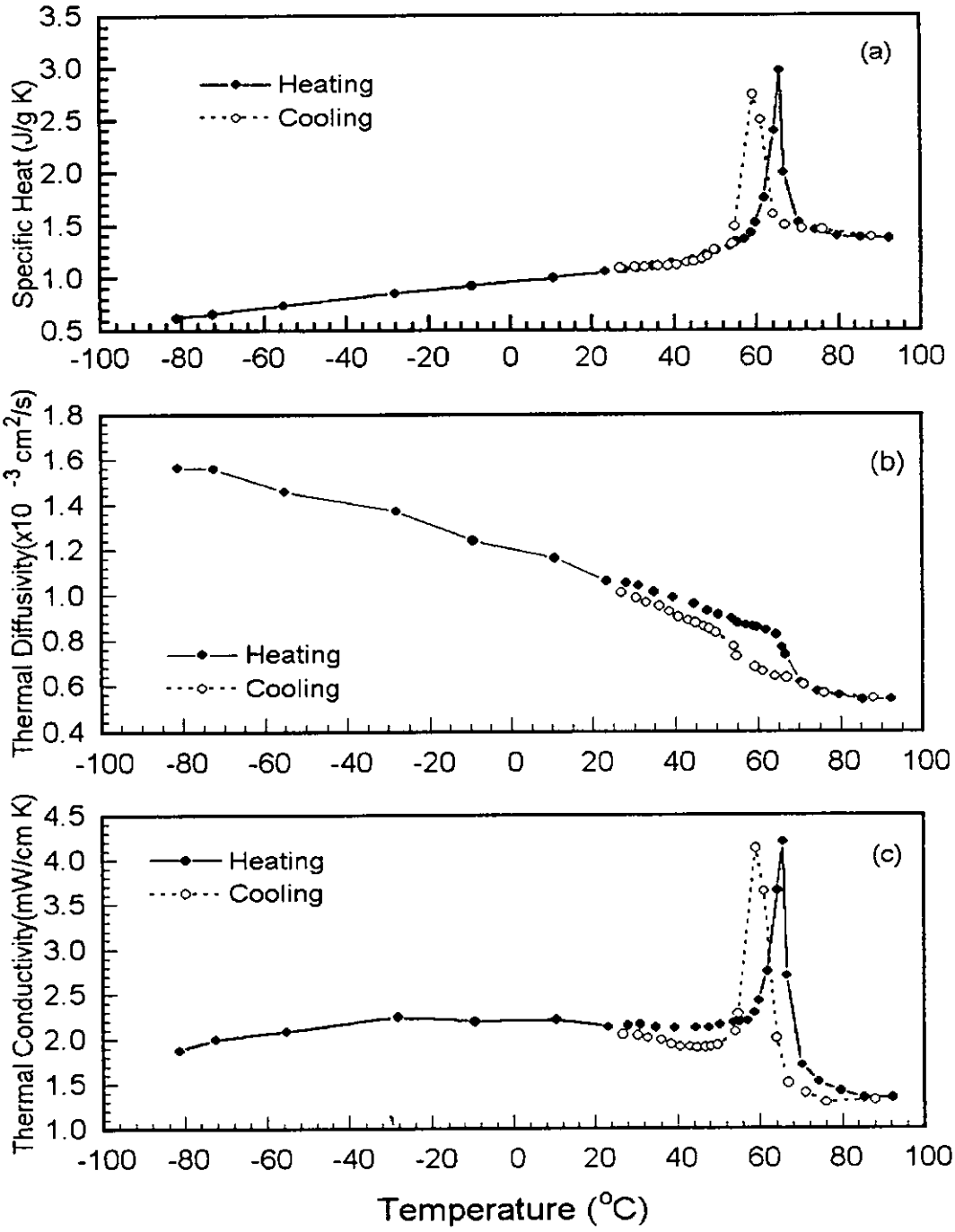

Figure 3.13 Temperature dependence of the (a) specific heat, (b) thermal diffusivity and (c) thermal conductivity of slow-cooled P(VDF/TrFE) 56/44 copolymer against temperature upon heating and cooling runs.

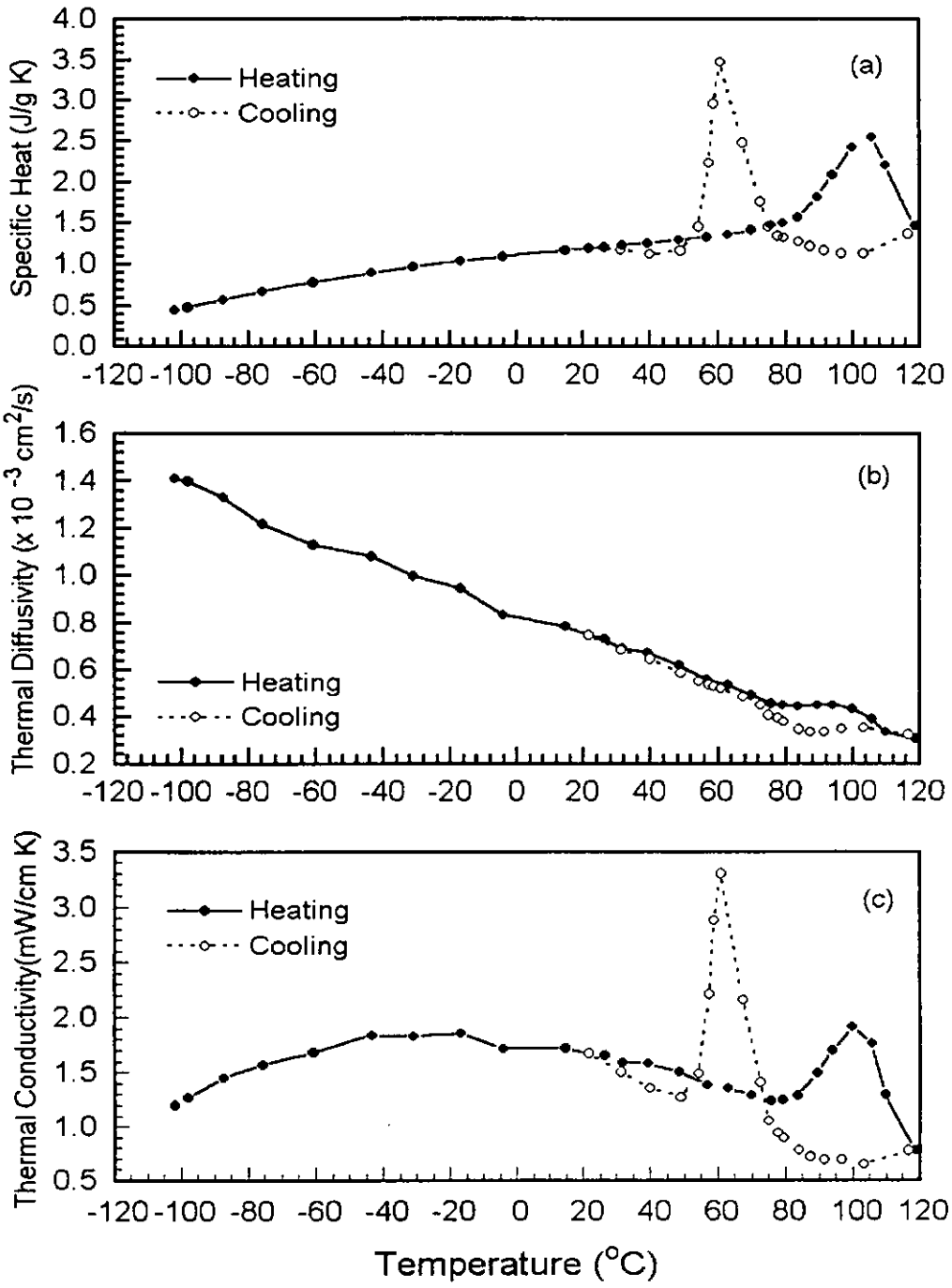

Figure 3.14 **Temperature dependence of the (a) specific heat, (b) thermal diffusivity and (c) thermal conductivity of quenched P(VDF/TrFE) 70/30 copolymer against temperature upon heating and cooling runs.**

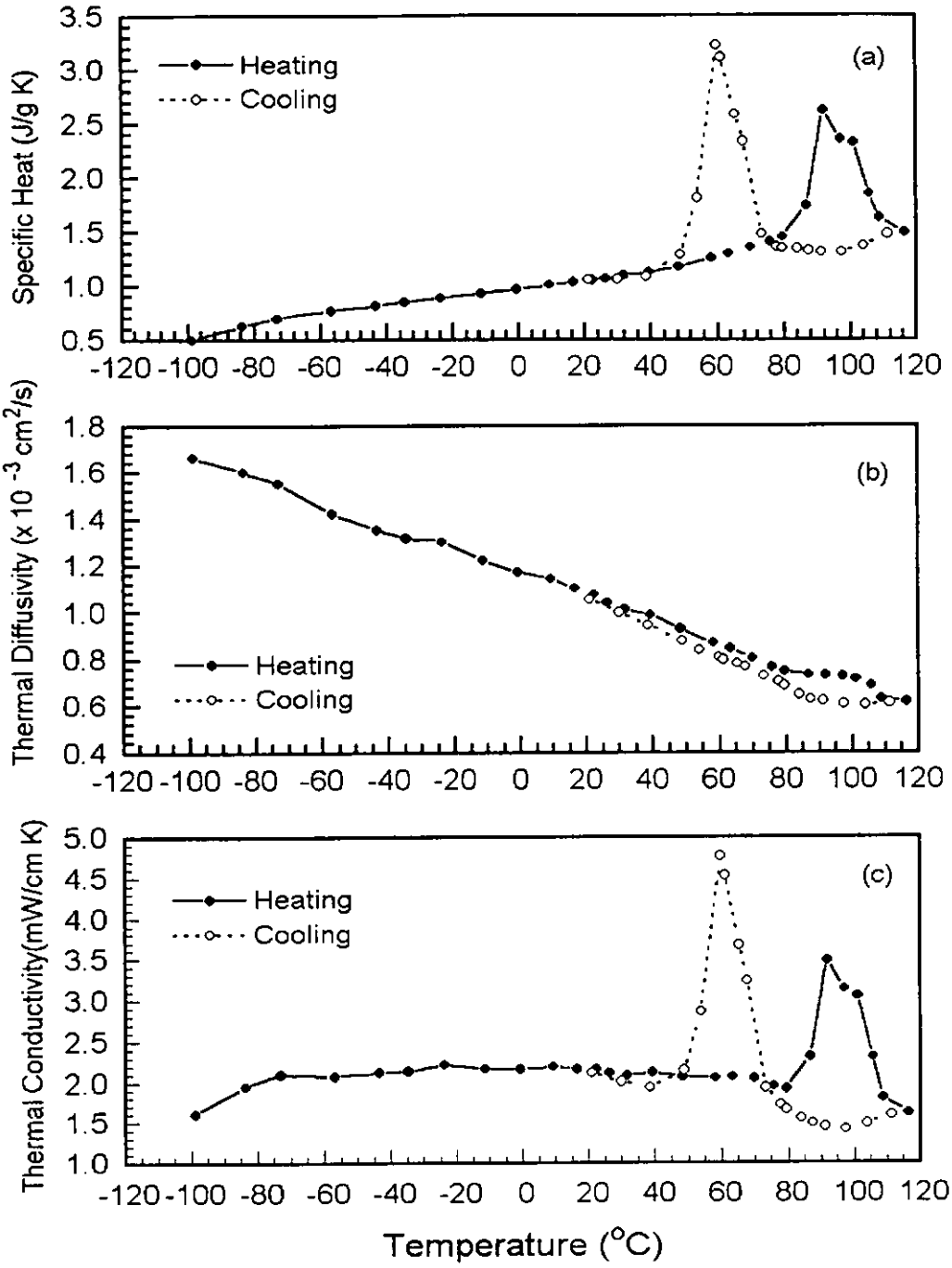

Figure 3.15 **Temperature dependence of the (a) specific heat, (b) thermal diffusivity and (c) thermal conductivity of slow-cooled P(VDF/TrFE) 70/30 copolymer against temperature upon heating and cooling runs.**

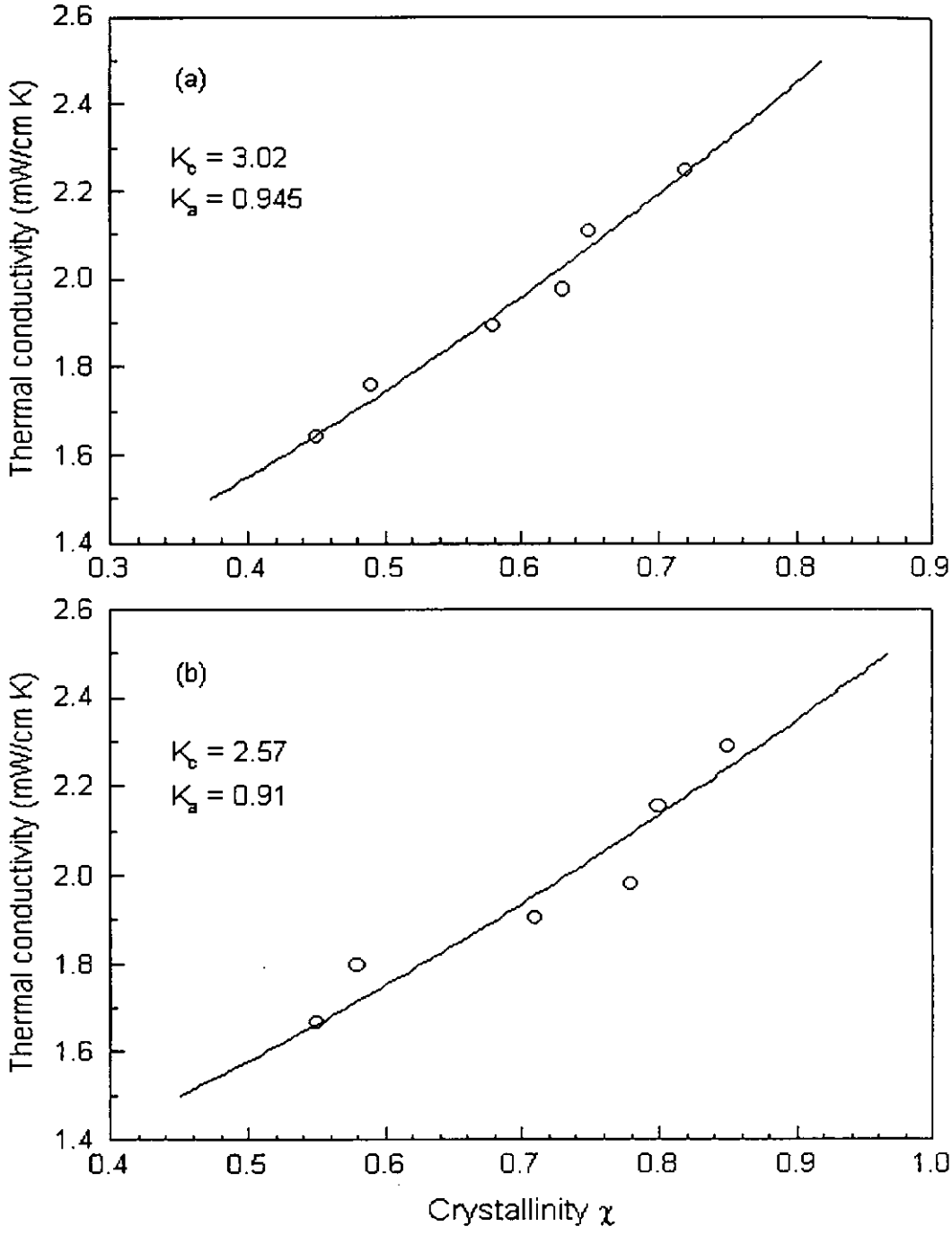

Figure 3.16 **Crystallinity dependence of the thermal conductivity measured at room temperature for (a) P(VDF/TrFE) 56/44 and (b) P(VDF/TrFE) 70/30 copolymer samples. K_c: average thermal conductivity of crystal, K_a: thermal conductivity of amorphous matrix.**

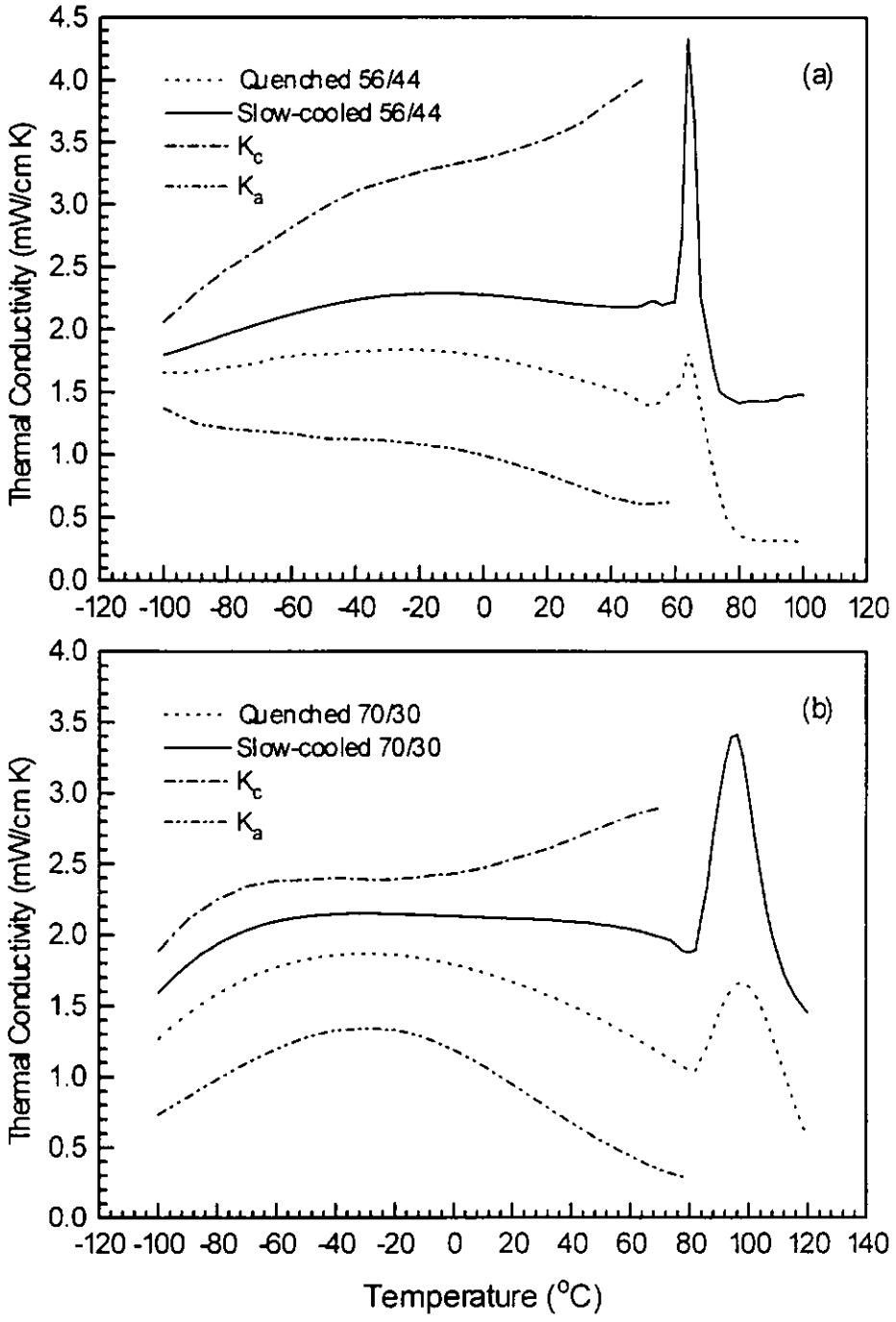

Figure 3.17 **Temperature dependence of the thermal conductivity measured for (a) P(VDF/TrFE) 56/44 and (b) P(VDF/TrFE) 70/30 copolymer samples. K_c: average thermal conductivity of crystal, K_a: thermal conductivity of amorphous matrix.**

The temperature dependence of the thermal conductivities depicted in Figures 3.12 (c), 3.13 (c), 3.14 (c) and 3.15 (c) all show a very sharp rise at the Curie transition both upon heating and cooling. This is largely due to the sharp rise in specific heat of the samples at phase transition (c.f. Figures 3.12 (a), 3.13 (a), 3.14 (a) and 3.15 (a)) because of equation 3.9.

Furthermore, the thermal conductivities at low temperature show a maximum at around -40 °C which is associated with glass transition of the semi-crystalline copolymers.

When comparing the thermal conductivities between the slow-cooled and quenched samples of both 56/44 and 70/30, one common feature is that as the temperature increases the difference of the conductivities becomes larger. For 56/44 at around –100 °C, the ratio of the conductivities of the slow-cooled to quenched samples is about 1.5. This ratio increases to 1.7 at 0 °C and becomes 3.1 at the phase transition temperature of 65 °C. The ratio is 6 at 90 °C. For 70/30 the corresponding ratios are 1.4 (-100 °C), 1.4 (0 °C), 2.3 (95 °C) and 2.9 (110 °C). The crystallinity ratio of the two 56/44 samples is 1.4 and is roughly the same for 70/30. From Figure 3.15, it can be seen that the conductivities of the slow-cooled samples do not have a larger temperature dependence; in other words, the quenched samples have a larger temperature dependence as revealed from the conductivity ratios at different temperatures. In addition, the conductivity of the quenched sample drops faster than the slow-cooled sample as the temperature increases. This may indicate that the

conductivity of the copolymer is mostly dominated by the amorphous region in the polymer. Thus, it is interesting to investigate the conductivity of the crystalline and amorphous phases of this copolymer.

The thermal conductivity of a two-phase system can be calculated by the Bruggeman model. It is assumed that the spherical crystalline particles of average conductivity K_c are dispersed in an amorphous matrix of conductivity K_a. If the volume fraction of the crystals is χ, then the bulk material's conductivity K_i can be related to the conductivities of the individual phases by the following equation:

$$\frac{K_c - K_i}{K_i^{1/3}} = (1-\chi)\frac{K_c - K_a}{K_a^{1/3}} \tag{3.10}$$

By fitting the crystallinities and the conductivity results of the slow-cooled and quenched samples to equation 3.10, the amorphous phase K_a and the crystallite K_c can be obtained. Figure 3.16 (a) depicts the room temperature conductivities of 56/44 as a function of crystallinity with a fitted curve based on the Bruggeman model. The K_c and K_a obtained are 3.02 mW/cmK and 0.95 mW/cmK respectively. The corresponding fitting for 70/30 is shown in Figure 3.16 (b) and the K_c and K_a obtained are 2.57 mW/cmK and 0.91 mW/cmK respectively. The temperature dependences of K_a and K_c of 56/44 and 70/30 are shown in Figures 3.17 (a) and 3.17 (b), respectively. In Figure 3.17 (a), it can be seen that the K_a of 56/44 decreases gradually from –100 °C to 90 °C while in Figure 3.17 (b), the K_a of 70/30 shows an obvious maximum at around –30 °C. For the 75/25 copolymer, the glass transition temperature T_g is –36 °C

and for 50/50, T_g is –28 °C [Teussedre, 1995]. It seems that the maximum conductivity at –30 °C of the 70/30 sample reveals the change of K_a at glass transition and then K_a decreases as the temperature increases further toward the Curie temperature. For the 56/44 sample, there is only a very slight change of K_a at around is –30 °C. In both figures, K_a shows another maximum at the Curie phase transition. It may not be real since the ferroelectric phase change could only occur at the crystalline phase. In other words, the model is not accurate in that region which involves change in crystal structure. The K_c obtained from the Bruggeman model show positive temperature dependence, i.e. the higher the temperature, the greater the average K_c of the spherical particles. The 56/44 copolymer has a greater slope of K_c against temperature. At around phase transition, the Bruggeman model is not applicable, so that the calculation of the K_c and K_a are below the phase transition temperature only.

CHAPTER 4

MECHANICAL PROPERTIES

The elastic properties of copolymers are influenced strongly by their molecular structure, and therefore the measurement of such properties is useful for further understanding of the copolymers. The Young's, shear and bulk moduli are the most representative parameters that can be used to illucidate the mechanical properties of the copolymer samples. These three parameters can be calculated from the elastic stiffness constants. One of the best ways to determine the stiffness constants of small samples is by the ultrasonic immersion method. Their temperature dependence can be easily measured by controlling the temperature of the immersion fluid.

4.1 ULTRASONIC METHODOLOGY

In an unbounded isotropic solid, two types of ultrasonic waves can be propagated. In the first type, the particles in the solid vibrate along the direction of propagation. This is called the longitudinal wave. In the second type, the particle motion is perpendicular to the direction of propagation. This is called the shear wave.

The velocities of the two types of ultrasonic waves are associated with the solid's stiffness and density, thus the elastic properties of the material can be deduced from measurements of the ultrasonic wave velocities. To study the propagation of ultrasonic waves in a solid, the solid sample is usually immersed in an oil bath and the ultrasonic wave from an ultrasound generator can be coupled to the sample through the oil medium and the emergent wave from the sample coupled again through the oil to the receiver. The oil bath can be temperature controlled so that the temperature dependence of the longitudinal and shear wave velocities in the sample can be measured.

4.1.1 Stiffness Constants and Ultrasonic Velocities

When an external stress σ is applied to a solid sample within the elastic range, the corresponding strain ε can be related to the stress by Hook's law

$$\sigma_{ij} = c_{ijkl}\varepsilon_{kl}$$

where σ_{ij}, ε_{kl} are the stress and strain components respectively in a Cartesian coordinate system and $c_{ijkl} = c_{klij}$ are the corresponding stiffness constants.

For simplicity, we adopt a more convenient designation for the subscripts which replaces two indices by one and four indices by two. The scheme of replacement is given below:

Full indices	11	22	33	23 or 32	31 or 13	12 or 2
Reduced indices	1	2	3	4	5	6

The stress-strain relation can be rewritten neatly with contracted symbols as

$$\sigma_p = c_{pq}\varepsilon_q \qquad (4.1)$$

where $p, q = 1 - 6$, with $c_{pq} = c_{qp}$.

Or it can be written in a matrix form

$$\begin{bmatrix}\sigma_1\\ \sigma_2\\ \sigma_3\\ \sigma_4\\ \sigma_5\\ \sigma_6\end{bmatrix} = \begin{bmatrix}c_{11} & c_{12} & c_{13} & c_{14} & c_{15} & c_{16}\\ c_{21} & c_{22} & c_{23} & c_{24} & c_{25} & c_{26}\\ c_{31} & c_{32} & c_{33} & c_{34} & c_{35} & c_{36}\\ c_{41} & c_{42} & c_{43} & c_{44} & c_{45} & c_{46}\\ c_{51} & c_{52} & c_{53} & c_{54} & c_{55} & c_{56}\\ c_{61} & c_{62} & c_{63} & c_{64} & c_{65} & c_{66}\end{bmatrix}\begin{bmatrix}\varepsilon_1\\ \varepsilon_2\\ \varepsilon_3\\ \varepsilon_4\\ \varepsilon_5\\ \varepsilon_6\end{bmatrix} \quad (4.2)$$

For an orthotropic material with symmetry axes along the 1, 2 and 3 directions (see Figure 4.1), there are only nine independent stiffness constants and the rest are zeros:

c_{11}, c_{22}, c_{33}, $c_{12} = c_{21}$, $c_{13} = c_{31}$, $c_{23} = c_{23}$, c_{44}, c_{55}, c_{66}.

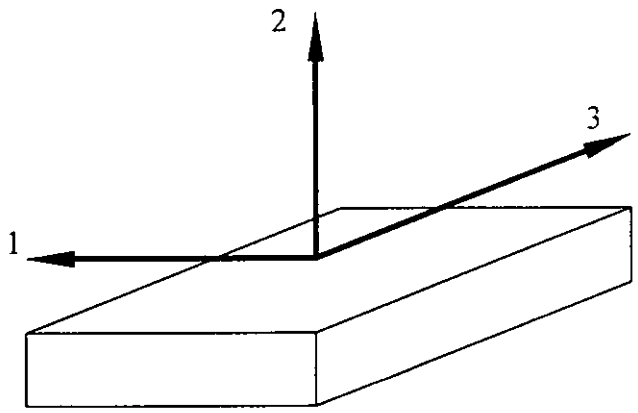

Figure 4.1 Cartesian coordinate system for a film with orthotropic symmetry.

For materials that have uniaxial symmetry about the 3-axis, there are only five independent stiffness constants:

$$c_{pq} = \begin{bmatrix} c_{11} & c_{12} & c_{13} & 0 & 0 & 0 \\ c_{12} & c_{11} & c_{13} & 0 & 0 & 0 \\ c_{13} & c_{13} & c_{33} & 0 & 0 & 0 \\ 0 & 0 & 0 & c_{44} & 0 & 0 \\ 0 & 0 & 0 & 0 & c_{55} & 0 \\ 0 & 0 & 0 & 0 & 0 & c_{66} \end{bmatrix} \qquad (4.3)$$

with $c_{12} = c_{11} - 2c_{66}$ and $c_{55} = c_{44}$.

Eventually an isotropic material needs only two independent stiffness constants to specify its elastic properties, they are e.g. c_{11} and c_{66}. For the two types of elastic waves propagating through an isotropic material, their velocities are related to the stiffness by the following equations:

$$c_{11} = \rho v_{11}^2 , \qquad c_{66} = \rho v_{66}^2 \qquad (4.4)$$

where ρ is the density, v_{11} and v_{66} are the longitudinal wave and shear wave velocities respectively.

4.1.2 Ultrasonic Velocity Measurement

The velocities of ultrasonic waves traveling in a specimen may be measured using the immersion method. The schematic setup is shown in Figure 4.2. A pair of 10 MHz transducers of 10 mm diameter were mounted in a stainless steel frame. The distance of transducers is 3.14 cm apart. The sample intervening the ultrasonic beam can also be rotated so that the angle of incidence of the beam can be varied. The whole setup is immersed in a silicon oil bath, 30 by 24 cm, 10 cm depth, with temperature controlled to an accuracy of $\pm$ 0.5°C. The silicon oil was supplied by Rhone-Poulenc of France company.

The block diagram depicted in Figure 4.3 shows the experimental arrangement. Ultrasonic pulses are generated by the pulse generator / analyser P and sent to the transmitter T1. The signal of the pulses that propagate through the sample and received by T2 is amplified by P before sending to the digital oscilloscope DSO for display. The transit time of a pulse can then be determined from the DSO trace.

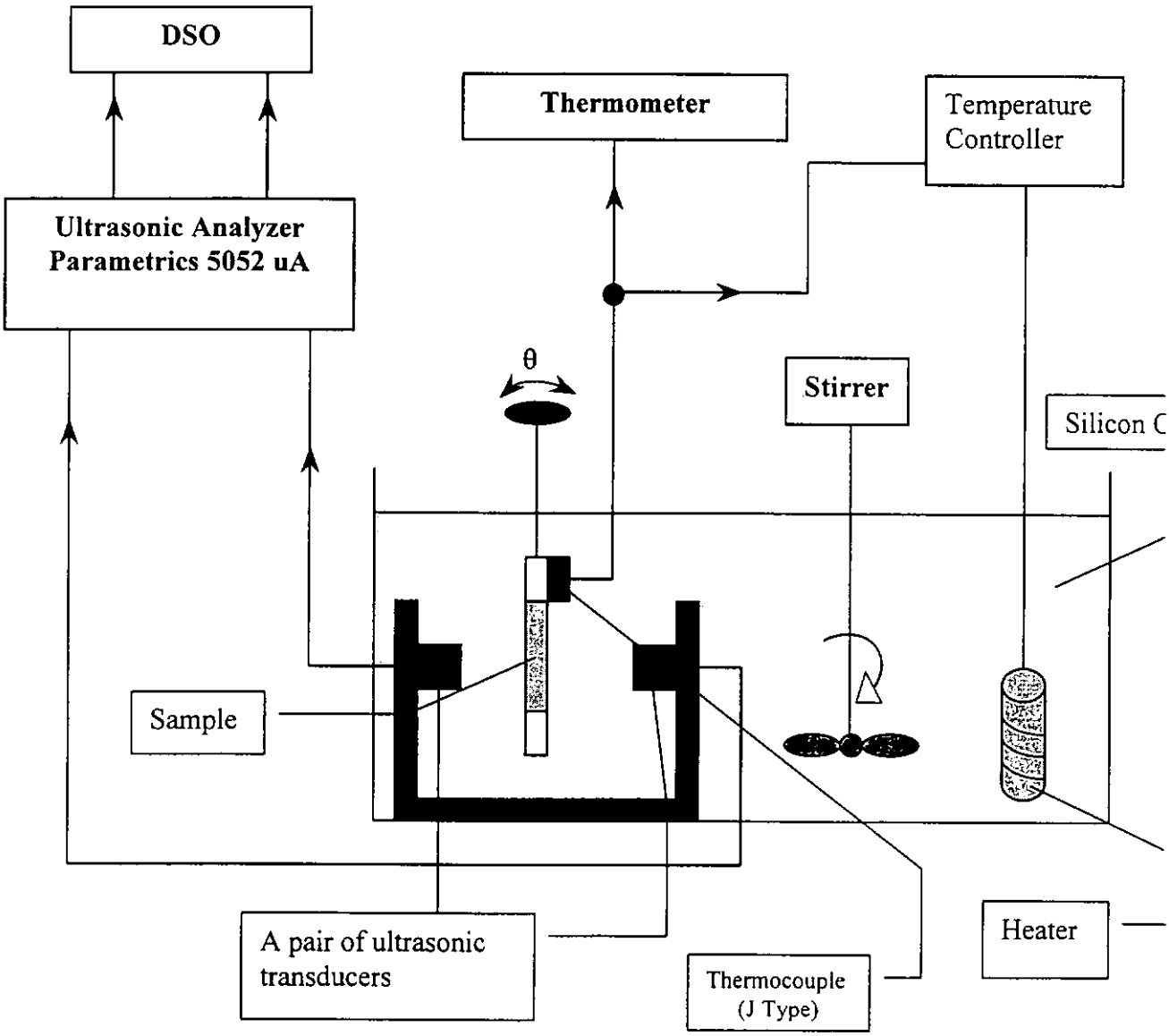

Figure 4.2 Immersion apparatus.

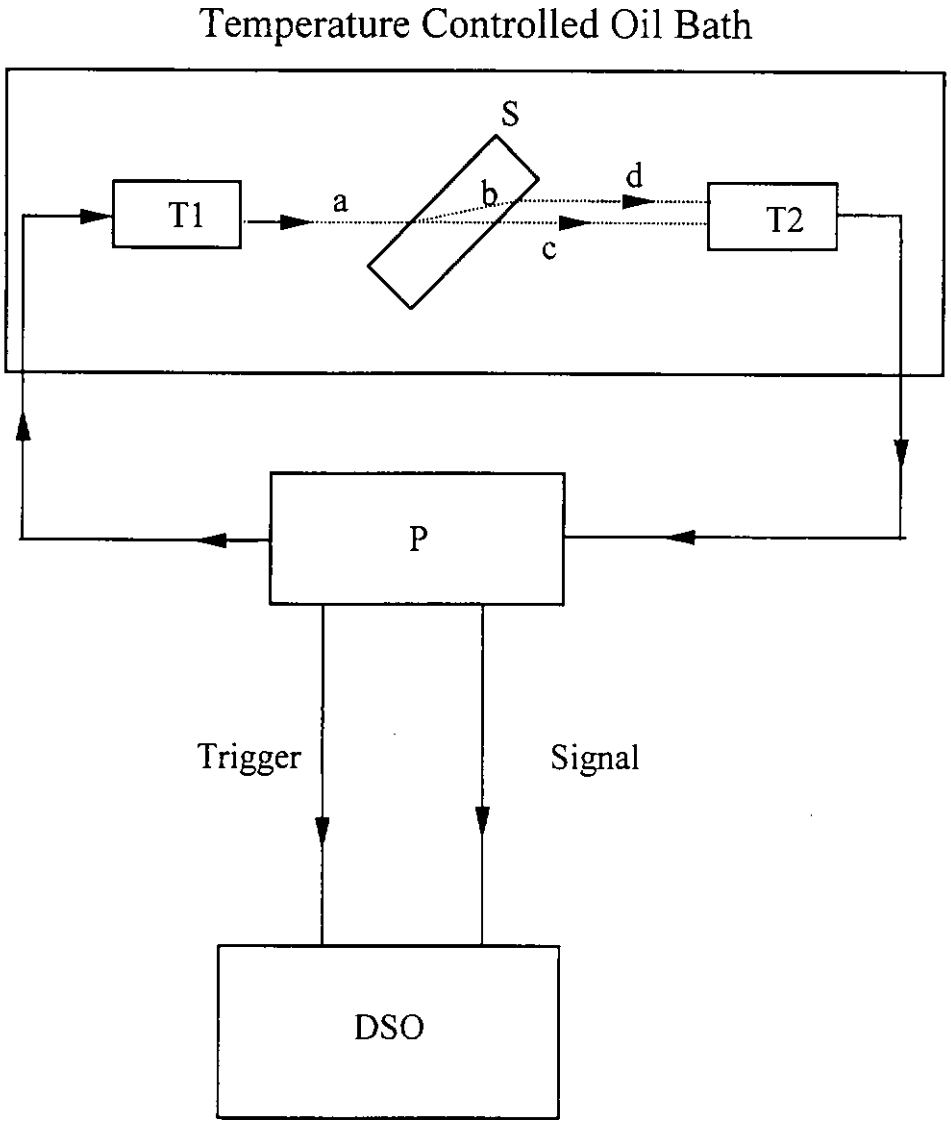

Figure 4.3 **Schematic representation of the ultrasonic method. S is the sample. The ultrasonic beam follows the path a, b, d when S is present; it follows a, c when S is not in place.**

At any off-normal incidence, both the shear and longitudinal waves are generated. They overlap with each other and are difficult to distinguish. However, if the wave velocity in oil is smaller than in the solid sample, there is a critical angle beyond which an internal total reflection of the longitudinal wave occurs and only the shear wave is received at T2. Therefore, the transit time of both the longitudinal wave and shear wave in the sample can be measured.

4.1.3 Determination of Wave Velocities

With the sample inserted between the transducers, the detected pulse is displayed on the oscilloscope and the position of the first pulse peak is noted. The sample is then removed from the path of the ultrasonic beam. Since the speed in the immersion liquid is less than the speed in the copolymer, the signal will take a longer time to reach the receiver; the difference in transmit times, Δt, is then determined. For a sample of thickness L placed perpendicularly to the beam, the transit time is L/v_r, where v_r is the wave speed in the sample. The transit time in the liquid layer of equal thickness is L/v_{liq}, where v_{liq} is the speed in the liquid. Therefore,

$$\Delta t = L/v_{liq} - L/v_r \qquad (4.5)$$

When the incident beam makes an angle ψ with the sample, it follows from Snell's law that

$$\sin\psi / v_{liq} = \sin\theta_r / v_r \qquad (4.6)$$

where θ_r is the angle of refraction of the longitudinal or shear wave. Figure 4.4 shows the propagation path of the ultrasonic wave at an incidence angle ψ.

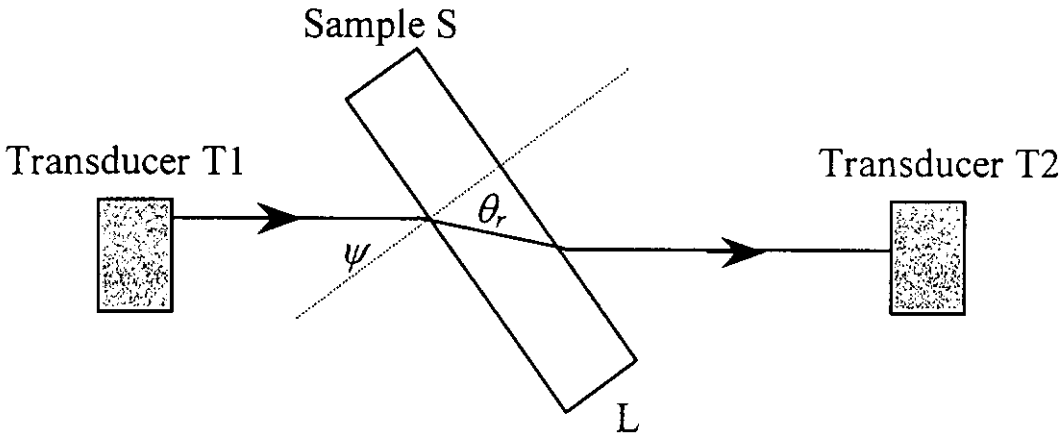

Figure 4.4 The propagation path of the ultrasonic wave.

The difference in transit times Δt_r can be obtained from the following equation:

$$\Delta t_r = \frac{L}{\cos\theta_r}\left[\frac{\cos(\theta_r - \psi)}{v_{liq}} - \frac{1}{v_r}\right] \tag{4.7}$$

It follows that

$$v_r = \frac{v_{liq}}{\sin\psi}\sin\left[\tan^{-1}\frac{L\sin\psi}{L\cos\psi - \Delta t_r v_{liq}}\right] \tag{4.8}$$

Thus the velocity of the wave in the sample can be calculated from the above equation. A detail derivation of the above equation is shown in Appendix E.

A typical example of an ultrasonic pulse propagated through the copolymer 56/44 sample is shown in the following figure. At normal incidence, only the longitudinal wave is observed (Figure 4.5 (a)). The velocity v_{11} of the longitudinal wave is obtained from Δt via equation 4.5. As the incident angle increases to about 50°, the shear wave emerged as shown in Figure 4.5 (b). The velocity v_{66} of the shear wave is calculated from knowledge of Δt_r via equation 4.8.

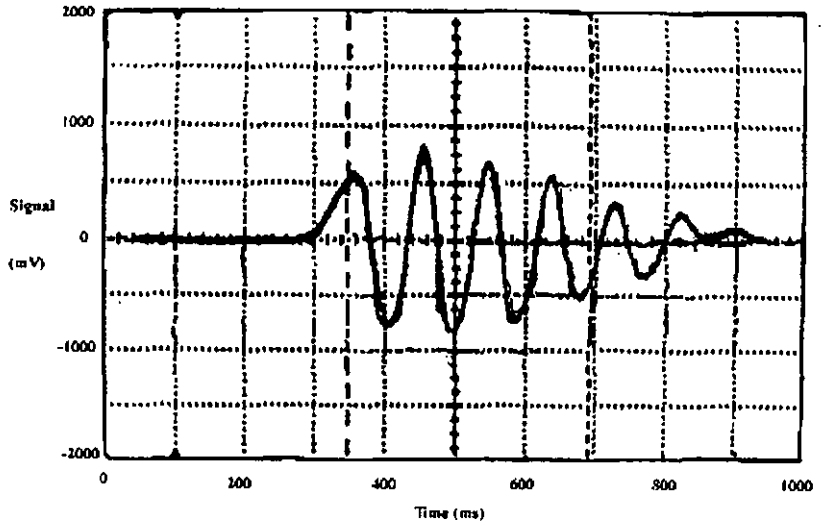

(a)

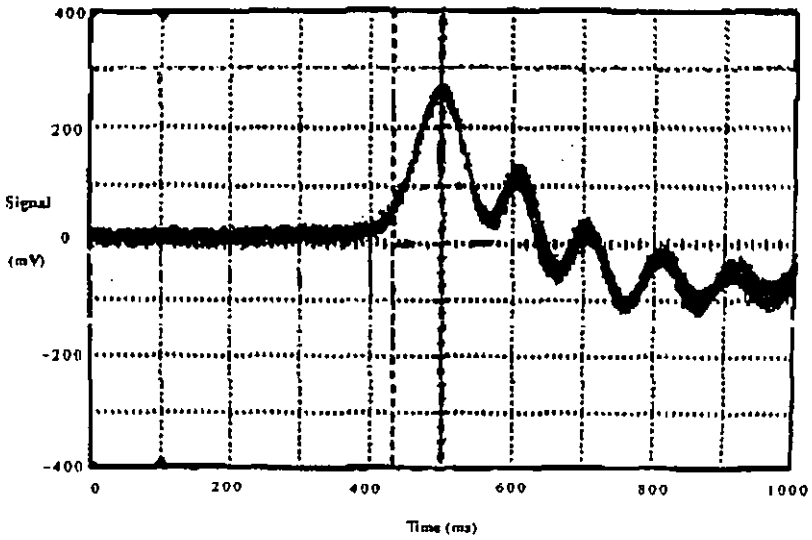

(b)

Figure 4.5 **Signal recorded at detector when the incident ultrasonic beam impinges on the sample surface (a) at normal incidence and (b) at 50^{o} off the normal. The longitudinal wave is observed in (a), the shear wave in (b).**

4.1.4. Calculation of Elastic Properties

Provided that the density is known, the stiffness constants c_{11} and c_{66} can now be obtained from equation 4.4. Eventually, the Young's modulus (E), bulk modulus (B) and Poisson's ratio (υ) of the samples can be calculated according to the following equations:

$$E = c_{66}(3c_{11} - 4c_{66})/(c_{11} - c_{66}) \tag{4.9}$$

$$B = c_{11} - \frac{4}{3}c_{66} \tag{4.10}$$

$$\upsilon = \frac{E}{2c_{66}} - 1 \tag{4.11}$$

4.2 RESULTS AND DISCUSSION

Since the ferroelectric to paraelectric transition in the copolymers is the result of the crystal structure change, it is expected that the elastic properties of the copolymers would change at the phase transition. The temperature dependence of the ultrasonic velocities of the longitudinal and shear waves measured for the quenched 56/44 copolymer samples show an anomalous behavior near the ferroelectric transition temperature (~ 60 °C) as depicted in Figure 4.6. Elastic moduli such as longitudinal (c_{11}) and shear (c_{66}) moduli are shown in Figure 4.7, and the bulk and Young's moduli are shown in Figure 4.8. Since these moduli are deduced from the ultrasonic velocities, they all show very similar features. As the temperature reaches the transition range, the velocities as well as the moduli drop abruptly and then only gradually as the temperature increases further. In the cooling measurements, the thermal hysteresis effect make the sample velocities as well as the moduli smaller than the values obtained at the transition temperature range in the heating measurements.

For slow-cooled 56/44 sample, the corresponding velocities and moduli are shown in Figures 4.9, 4.10 and 4.11. As expected, slow-cooled 56/44 is similar to the quenched counter part.

For the 70/30 copolymer, the velocities and moduli of the quenched samples are shown in Figures 4.12, 4.13 and 4.14. The corresponding results of the slow-cooled samples are given in Figures 4.15, 4.16 and 4.17. The 70/30 copolymer

shows a more prominent thermal hysteresis as compared with the 56/44 copolymer and is consistent with the results observed in thermal conductivities.

In addition, the higher crystallinity of the slow-cooled samples gives rise to higher elastic moduli as the moduli of the crystallites are expected to be higher than those of the amorphous phase. The degree of thermal hysteresis increases with VDF content as observed by the ultrasonic measurement, such an observation was made also by Kruger et al. [Kruger et al., 1986]. The anomalous behavior of the ultrasonic velocity is not limited to the 56 and 70 mol% VDF samples, but is found to occur in the structural transition region for copolymer samples of other mole fractions of VDF, although the degree of drastic change in ultrasonic velocity becomes less as the VDF content decreases. Thermal hystersis occurs over a large temperature range and is determined by the transition temperature of the crystallites. Nevertheless, plots of the Young's moduli of 56/44 and 70/30 versus the crystallinity as shown in Figures 4.18 (a) and 4.18 (b) respectively reveal the fact that the mechanical properties of the copolymers are enhanced by the presence of the crystalline phase. It is a common feature for most of the semicrystalline polymers. On the other hand, the polymer will become more brittle as crystallinity increases. Brittleness might be a limiting factor if applications as an actuator/sensor material are conceived.

The calculated Poisson's ratios are tabulated in Appendix D. The results show typical values of semicrystalline polymers. As the temperature increases, the Poisson ratio approaches 0.5 which indicates that all the samples become rubber-like at high temperature.

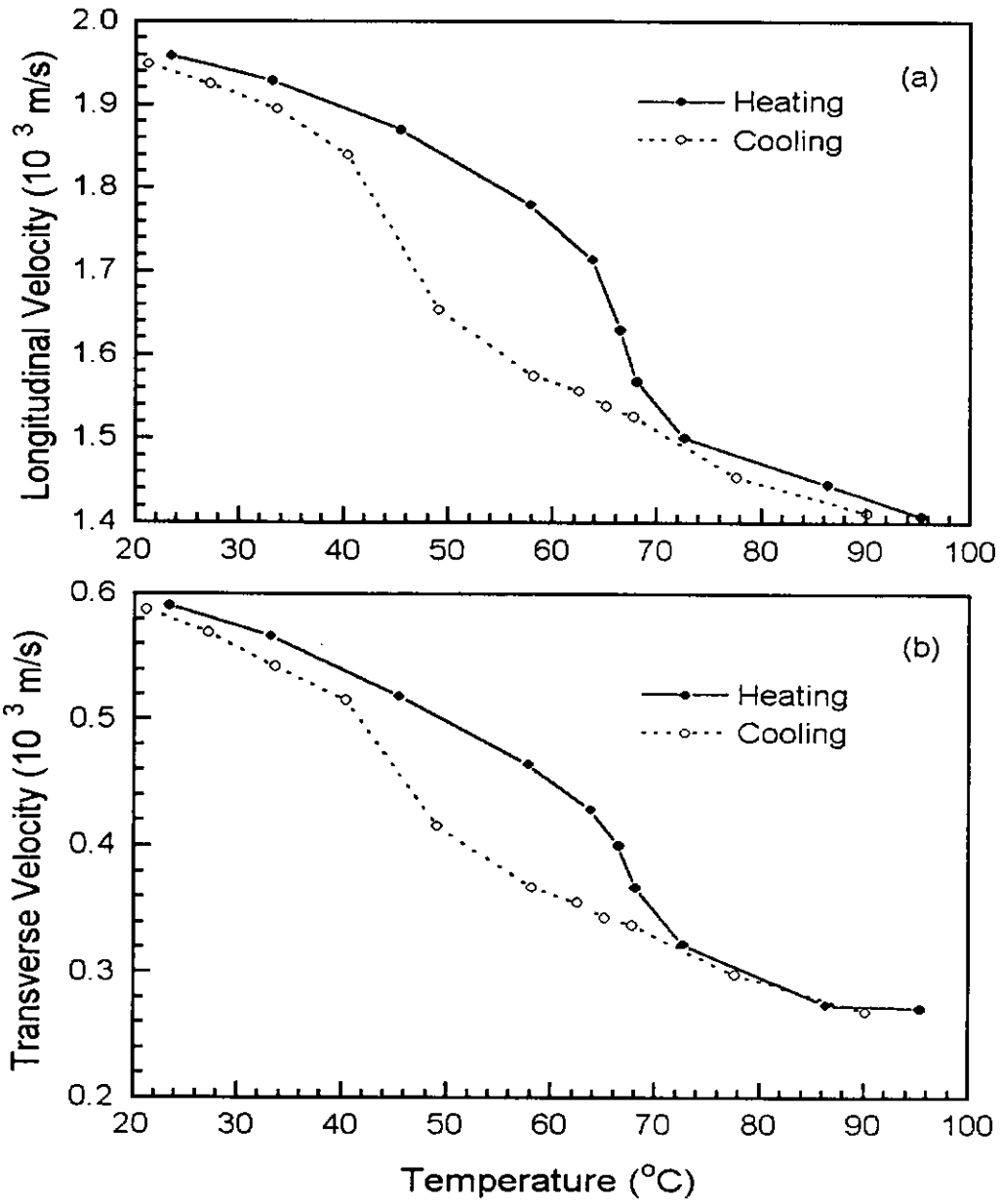

Figure 4.6 **Temperature dependence of the (a) longitudinal velocity and (b) transverse velocity of the quenched 56/44 copolymer in heating and cooling measurements.**

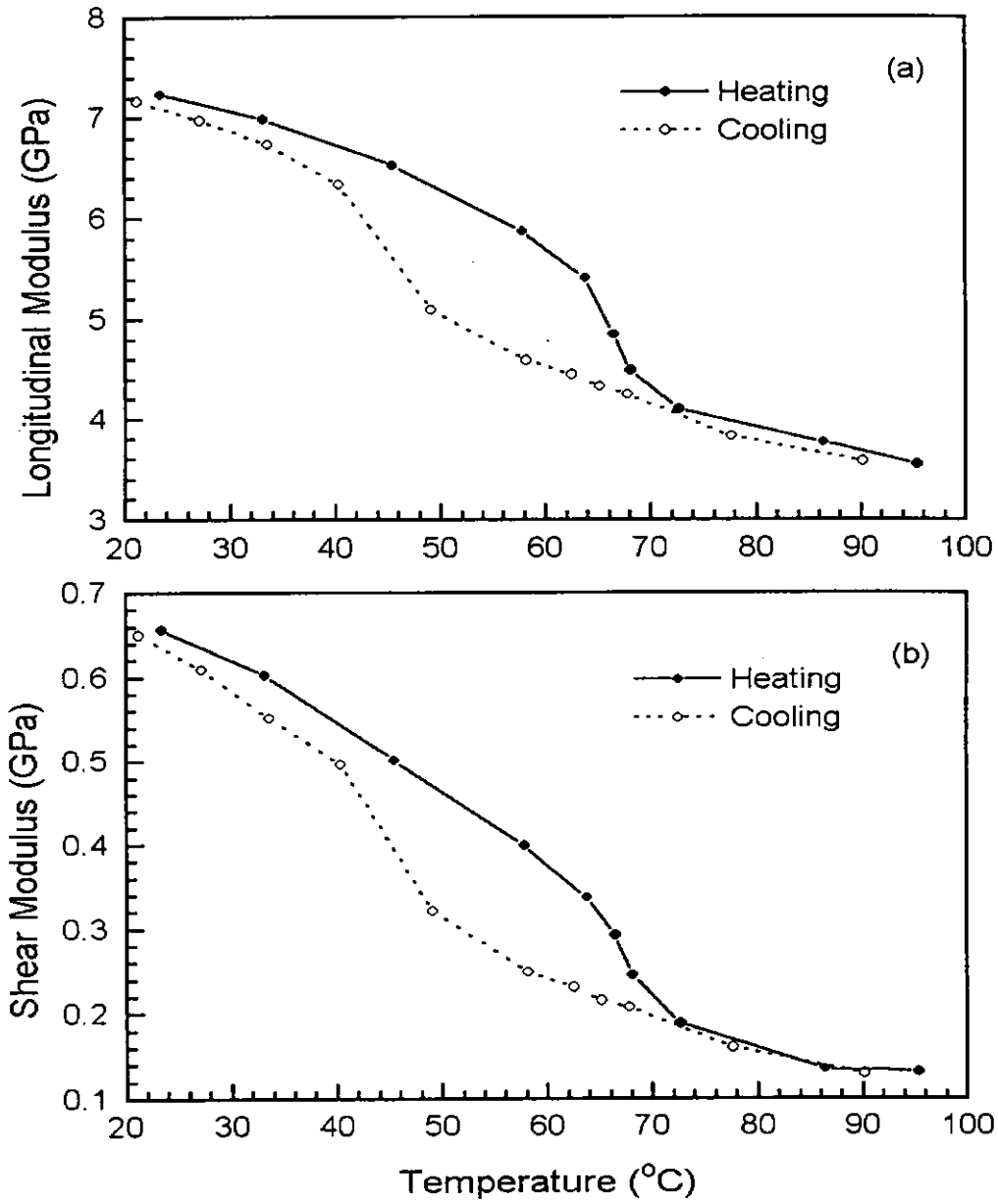

Figure 4.7 **Temperature dependence of the (a) longitudinal modulus (c_{11}) and (b) shear modulus (c_{66}) of the quenched 56/44 copolymer in heating and cooling measurements.**

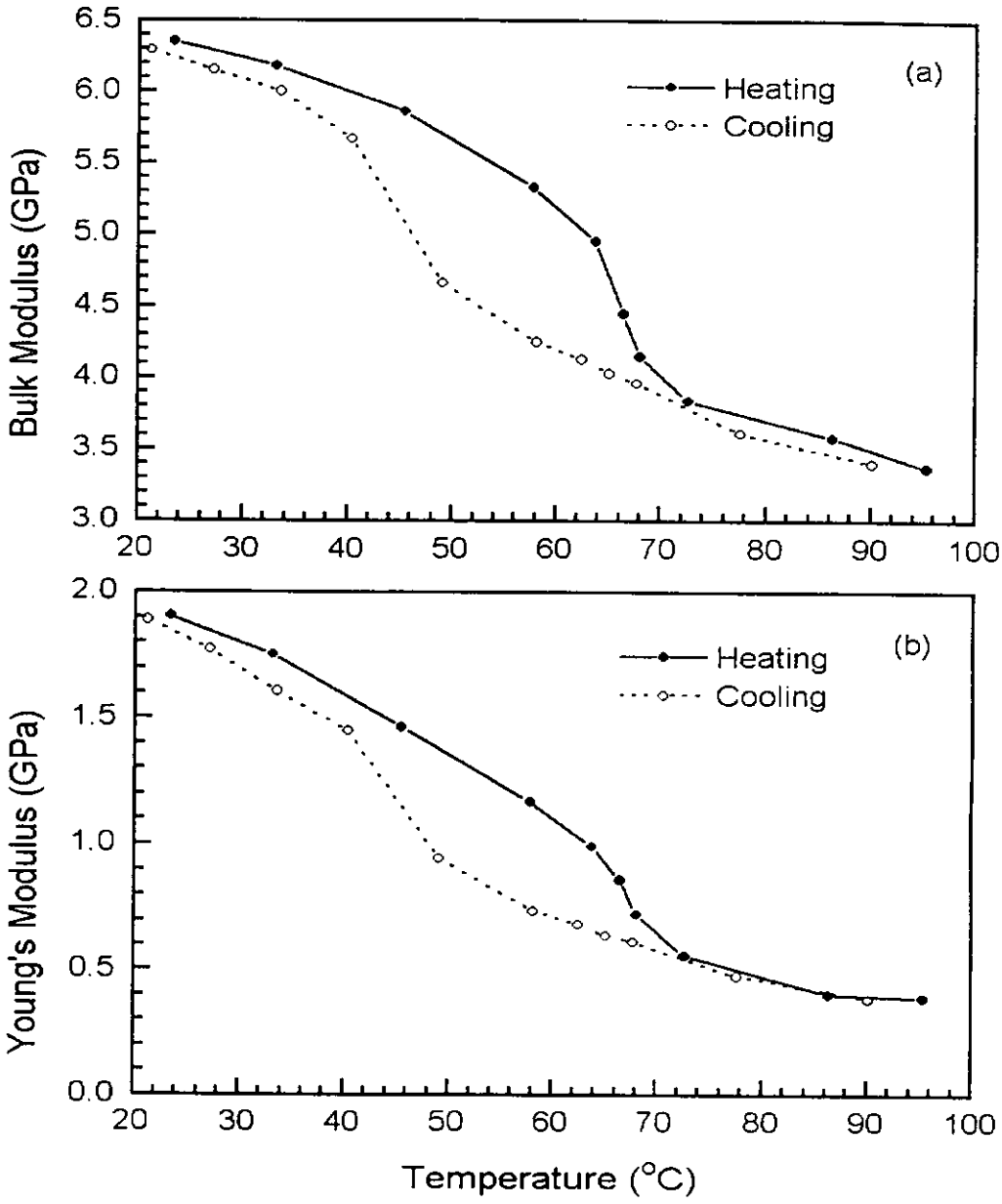

Figure 4.8 **Temperature dependence of the (a) bulk modulus and (b) Young's modulus of the quenched 56/44 copolymer in heating and cooling measurements.**

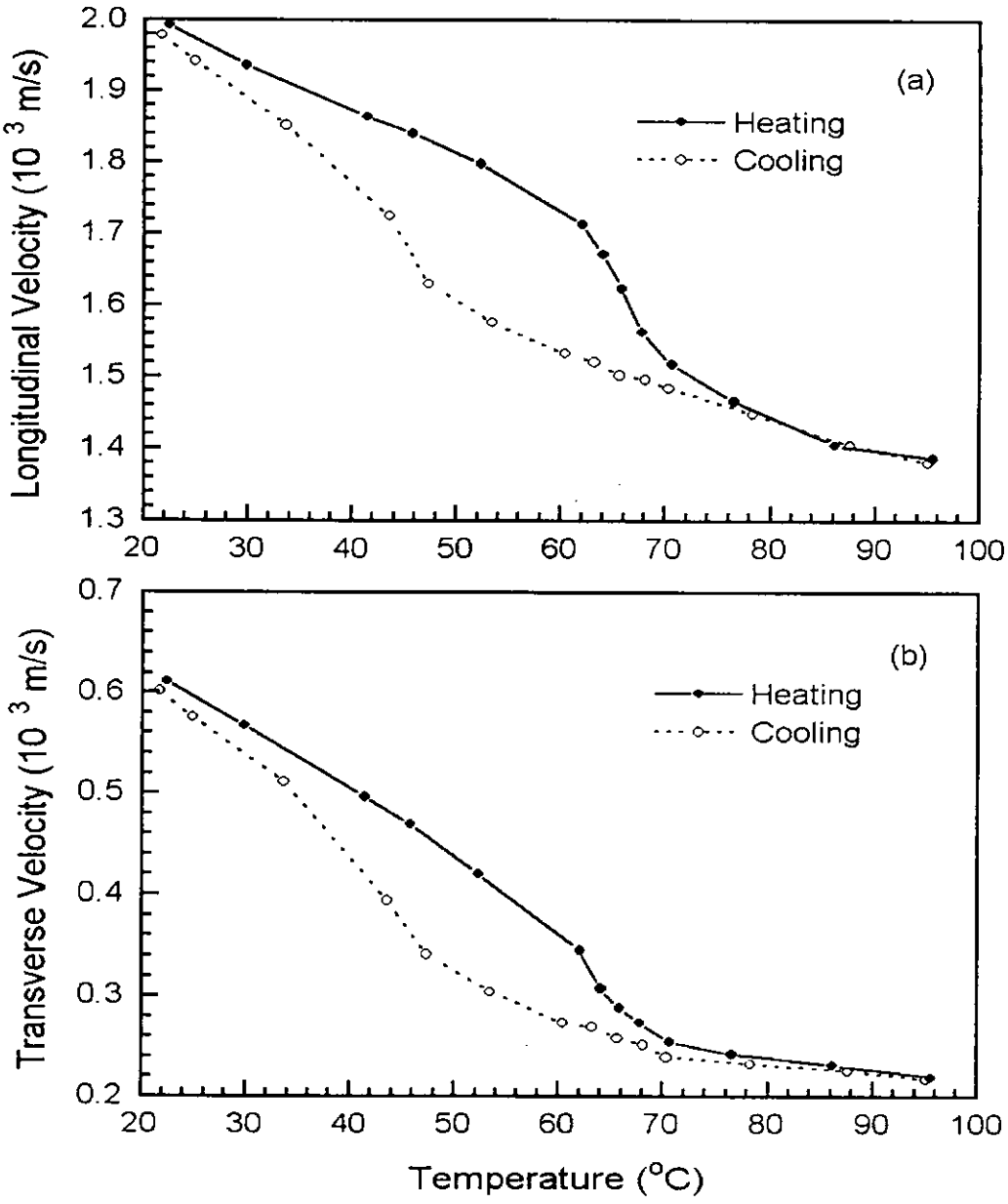

Figure 4.9 **Temperature dependence of the (a) longitudinal velocity and (b) transverse velocity of the slow-cooled 56/44 copolymer in heating and cooling measurements.**

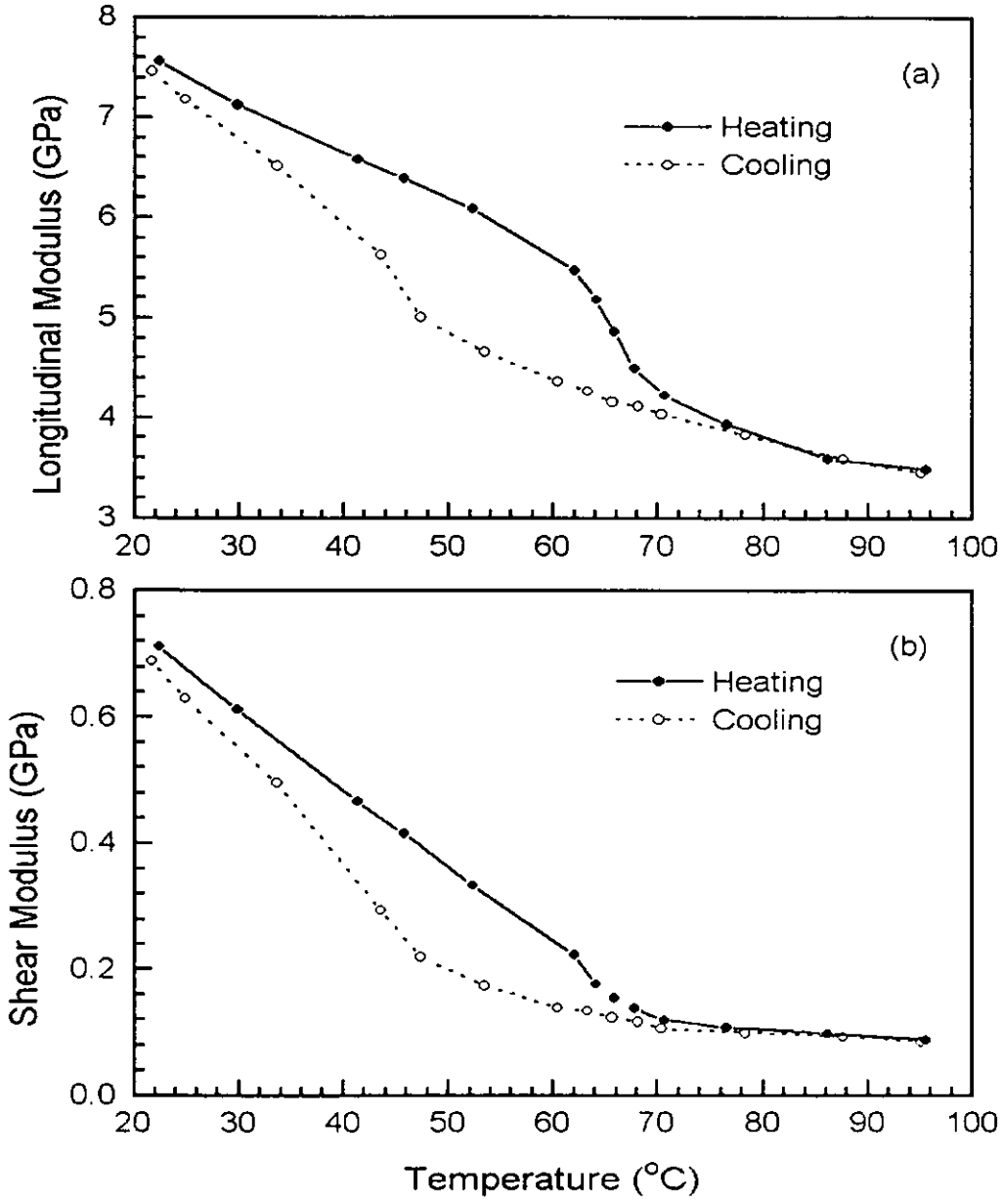

Figure 4.10 **Temperature dependence of the (a) longitudinal modulus (c_{11}) and (b) shear modulus (c_{66}) of the slow-cooled 56/44 copolymer in heating and cooling measurements.**

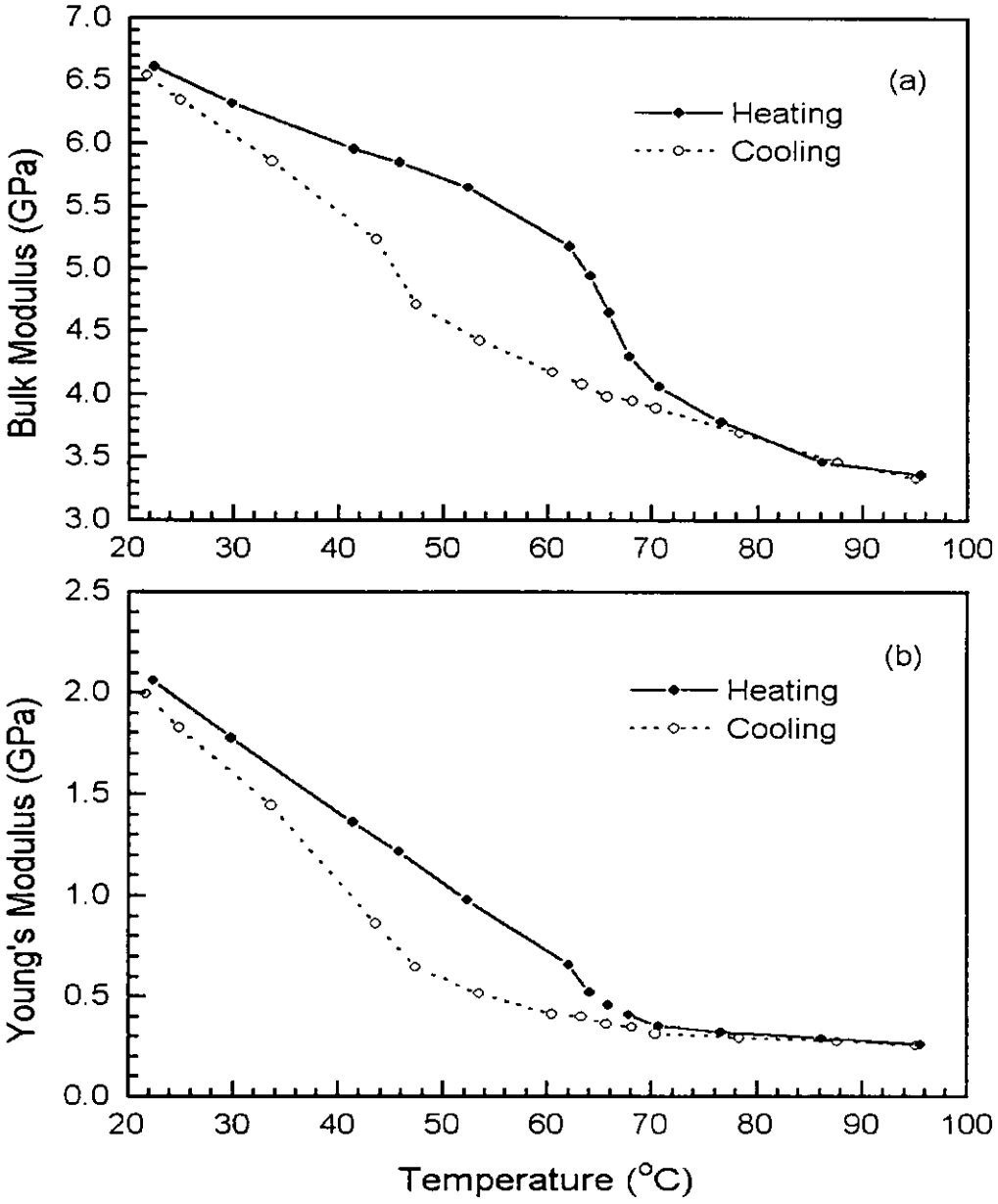

Figure 4.11 **Temperature dependence of the (a) bulk modulus and (b) Young's modulus of the slow-cooled 56/44 copolymer in heating and cooling measurements.**

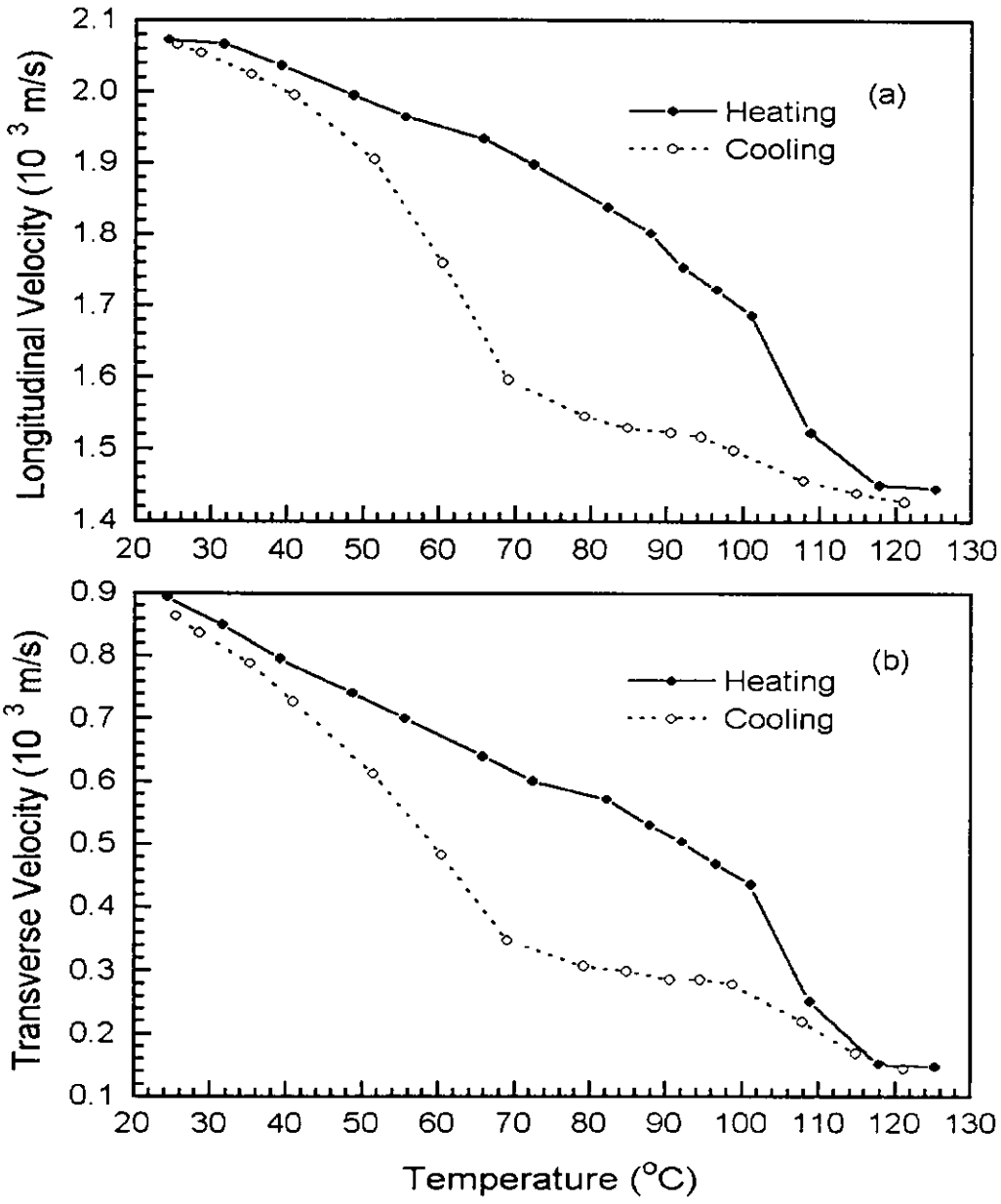

Figure 4.12 **Temperature dependence of the (a) longitudinal velocity and (b) transverse velocity of the quenched 70/30 copolymer in heating and cooling measurements.**

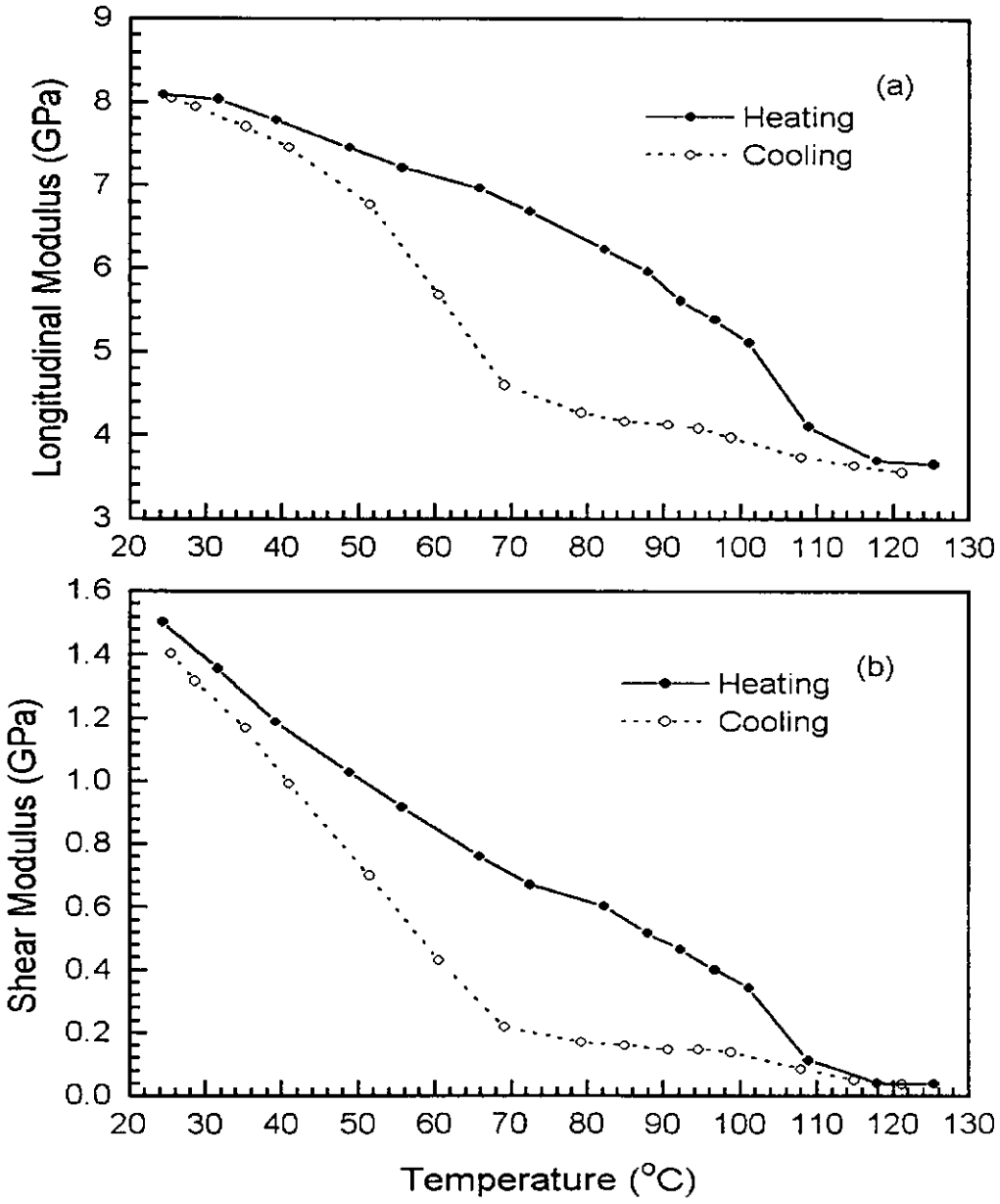

Figure 4.13 **Temperature dependence of the (a) longitudinal modulus (c_{11}) and (b) shear modulus (c_{66}) of the quenched 70/30 copolymer in heating and cooling measurements.**

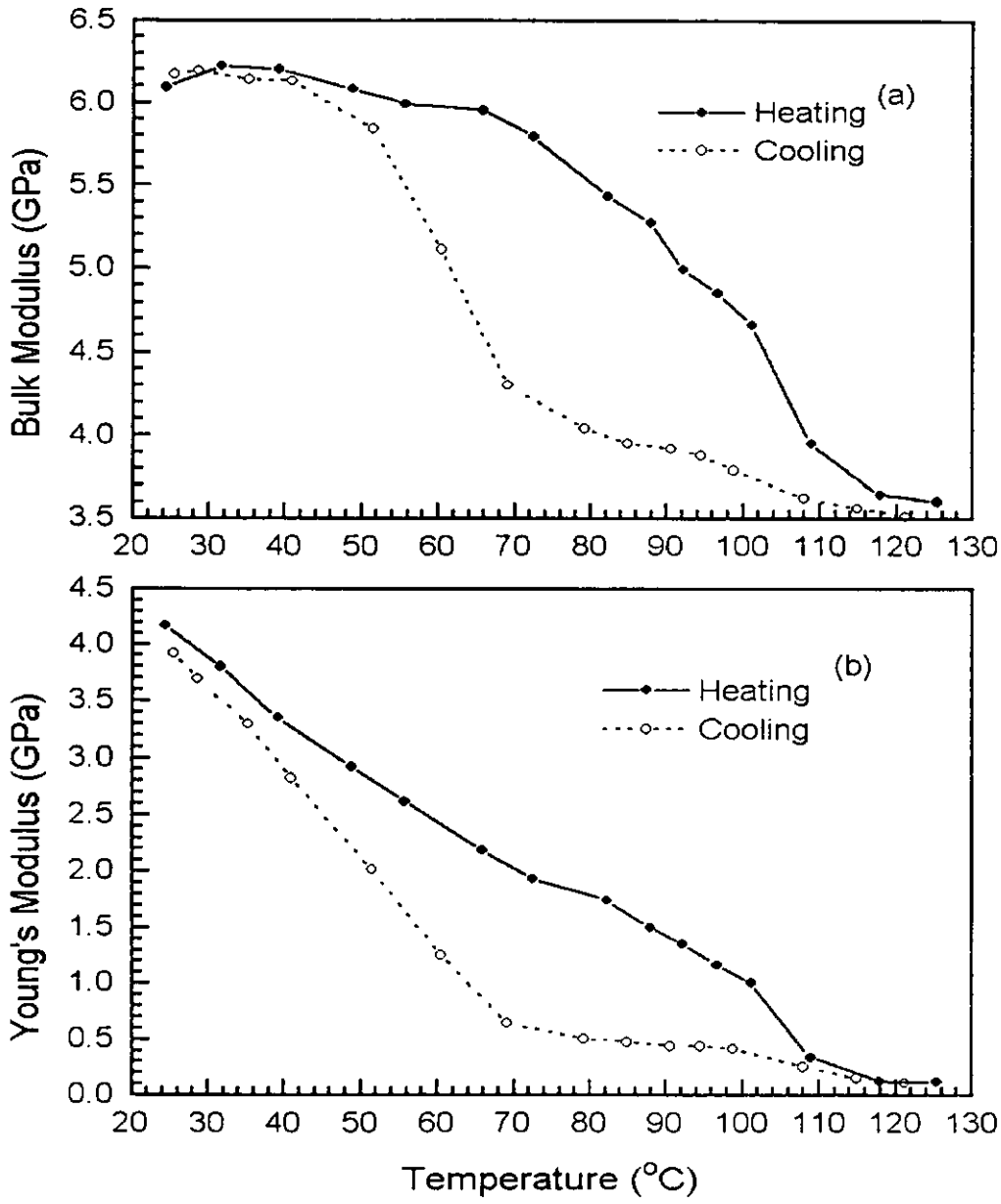

Figure 4.14 **Temperature dependence of the (a) bulk modulus and (b) Young's modulus of the quenched 70/30 copolymer in heating and cooling measurements.**

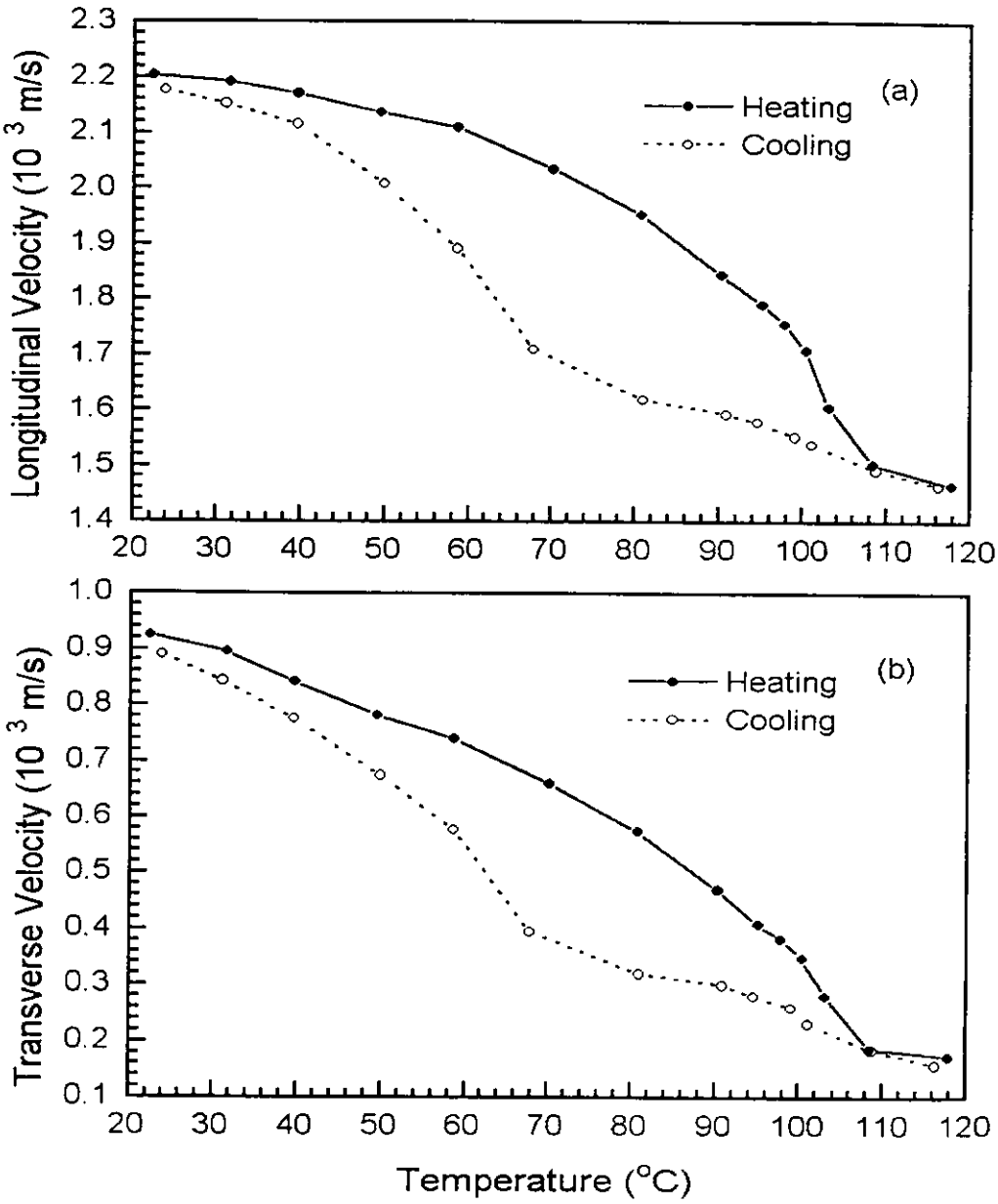

Figure 4.15 **Temperature dependence of the (a) longitudinal velocity and (b) transverse velocity of the slow-cooled 70/30 copolymer in heating and cooling measurements.**

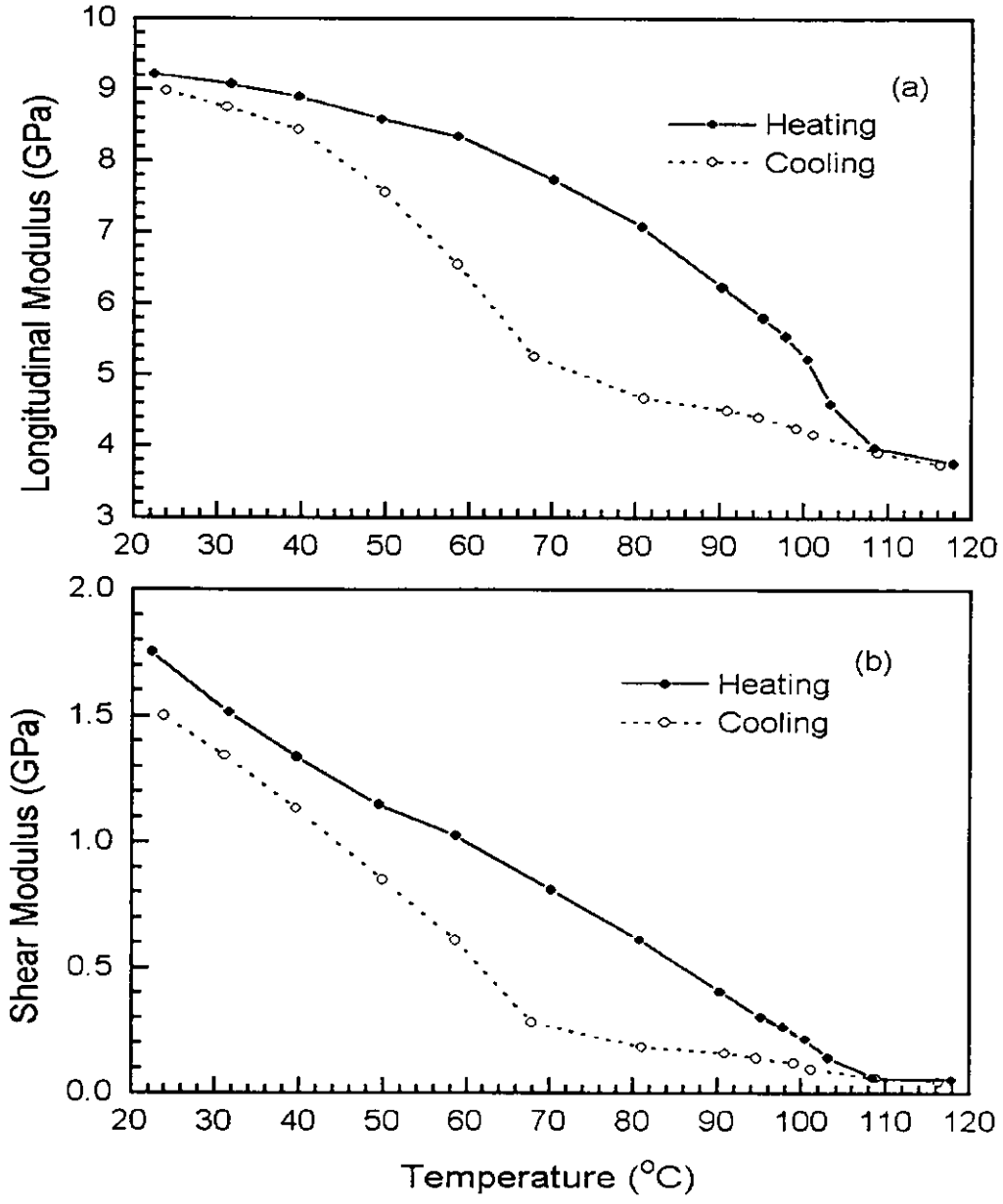

Figure 4.16 **Temperature dependence of the (a) longitudinal modulus (c_{11}) and (b) shear modulus (c_{66}) of the slow-cooled 70/30 copolymer in heating and cooling measurements.**

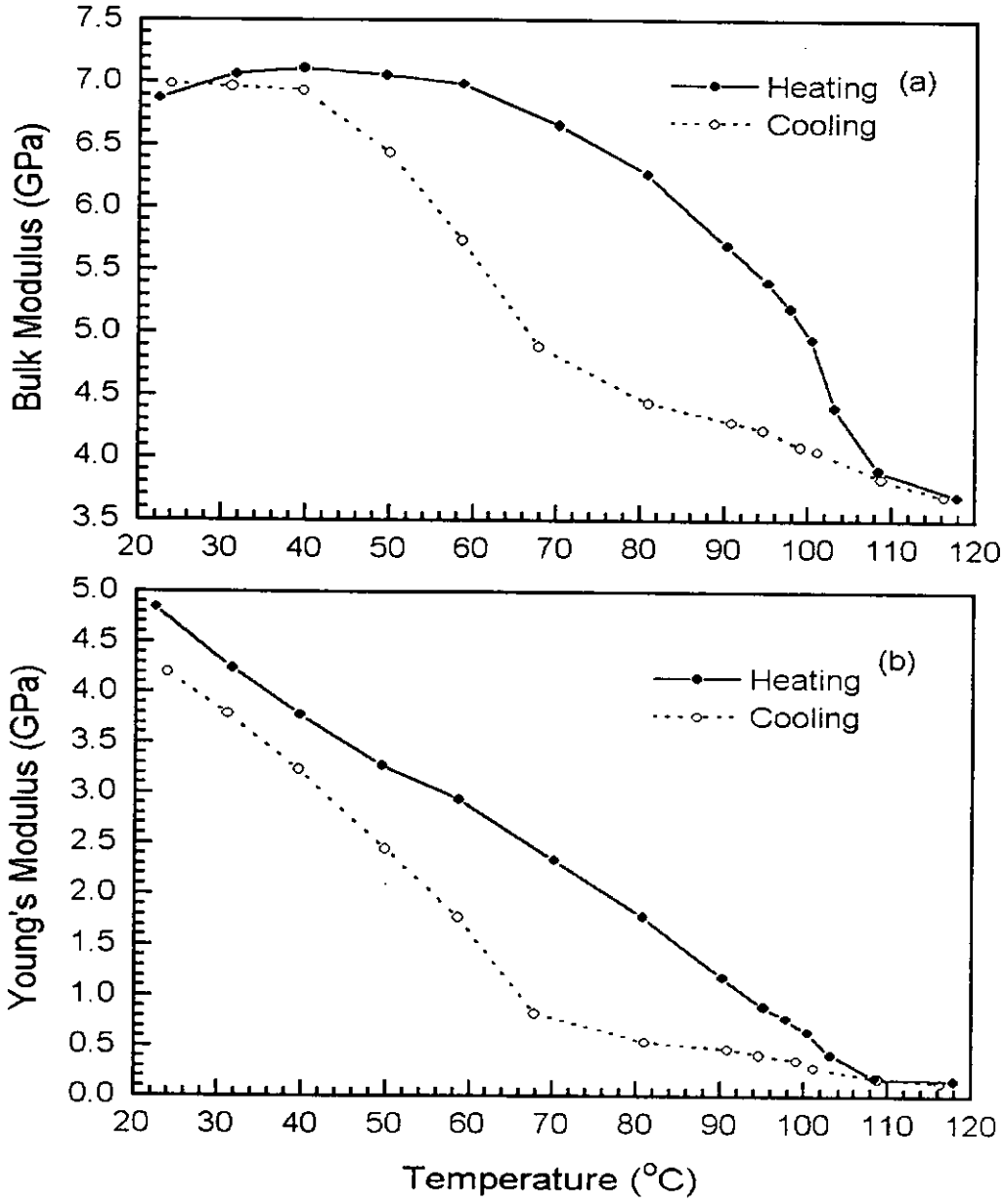

Figure 4.17 **Temperature dependence of the (a) bulk modulus and (b) Young's modulus of the slow-cooled 70/30 copolymer in heating and cooling measurements.**

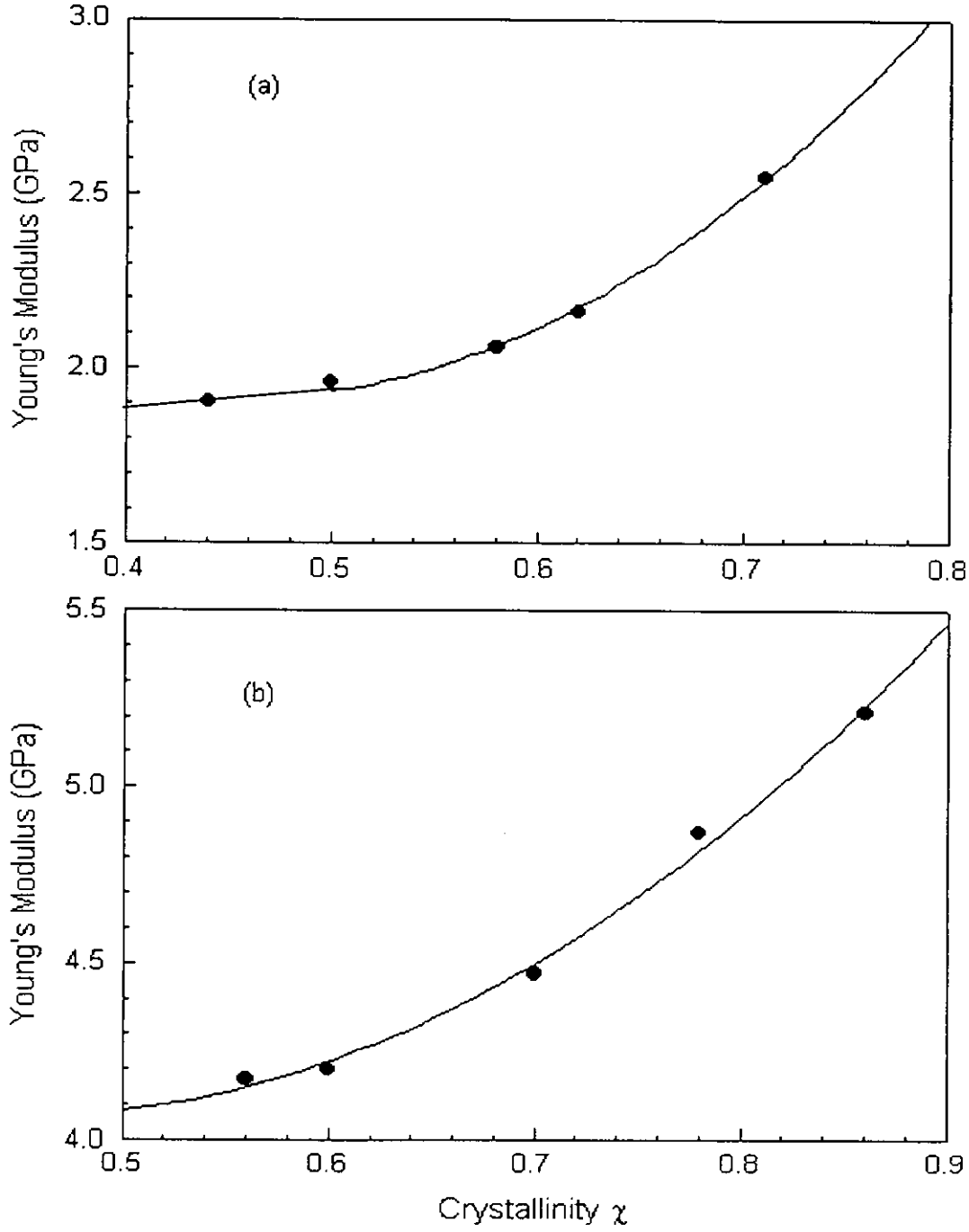

Figure 4.18 Crystallinity dependence of the Young's modulus measured at room temperature for (a) P(VDF/TrFE) 56/44 and (b) P(VDF/TrFE) 70/30 copolymer samples.

CHAPTER 5

CONCLUSIONS

The thermal and mechanical properties of the copolymers P(VDF/TrFE) of VDF mole fraction 56% and 70% were investigated. The corresponding results have been shown and analysed in the previous chapters.

The samples used in this study were prepared by the hot-press method, then followed by a quenching or slow-cooling process. Some quenched samples were also annealed at above re-crystallization temperature. They are isotropic in nature since no drawing is applied.

Density of the samples at room temperature was determined by the flotation method, and the density as a function of temperature was evaluated from the results of thermal expansivity measurement. All of the samples show a drastic change in thermal expansivity and hence density at around the ferroelectric phase transition temperature, manifested by a change in crystal structure.

Wide angle X-ray diffraction was used to determine the samples' crystallinity. From the results, it can be seen that annealing at a higher temperature gives a higher crystallinity.

The specific heat and the enthalpy change of the samples as a function of temperature were determined by using a Differential Scanning Calorimeter (DSC). It was shown that the specific heat of the copolymer samples increased almost linearly with temperature from –30 °C to the temperature before T_c. The two endothermic peaks observed in the DSC curves were identified with the Curie transition temperature (T_c) and melting temperature (T_m). Higher VDF content copolymer has a higher T_c. In the 70/30 copolymer, T_c shifts to a notedly lower temperature in cooling measurements. This thermal hysteresis phenomenon is common to ferroelectric materials undergoing first order phase transition. It indicates that the crystal structure change from paraelectric to ferroelectric has to release more energy for the rotation of dipoles in the molecular chains. On the other hand, thermal hysteresis is less pronounced in the 56/44 copolymer.

In evaluating the thermal conductivity of the copolymers, we have used the laser flash radiometry method to obtain the thermal diffusivity D which, together with the earlier results of density and specific heat, is used to calculate the thermal conductivity. The results indicate that the room temperature thermal conductivity of low VDF content copolymer is higher at a similar degree of

crystallinity. This may be interpreted to mean that phonon transportation is more efficient in the crystal phase of the low VDF copolymer.

The mechanical properties of the copolymers as revealed by their elastic moduli are investigated by the ultrasonic immersion method. As expected, the elastic moduli (including the Young's, bulk and shear moduli) of the copolymer exhibit an obvious drop when going from the ferroelectric phase to the paraelectric phase. The thermal hysteresis effect is observed in the elastic moduli and the effect is more prominent for high VDF copolymers, i.e. the phase transition occurs at a lower temperature in sample cooling. The results are consistent with the DSC observations. The elastic moduli of the copolymer increase with crystallinity, which indicates a strengthening effect by the crystallites.

The ferroelectric copolymer P(VDF/TrFE) exhibits ferroelectric phase transition at a critical temperature which depends on the mole fraction of VDF. In addition, since the ferroelectric transition is a result of crystal structure change, both the mechanical and thermal properties are also sensitive to this phase transition. It is clear that these two kinds of properties are well-correlated to the degree of crystallinity.

REFERENCES

Abkovitz, M. and Pfister, G., (1975). *J. Appl. Phys.*, **46**, 2559, 1975.

Aharony, (1976). *Phys. Rev. B*, **13**, 2092, 1976.

Bhatacharjee, J.K. and Ferrel, R.A., (1981). *Phys. Rev. A*, **24**, pp.1643, 1981.

Carlsaw, H.S. and Jaeger, J.C., (1959). *"Conduction of Heat in Solids, 2nd edition"*, Clarendon Oxford, 1959.

Choy, C.L., Leung, W.P. and Yee, A.F., (1992). *Polym.*, **33**, No.8, 1788, 1992.

Fernandezetal, M.V., (1987). *Macromolecules*, **20**, 1811-1818, 1987.

Ferrell, R.A. and Bhatacharjee, J.K., (1981). *Phys. Rev. A*, **24**, 4095. 1981.

Fixman, M., (1962). *J. Chem. Phys.*, **50**, 1961, 1962.

Furukawa, T., (1989). *IEEE Trans. Electr. Insul.*, **24(3)**, 375, 1989.

Furukawa, T., (1984). *"Key Engineering Materials Vols. 92-93 - Chapter 2: Structure and Properties of Ferroelectric Polymers"*, Trans Tech Publications, Switzerland, 15-18, 1984.

Furukawa, T., Date, M., Fukada, E., Tajitsu, Y. and Chiba, T., (1980). *Jpn. J. Appl. Phys.*, **19**, L109, 1980.

Furukawa, T., Wen, J.X., Suzuki, K., Tashian, Y. and Date, M., (1984). "*Piezoelectricity and Pyroelectricity in Vinylidene Fluoride/Trifluoroethylene Copolymers*", *J. Appl. Phys.*, **56(3)**, 829-834, 1984.

Harris, A.B., (1974). *J. Phys. C*, **7**, 1671, 1974.

Hikosaka, M., (1987). *Polymer*, **28**, 1257, 1987.

Ikeda, S., Shimojima, Z. and Kutani, M., (1990). *"Correlation between Ferroelectric Phase Transition and Crystallization Behavior of Ferroelectric Polymers", Ferroelectrics*, **109**, 297-301, 1990.

Kepler, R.G., (1978). *Ann. Rev. Phys. Chem.*, **20**, 497, 1978.

Kitayama, T., Ueda, T. and Yamada, T., (1980). *Ferroelectrics*, **19**, 301, 1980.

Koga, K.K. and Ohigashi, H., (1986). "*Piezoelectricity and Related Properties of Vinylidene Fluoride and Trifluoroethylene Copolymers*", *J. Appl. Phys.*, **59(6)**, 2142-2150, 1986.

Koizumi, N., Haikawa, N. and Habuka, H., (1984). *Ferroelectrics*, **57**, 99, 1984.

Kruger, J.K., Petzett, J. and Legrand, J.F., (1986). *Colloid. Polym. Sci*, **264**, 7915, 1986.

Lando, J.B. and Doll, W.W., (1968). "*The Polymorphism of Poly(vinylidene fluoride): 1. The Effect of Head-to-head Structure*", *J. Macromol. Sci. Phys.*, **132**, 205-218, 1968.

Legrand, J.F., Frick, B., Meurer, B., Schmidt, V.H., Bee, M. and Lajzerowicz, J., (1990). *Ferroelectrics*, **109**, 321-326, 1990.

Legrand, J.F., Lajzerowicz, J., Berge, B., Delzenne, P., Macchi, F., Bourgaux-Leonard, C., Wicker, A. and Kruger, J.K., (1988). *Ferroelectrics*, **78**, 151, 1988.

Leung, W.P. and Tam, A.C., (1984a). *J. Appl. Phy.*, **56**, 153, 1984.

Leung, W.P. and Tam, A.C., (1984b). *Optics Lett.*, **9**, 93, 1984.

Lovinger, A.J., (1983c). *"Ferroelectric Polymers", Science*, **220**, 4602, 1983.

Lovinger, A.J., Davis, G.T., Furukawa, T. and Broadhurst, M.G., (1982). *Macromolecules*, **15**, 323, 1982.

Lovinger, A.J., Davis, G.T., Furukawa, T., Broadhurst, M.G., (1983a). *Polymer*, **24**, 1225-1233, 1983.

Lovinger, A.J., Furukawa, T., Davis, G.T. and Broadhurst, M.G., (1983d). "*Curie Transitions in Copolymers of Vinylidene Fluoride", Ferroelectrics*, **50**, 227-236, 1983.

Lovinger, A.J., Furukawa, T., Davis, G.T. and Broadhurst, M.G., (1983b). *Ferroelectrics*, **50**, 553, 1983.

Maeda, K., Yamauchi, T. and Tsutsumi, K., (1990). *Polym. J.*, 1990.

Marcus, M.A., (1984). "*Ferroelectric Polymers and Their Applications*", Research Laboratories, Eastman Kodak Company, USA, 1984.

Naokazu, K., (1994). *Key Engineering Materials*, **92-93**, 161-180, 1994.

Ohigashi, H. and Koga, K., (1983). *Jpn. J. Appl. Phys.*, **21**, L455, 1983.

Peierls, R.E., (1929). *Ann. Phys.*, **3**, 1055, 1929.

Tadokoro, H., (1979). *"Structure of Crystalline Polymers", John Wiley, New York*, 1979.

Tanaka, H. and Wada, Y., (1985). *Phys. Rev. A*, **32**, 512, 1985.

Tanaka, H. and Lovinger, A.J., (1987). *Macromolecules*, **20**, 2638, 1987.

Tanaka, M., Yukawa, H. and Nishi, T., (1988). *Macromolecules*, **21**, 2469, 1988.

Tasaka, S. and Miyata, S., (1985). "*Effects of Crystal Structure on Piezoelectric and Ferroelectric Properties of Copoly(vinylidene fluoride-tetrofluoroethylene)*", *J. Appl. Phys.*, **57**, 906-910, 1985.

Tashiro, K., Itoh, Y., Nishimura, S. and Kobayashi, M., (1991). *"Vibrational Spectroscopic Study on Ferroelectric Phase Transition of Vinylidene Fluoride-Trifluoroethylene Copolymers: 2. Temperature Dependences of the Far-Infrared Absorption Spectra and Ultrasonic Velocity", Polymer*, **32 (6)**, 1017-1025, 1991.

Tashiro, K., Takano, K., Kobayash, M., Chatani, Y. and Tadokoro, H., (1981). *Polymer*, **22**, 1312, 1981.

Tashiro, K., Takano, K., Kobayash, M., Chatani, Y. and Tadokoro, H., (1984a). *Polymer*, **25**, 195, 1984.

Tashiro, K., Takano, K., Kobayash, M., Chatani, Y. and Tadokoro, H., (1984b). *Ferroelectrics*, **57**, 297, 1984.

Wen, J.X., (1984). "*Piezoelectric Properties in Uniaxially Drawn Copolymers of Vinylidene Fluoride and Trifluoroethylene*", *Jpn. J. Appl. Phys.*, **23**, 1434-1439, 1984.

Yagi, T., (1979a). *Polymer. J.*, **11**, 353, 1979.

Yagi, T. and Tatemoto, M., (1979b). *Polymer J.*, **11**, 429, 1979.

Yagi, T., Tatemoto, M. and Sako, J., (1980a). *Polymer. J.*, **12**, 209, 1980.

Yagi, T., Tatemoto, M. and Sako, J., (1980b). "*Transition Behavior and Dielectric Properties in Trifluoroethylene and Vinylidene Fluoride Copolymers*", *J. Polymer*, **12(4)**, 209-223, 1980.

Yagi, T., Tatemoto, M. and Sako, J.I., (1980c). *J. Polymer*, **12**, 222, 1980.

APPENDIX A CRYSTALLINITY DEPENDENCE OF THE THERMAL PROPERTIES AND ELASTIC MODULI OF THE COPOLYMERS

Crystallinity : χ

Density : ρ (g/cm^3)

Specific Heat : C_p (J/g K)

Diffusivity : D (x 10^{-3} cm^2/s)

Conductivity : K (mW/cm K)

Elastic Stiffness Coefficient : $C_{11} = \rho V_{11}^2$ (GPa)

Shear Modulus : $C_{66} = \rho V_{66}^2 = G$ (GPa)

Young's Modulus : $E = C_{66} (3C_{11} - 4C_{66}) / (C_{11} - C_{66})$ (GPa)

Bulk Modulus : $B = C_{11} - \frac{4}{3} C_{66}$ (GPa)

CRYSTALLINITY DEPENDENCE OF THE THERMAL PROPERTIES

P(VDF/TrFE) 56/44 COPOLYMER					
SAMPLES	χ	ρ (g/cm^3)	C_P (J/g K)	D ($\times 10^{-3}$ cm^2/s)	K (mW/cm K)
Quenched	0.45	1.885	1.195	0.730	1.644
Annealed at 100 °C	0.49	1.886	1.150	0.810	1.757
Annealed at 120 °C	0.58	1.894	1.115	0.896	1.892
Annealed at 130 °C	0.63	1.905	1.068	0.971	1.976
Slow-Cooled	0.65	1.907	1.043	1.060	2.108
Annealed at 140 °C	0.72	1.917	1.011	1.160	2.248

P(VDF/TrFE) 70/30 COPOLYMER					
SAMPLES	χ	ρ (g/cm^3)	C_P (J/g K)	D ($\times 10^{-3}$ cm^2/s)	K (mW/cm K)
Quenched	0.55	1.886	1.188	0.745	1.669
Annealed at 100 °C	0.58	1.887	1.141	0.836	1.799
Annealed at 120 °C	0.71	1.897	1.103	0.911	1.906
Annealed at 130 °C	0.78	1.908	1.059	0.981	1.982
Slow-Cooled	0.80	1.911	1.044	1.080	2.155
Annealed at 140 °C	0.85	1.920	1.010	1.180	2.288

Crystallinity Dependence of the Elastic Moduli

P(VDF/TrFE) 56/44 COPOLYMER						
SAMPLES	χ	ρ (g/cm^3)	C_{11} (GPa)	G (GPa)	E (GPa)	B (GPa)
Quenched	0.44	1.889	7.24	0.657	1.905	6.36
Annealed at 100 °C	0.50	1.890	7.34	0.676	1.959	6.44
Annealed at 120 °C	0.58	1.899	7.52	0.711	2.059	6.57
Annealed at 130 °C	0.62	1.911	7.79	0.746	2.159	6.80
Slow-Cooled	0.66	1.913	7.88	0.751	2.174	6.88
Annealed at 140 °C	0.71	1.925	8.05	0.885	2.546	6.87

P(VDF/TrFE) 70/30 COPOLYMER						
SAMPLES	χ	ρ (g/cm^3)	C_{11} (GPa)	G (GPa)	E (GPa)	B (GPa)
Quenched	0.56	1.887	8.09	1.504	4.17	6.08
Annealed at 100 °C	0.60	1.890	8.17	1.514	4.20	6.15
Annealed at 120 °C	0.70	1.903	8.72	1.611	4.47	6.57
Annealed at 130 °C	0.78	1.913	9.17	1.763	4.87	6.82
Slow-Cooled	0.81	1.915	9.27	1.786	4.93	6.89
Annealed at 140 °C	0.86	1.927	9.67	1.887	5.21	7.15

APPENDIX B TEMPERATURE DEPENDENCE OF THE THERMAL EXPANSION OF THE COPOLYMERS

Length of sample at room temperature : l_0

Expansion Coefficient : α (K^{-1})

QUENCHED 56/44 P(VDF/TrFE) COPOLYMER IN HEATING RUN								
TEMP. (^{o}C)	$\Delta l/l_0$ (%)	α (x 10^{-4} K^{-1})	TEMP. (^{o}C)	$\Delta l/l_0$ (%)	α (x 10^{-4} K^{-1})	TEMP. (^{o}C)	$\Delta l/l_0$ (%)	α (x 10^{-4} K^{-1})
-160	-1.363	0.527	-30	-0.571	0.820	70	1.246	3.066
-150	-1.314	0.530	-20	-0.488	0.887	75	1.383	2.460
-140	-1.258	0.539	-10	-0.394	0.972	80	1.498	2.247
-130	-1.208	0.551	0	-0.294	1.066	85	1.608	2.170
-120	-1.147	0.560	10	-0.183	1.150	90	1.714	2.052
-110	-1.097	0.567	20	-0.061	1.222	95	1.813	1.992
-100	-1.036	0.577	30	0.059	1.308	100	1.915	1.990
-90	-0.981	0.595	40	0.203	1.610	105	2.011	1.878
-80	-0.920	0.619	45	0.285	1.743			
-70	-0.854	0.651	50	0.380	2.007			
-60	-0.793	0.685	55	0.492	2.551			
-50	-0.721	0.723	60	0.647	3.887			
-40	-0.648	0.763	65	0.972	10.46			

l_0 = 1.804 mm

QUENCHED 56/44 P(VDF/TrFE) COPOLYMER IN COOLING RUN								
TEMP. (^{o}C)	$\Delta l/l_0$ (%)	α (x 10^{-4} K^{-1})	TEMP. (^{o}C)	$\Delta l/l_0$ (%)	α (x 10^{-4} K^{-1})	TEMP. (^{o}C)	$\Delta l/l_0$ (%)	α (x 10^{-4} K^{-1})
-160	-1.422	0.513	-30	-0.613	0.896	70	1.276	2.662
-150	-1.374	0.523	-20	-0.521	0.986	75	1.403	2.375
-140	-1.319	0.535	-10	-0.417	1.070	80	1.513	2.139
-130	-1.268	0.547	0	-0.302	1.132	85	1.619	2.080
-120	-1.209	0.561	10	-0.176	1.166	90	1.720	2.081
-110	-1.154	0.572	20	-0.062	1.212	95	1.823	2.079
-100	-1.098	0.591	30	0.067	1.371	100	1.925	1.088
-90	-1.036	0.613	40	0.220	1.730	105	2.030	0.911
-80	-0.976	0.640	45	0.310	1.872			
-70	-0.909	0.674	50	0.414	2.329			
-60	-0.842	0.712	55	0.545	3.068			
-50	-0.771	0.759	60	0.748	5.821			
-40	-0.695	0.818	65	1.112	4.849			

l_o = 1.805 mm

SLOW-COOLED 56/44 P(VDF/TrFE) COPOLYMER IN HEATING RUN								
TEMP. (°C)	$\Delta l/l_0$ (%)	α (x 10^{-4} K^{-1})	TEMP. (°C)	$\Delta l/l_0$ (%)	α (x 10^{-4} K^{-1})	TEMP. (°C)	$\Delta l/l_0$ (%)	α (x 10^{-4} K^{-1})
-160	-1.348	0.514	-30	-0.530	0.804	70	1.309	3.017
-150	-1.301	0.520	-20	-0.448	0.865	75	1.441	2.395
-140	-1.245	0.545	-10	-0.359	0.925	80	1.554	2.203
-130	-1.192	0.567	0	-0.264	0.997	85	1.662	2.074
-120	-1.134	0.588	10	-0.160	1.038	90	1.760	1.896
-110	-1.074	0.609	20	-0.049	1.084	95	1.851	1.851
-100	-1.011	0.624	30	-0.059	1.222	100	1.934	1.805
-90	-0.948	0.640	40	0.191	1.488			
-80	-0.884	0.656	45	0.271	1.657			
-70	-0.817	0.669	50	0.362	2.015			
-60	-0.750	0.694	55	0.472	2.607			
-50	-0.681	0.718	60	0.634	4.197			
-40	-0.607	0.765	65	1.072	1.074			

l_0 = 1.431 mm

SLOW-COOLED 56/44 P(VDF/TrFE) COPOLYMER IN COOLING RUN								
TEMP. (^{o}C)	$\Delta l/l_0$ (%)	α (x 10^{-4} K^{-1})	TEMP. (^{o}C)	$\Delta l/l_0$ (%)	α (x 10^{-4} K^{-1})	TEMP. (^{o}C)	$\Delta l/l_0$ (%)	α (x 10^{-4} K^{-1})
-160	-1.396	0.493	-30	-0.586	0.854	70	1.356	2.630
-150	-1.348	0.518	-20	-0.499	0.917	75	1.476	2.212
-140	-1.294	0.544	-10	-0.402	0.986	80	1.582	2.049
-130	-1.239	0.568	0	-0.301	1.073	85	1.680	1.958
-120	-1.180	0.582	10	-0.191	1.181	90	1.777	1.921
-110	-1.121	0.590	20	-0.067	1.287	95	1.871	1.860
-100	-1.063	0.596	30	0.063	1.362	100	1.960	1.622
-90	-1.003	0.604	40	0.207	1.640			
-80	-0.943	0.621	45	0.298	1.889			
-70	-0.879	0.647	50	0.408	2.520			
-60	-0.815	0.691	55	0.553	3.445			
-50	-0.744	0.735	60	0.831	10.96			
-40	-0.667	0.793	65	1.205	3.986			

l_0 = 1.431 mm

QUENCHED 70/30 P(VDF/TrFE) COPOLYMER IN HEATING RUN								
TEMP. (^oC)	$\Delta l/l_o$ (%)	α (x 10^{-4} K^{-1})	TEMP. (^oC)	$\Delta l/l_o$ (%)	α (x 10^{-4} K^{-1})	TEMP. (^oC)	$\Delta l/l_o$ (%)	α (x 10^{-4} K^{-1})
-160	-1.057	0.573	-30	-0.414	0.686	70	0.482	1.052
-150	-1.021	0.576	-20	-0.351	0.700	75	0.568	1.155
-140	-0.971	0.584	-10	-0.273	0.713	80	0.677	1.469
-130	-0.927	0.594	0	-0.198	0.722	85	0.818	1.815
-120	-0.867	0.603	10	-0.120	0.733	90	1.015	2.293
-110	-0.804	0.607	20	-0.041	0.751	95	1.272	2.874
-100	-0.750	0.610	30	0.051	0.782	100	1.591	3.338
-90	-0.711	0.617	40	0.149	0.804	105	1.976	4.194
-80	-0.673	0.628	45	0.191	0.816	110	2.391	2.746
-70	-0.626	0.643	50	0.240	0.828	115	2.565	1.391
-60	-0.579	0.654	55	0.291	0.845	120	2.666	1.243
-50	-0.522	0.665	60	0.348	0.889	125	2.761	1.243
-40	-0.472	0.676	65	0.410	0.950			

l_o = 1.724 mm

QUENCHED 70/30 P(VDF/TrFE) COPOLYMER IN COOLING RUN								
TEMP. (^{o}C)	$\Delta l/l_o$ (%)	α (x 10^{-4} K^{-1})	TEMP. (^{o}C)	$\Delta l/l_o$ (%)	α (x 10^{-4} K^{-1})	TEMP. (^{o}C)	$\Delta l/l_o$ (%)	α (x 10^{-4} K^{-1})
-160	-1.220	0.570	-30	-0.492	0.687	70	1.646	2.608
-150	-1.182	0.570	-20	-0.410	0.701	75	1.842	1.540
-140	-1.132	0.581	-10	-0.330	0.714	80	1.961	1.268
-130	-1.085	0.594	0	-0.244	0.732	85	2.270	1.173
-120	-1.030	0.601	10	-0.153	0.754	90	2.155	1.127
-110	-0.975	0.606	20	-0.050	0.767	95	2.248	1.154
-100	-0.928	0.608	30	0.046	0.801	100	2.343	1.186
-90	-0.867	0.610	40	0.163	0.863	105	2.442	1.236
-80	-0.815	0.620	45	0.229	0.910	110	2.544	1.269
-70	-0.757	0.631	50	0.298	1.024	115	2.652	1.316
-60	-0.691	0.644	55	0.418	2.010	120	2.767	1.332
-50	-0.627	0.653	60	0.831	5.713	125	2.937	1.332
-40	-0.558	0.670	65	1.291	3.708			

l_o = 1.725 mm

SLOW-COOLED 70/30 P(VDF/TrFE) COPOLYMER IN HEATING RUN								
TEMP. (°C)	$\Delta l/l_o$ (%)	α (x 10^{-4} K^{-1})	TEMP. (°C)	$\Delta l/l_o$ (%)	α (x 10^{-4} K^{-1})	TEMP. (°C)	$\Delta l/l_o$ (%)	α (x 10^{-4} K^{-1})
-160	-1.119	0.493	-30	-0.415	0.651	70	0.498	1.594
-150	-1.068	0.494	-20	-0.349	0.693	75	0.587	1.948
-140	-1.020	0.501	-10	-0.277	0.735	80	0.714	3.026
-130	-0.971	0.509	0	-0.203	0.773	85	0.899	4.565
-120	-0.917	0.517	10	-0.126	0.808	90	1.190	7.494
-110	-0.869	0.525	20	-0.044	0.889	95	1.628	9.033
-100	-0.814	0.531	30	0.051	0.981	100	2.043	7.617
-90	-0.762	0.544	40	0.154	1.039	105	2.404	6.831
-80	-0.706	0.556	45	0.207	1.065	110	2.671	3.446
-70	-0.656	0.569	50	0.261	1.089	115	2.804	2.408
-60	-0.601	0.579	55	0.315	1.090	120	2.915	2.084
-50	-0.540	0.598	60	0.368	1.127	125	3.017	1.985
-40	-0.479	0.627	65	0.429	1.317			

l_o = 1.537 mm

SLOW-COOLED 70/30 P(VDF/TrFE) COPOLYMER IN COOLING RUN								
TEMP. (^{o}C)	$\Delta l/l_0$ (%)	α (x 10^{-4} K^{-1})	TEMP. (^{o}C)	$\Delta l/l_0$ (%)	α (x 10^{-4} K^{-1})	TEMP. (^{o}C)	$\Delta l/l_0$ (%)	α (x 10^{-4} K^{-1})
-160	-1.152	0.491	-30	-0.444	0.668	70	1.983	2.972
-150	-1.107	0.492	-20	-0.378	0.699	75	2.109	2.159
-140	-1.059	0.504	-10	-0.305	0.755	80	2.208	1.884
-130	1.011	0.515	0	-0.228	0.820	85	2.302	1.895
-120	-0.959	0.525	10	-0.141	0.877	90	2.398	1.958
-110	-0.910	0.533	20	-0.049	0.971	95	2.495	1.970
-100	-0.859	0.545	30	0.053	1.087	100	2.597	2.035
-90	-0.806	0.555	40	0.166	1.199	105	2.698	2.060
-80	-0.751	0.567	45	0.238	1.511	110	2.803	2.141
-70	-0.690	0.586	50	0.326	2.335	115	2.913	2.196
-60	-0.633	0.605	55	0.628	15.16	120	3.026	2.244
-50	-0.568	0.619	60	1.431	10.42	125	3.137	2.464
-40	-0.507	0.641	65	1.785	5.885			

l_0 = 1.538 mm

APPENDIX C TEMPERATURE DEPENDENCE OF SPECIFIC HEAT, THERMAL DIFFUSIVITY AND THERMAL CONDUCTIVITY OF THE COPOLYMERS

Density : ρ (g/cm^3)

Specific Heat : C_p (J/g K)

Diffusivity : D (cm^2/s)

Conductivity : K (mW/cm K)

QUENCHED 56/44 P(VDF/TrFE) COPOLYMER IN HEATING RUN				
TEMP. (°C)	ρ (g/cm^3)	C_P (J/g K)	D (x 10^{-3} cm^2/s)	K (mW/cm K)
-99.6	1.943	0.5394	1.3638	1.4293
-92.9	1.941	0.5594	1.3240	1.4376
-85.1	1.938	0.6062	1.2514	1.4702
-73.5	1.934	0.6797	1.1624	1.5280
-65.2	1.931	0.7320	1.1214	1.5851
-55.2	1.928	0.7897	1.0714	1.6313
-43.9	1.923	0.8570	0.9984	1.6454
-33.9	1.918	0.9151	0.9524	1.6716
-18.3	1.931	1.0039	0.8834	1.7125
-3.2	1.903	1.0819	0.8439	1.7375
10.9	1.895	1.1391	0.7920	1.7096
20.4	1.889	1.1791	0.7522	1.6754
25.5	1.885	1.1950	0.7300	1.6444
30.5	1.882	1.2180	0.7124	1.6330
34.8	1.878	1.2421	0.6914	1.6128
39.5	1.875	1.2706	0.6635	1.5807
44.0	1.871	1.3172	0.6369	1.5696
47.4	1.868	1.3441	0.6061	1.5218
50.2	1.865	1.3719	0.5925	1.5160
52.7	1.862	1.4133	0.5784	1.5221
55.6	1.858	1.4664	0.5695	1.5516
57.9	1.855	1.5387	0.5695	1.6255
60.2	1.850	1.5755	0.5648	1.6462
61.3	1.848	1.6235	0.5648	1.6945
65.5	1.831	2.0179	0.5512	2.0366
66.5	1.827	2.1753	0.5215	2.0726
67.6	1.824	2.3841	0.4595	1.9982
68.1	1.823	2.2911	0.4197	1.7530
69.8	1.820	2.0791	0.3401	1.2869
72.6	1.816	1.7468	0.2999	0.9513
78.8	1.809	1.5636	0.2736	0.7739
87.2	1.800	1.4912	0.2646	0.7102
92.8	1.794	1.4750	0.2691	0.7121

QUENCHED 56/44 P(VDF/TrFE) COPOLYMER IN COOLING RUN				
TEMP. (^{o}C)	ρ (g/cm^3)	C_P (J/g K)	D (x 10^{-3} cm^2/s)	K (mW/cm K)
21.5	1.885	1.2000	0.7278	1.64628
27.9	1.881	1.2400	0.7049	1.64414
30.8	1.879	1.2410	0.6820	1.59031
35.0	1.876	1.2411	0.6638	1.54553
36.7	1.874	1.2411	0.6456	1.50155
37.9	1.873	1.2409	0.6270	1.45728
40.2	1.871	1.2410	0.6088	1.41358
41.4	1.870	1.2410	0.5952	1.38126
42.8	1.869	1.2411	0.5723	1.32752
44.5	1.867	1.2407	0.5541	1.28351
46.3	1.865	1.2537	0.5219	1.22028
47.4	1.864	1.2788	0.5037	1.20066
49.8	1.861	1.3786	0.4762	1.22173
52.7	1.857	1.5788	0.4626	1.35627
56.1	1.852	2.0775	0.4533	1.74409
59.0	1.846	2.8046	0.4487	2.32305
61.3	1.839	2.3514	0.4440	1.91996
64.3	1.827	1.6448	0.4076	1.22486
66.6	1.821	1.5182	0.3754	1.03784
70.1	1.816	1.4831	0.3366	0.90658
71.9	1.814	1.4779	0.3094	0.82936
74.2	1.811	1.4779	0.2945	0.78821
76.0	1.809	1.4837	0.2784	0.74721
79.5	1.805	1.4787	0.2706	0.72211
84.8	1.799	1.4803	0.2656	0.7073
88.9	1.795	1.4826	0.2656	0.70682
93.0	1.791	1.4905	0.2652	0.7079

SLOW-COOLED 56/44 P(VDF/TrFE) COPOLYMER IN HEATING RUN				
TEMP. (^oC)	ρ (g/cm^3)	C_P (J/g K)	D ($x\ 10^{-3}\ cm^2/s$)	K (mW/cm K)
-81.3	1.955	0.6143	1.5638	1.878
-72.4	1.952	0.6555	1.5600	1.996
-55.2	1.945	0.7353	1.4581	2.085
-28.2	1.934	0.8472	1.3700	2.245
-9.4	1.925	0.9179	1.2400	2.191
10.7	1.913	0.9964	1.1600	2.211
23.2	1.906	1.0551	1.0600	2.132
28.0	1.903	1.0751	1.0500	2.148
31.0	1.901	1.0906	1.0400	2.156
34.8	1.898	1.1093	1.0100	2.127
39.4	1.895	1.1356	0.9860	2.122
44.4	1.891	1.1681	0.9580	2.116
47.8	1.888	1.2121	0.9270	2.121
50.4	1.885	1.2546	0.9100	2.152
53.6	1.881	1.2951	0.8930	2.175
55.1	1.879	1.3363	0.8720	2.190
57.2	1.876	1.3577	0.8628	2.198
58.8	1.873	1.4201	0.8581	2.282
59.8	1.871	1.5137	0.8533	2.417
61.9	1.866	1.7491	0.8405	2.743
64.3	1.859	2.3881	0.8210	3.645
65.7	1.845	2.9664	0.7660	4.192
66.6	1.842	1.9916	0.7340	2.693
70.2	1.836	1.5147	0.6120	1.702
74.4	1.830	1.4452	0.5718	1.512
79.7	1.824	1.3896	0.5542	1.405
85.4	1.818	1.3731	0.5340	1.333
92.3	1.811	1.3647	0.5373	1.328

SLOW-COOLED 56/44 P(VDF/TrFE) COPOLYMER IN COOLING RUN				
TEMP. (^{o}C)	ρ (g/cm^3)	C_P (J/g K)	D (x 10^{-3} cm^2/s)	K (mW/cm K)
26.9	1.902	1.088	1.008	2.047
30.5	1.9	1.097	0.985	2.034
32.9	1.898	1.097	0.965	2.009
36.2	1.895	1.107	0.948	1.989
38.5	1.893	1.107	0.925	1.938
40.8	1.891	1.12	0.902	1.910
43.1	1.889	1.142	0.884	1.907
44.9	1.887	1.153	0.873	1.899
46.8	1.885	1.176	0.858	1.902
48.3	1.884	1.198	0.847	1.912
49.9	1.882	1.261	0.831	1.927
54.2	1.877	1.317	0.771	2.076
54.8	1.873	1.48	0.726	2.273
59.2	1.863	2.735	0.680	4.122
61.2	1.851	2.492	0.661	3.644
64.2	1.841	1.596	0.640	1.999
66.9	1.837	1.491	0.631	1.496
71.1	1.831	1.459	0.600	1.383
76.1	1.825	1.447	0.563	1.281
88.1	1.813	1.379	0.541	1.310

QUENCHED 70/30 P(VDF/TrFE) COPOLYMER IN HEATING RUN				
TEMP. (^{o}C)	ρ (g/cm^3)	C_P (J/g K)	D (x 10^{-3} cm^2/s)	K (mW/cm K)
-101.7	1.927	0.4416	1.4090	1.1990
-97.8	1.926	0.4719	1.3990	1.2715
-87.3	1.924	0.5670	1.3290	1.4498
-75.7	1.921	0.6692	1.2180	1.5658
-60.7	1.917	0.7772	1.1290	1.6821
-43.2	1.912	0.8904	1.0800	1.8386
-30.8	1.908	0.9626	0.9960	1.8293
-16.7	1.903	1.0319	0.9450	1.8557
-4.1	1.897	1.0862	0.8320	1.7144
14.7	1.889	1.1632	0.7820	1.7183
21.9	1.886	1.1873	0.7450	1.6682
26.4	1.884	1.2025	0.7290	1.6516
31.6	1.881	1.2258	0.6890	1.5886
39.4	1.877	1.2558	0.6700	1.5793
48.5	1.873	1.2985	0.6170	1.5006
57.0	1.868	1.3313	0.5560	1.3827
62.9	1.864	1.3616	0.5330	1.3528
70.0	1.859	1.4146	0.4900	1.2886
75.8	1.854	1.4718	0.4530	1.2361
79.1	1.851	1.5001	0.4480	1.2440
83.6	1.844	1.5713	0.4430	1.2836
89.5	1.833	1.8148	0.4480	1.4903
94.1	1.821	2.0837	0.4480	1.6999
99.9	1.831	2.4188	0.4320	1.9133
105.8	1.781	2.5454	0.3880	1.7589
109.8	1.765	2.2064	0.3320	1.2929
118.7	1.753	1.4669	0.3030	0.7792

QUENCHED 70/30 P(VDF/TrFE) COPOLYMER IN COOLING RUN				
TEMP. (^{o}C)	ρ (g/cm^3)	C_P (J/g K)	D (x 10^{-3} cm^2/s)	K (mW/cm K)
21.7	1.886	1.1900	0.7456	1.6734
31.5	1.881	1.1730	0.6802	1.5008
40.0	1.876	1.1210	0.6442	1.3548
49.1	1.869	1.1640	0.5844	1.2714
54.3	1.863	1.4550	0.5484	1.4865
57.6	1.855	2.2330	0.5340	2.2119
58.9	1.849	2.9550	0.5270	2.8794
60.9	1.834	3.4670	0.5185	3.2969
67.4	1.808	2.4750	0.4825	2.1591
72.7	1.794	1.7550	0.4470	1.4074
75.2	1.790	1.4520	0.4050	1.0526
77.9	1.787	1.3390	0.3928	0.9399
79.6	1.785	1.3240	0.3780	0.8933
83.9	1.781	1.2730	0.3440	0.7799
87.6	1.778	1.2150	0.3330	0.7194
91.5	1.774	1.1640	0.3330	0.6876
96.8	1.770	1.1240	0.3451	0.6866
103.3	1.635	1.1240	0.3512	0.6454
116.8	1.750	1.3680	0.3220	0.7709

SLOW-COOLED 70/30 P(VDF/TrFE) COPOLYMER IN HEATING RUN				
TEMP. (^{o}C)	ρ (g/cm^3)	C_P (J/g K)	D (x 10^{-3} cm^2/s)	K (mW/cm K)
-98.8	1.961	0.4919	1.6600	1.6013
-83.7	1.956	0.6229	1.6000	1.9494
-73.1	1.953	0.6921	1.5500	2.0951
-56.8	1.948	0.7590	1.4196	2.0699
-43.2	1.943	0.8075	1.3500	2.1181
-34.5	1.940	0.8385	1.3149	2.1310
-23.7	1.936	0.8785	1.3000	2.2110
-11.3	1.931	0.9196	1.2200	2.1664
-0.5	1.927	0.9572	1.1700	2.1581
9.5	1.922	0.9986	1.1400	2.1880
16.6	1.919	1.0220	1.1000	2.1573
22.5	1.917	1.0430	1.0749	2.1594
26.4	1.915	1.0597	1.0400	2.1105
31.6	1.912	1.0899	1.0099	2.0839
39.4	1.907	1.1192	0.9872	2.1172
48.4	1.902	1.1698	0.9280	2.0648
58.2	1.896	1.2494	0.8670	2.0538
63.4	1.893	1.2911	0.8440	2.0628
69.9	1.888	1.3515	0.8010	2.0439
75.8	1.883	1.4006	0.7635	1.9490
79.5	1.875	1.4467	0.7464	1.9205
86.8	1.863	1.7300	0.7306	2.3077
92.0	1.844	2.6109	0.7279	3.4809
97.2	1.820	2.3479	0.7230	3.1322
101.1	1.806	2.3130	0.7143	3.0452
105.8	1.790	1.8407	0.6841	2.3031
108.9	1.781	1.6169	0.6270	1.8056
116.6	1.771	1.4816	0.6140	1.6111

SLOW-COOLED 70/30 P(VDF/TrFE) COPOLYMER IN COOLING RUN				
TEMP. (^{o}C)	ρ (g/cm^3)	C_P (J/g K)	D (x 10^{-3} cm^2/s)	K (mW/cm K)
21.2	1.917	1.048	1.0524	2.114
30.0	1.912	1.052	0.9984	2.008
38.7	1.907	1.078	0.9433	1.939
49.0	1.899	1.287	0.8760	2.141
54.0	1.888	1.808	0.8372	2.858
60.0	1.840	3.214	0.8050	4.761
61.3	1.835	3.104	0.7948	4.527
65.5	1.821	2.580	0.7800	3.665
68.0	1.815	2.327	0.7657	3.234
73.5	1.808	1.473	0.7257	1.933
77.7	1.804	1.359	0.7011	1.719
77.8	1.804	1.353	0.7030	1.716
79.6	1.802	1.343	0.6841	1.656
83.9	1.798	1.334	0.6451	1.547
87.6	1.795	1.320	0.6259	1.483
91.2	1.791	1.304	0.6172	1.441
97.4	1.785	1.303	0.6047	1.406
104.1	1.809	1.362	0.6005	1.480
111.4	1.772	1.470	0.6090	1.586

APPENDIX D TEMPERATURE DEPENDENCE OF ELASTIC MODULI OF THE COPOLYMERS DETERMINED BY ULTRASONIC IMMERSION METHOD

Density : ρ **(g/cm^3)**

Elastic Stiffness Coefficient : $C_{11} = \rho V_{11}^2$ **(GPa)**

Shear Modulus : $C_{66} = \rho V_{66}^2$ **(GPa)**

Young's Modulus : $E = C_{66} (3C_{11} - 4C_{66}) / (C_{11} - C_{66})$ **(GPa)**

Bulk Modulus : $B = C_{11} - \frac{4}{3} C_{66}$ **(GPa)**

Poisson's Ratio : $\upsilon = \frac{E}{2C_{66}} - 1$

QUENCHED 56/44 P(VDF/TrFE) COPOLYMER IN HEATING RUN

TEMP. (°C)	ρ (g/cm³)	V_{11} (x10³ m/s)	V_{66} (x10³ m/s)	C_{11} (GPa)	C_{66} (GPa)	E (GPa)	B (GPa)	υ
23.4	1.885	1.958	0.590	7.23	0.656	1.902	6.35	0.449
33.2	1.878	1.928	0.566	6.98	0.602	1.749	6.18	0.453
45.5	1.867	1.869	0.518	6.52	0.501	1.461	5.86	0.458
57.8	1.853	1.779	0.464	5.86	0.399	1.168	5.33	0.464
63.8	1.838	1.713	0.428	5.40	0.337	0.989	4.95	0.467
66.5	1.825	1.629	0.400	4.84	0.292	0.857	4.45	0.467
68.1	1.821	1.568	0.367	4.48	0.245	0.721	4.15	0.471
72.7	1.814	1.501	0.322	4.09	0.188	0.555	3.84	0.476
86.4	1.798	1.445	0.274	3.76	0.135	0.400	3.58	0.481
95.4	1.789	1.407	0.271	3.54	0.131	0.388	3.37	0.481

QUENCHED 56/44 P(VDF/TrFE) COPOLYMER IN COOLING RUN								
TEMP. (°C)	ρ (g/cm^3)	V_{11} ($x10^3$ m/s)	V_{66} ($x10^3$ m/s)	C_{11} (GPa)	C_{66} (GPa)	E (GPa)	B (GPa)	υ
21.3	1.886	1.948	0.587	7.16	0.650	1.885	6.29	0.450
27.2	1.882	1.924	0.569	6.97	0.609	1.769	6.15	0.452
33.6	1.877	1.894	0.542	6.73	0.551	1.604	6.00	0.456
40.4	1.871	1.839	0.515	6.33	0.496	1.446	5.67	0.458
49.1	1.862	1.653	0.415	5.09	0.321	0.941	4.66	0.466
58.2	1.848	1.574	0.367	4.58	0.249	0.733	4.25	0.472
62.5	1.833	1.556	0.355	4.44	0.231	0.680	4.13	0.472
65.2	1.824	1.538	0.343	4.32	0.215	0.634	4.03	0.474
67.8	1.819	1.526	0.337	4.24	0.207	0.610	3.96	0.473
77.7	1.807	1.454	0.298	3.82	0.160	0.473	3.61	0.478
90.2	1.794	1.411	0.268	3.57	0.129	0.382	3.40	0.481

SLOW-COOLED 56/44 P(VDF/TrFE) COPOLYMER IN HEATING RUN

TEMP. (°C)	ρ (g/cm^3)	V_{11} (x10^3 m/s)	V_{66} (x10^3 m/s)	C_{11} (GPa)	C_{66} (GPa)	E (GPa)	B (GPa)	υ
22.4	1.905	1.992	0.611	7.56	0.711	2.059	6.61	0.448
29.9	1.901	1.936	0.567	7.12	0.611	1.776	6.310	0.453
41.4	1.892	1.864	0.496	6.58	0.466	1.362	5.95	0.461
45.8	1.889	1.840	0.469	6.39	0.415	1.216	5.84	0.465
52.3	1.882	1.797	0.420	6.08	0.332	0.977	5.95	0.471
62.1	1.864	1.713	0.345	5.47	0.222	0.657	5.17	0.480
64.1	1.853	1.671	0.307	5.18	0.175	0.519	4.94	0.483
65.9	1.843	1.623	0.288	4.86	0.153	0.454	4.65	0.484
67.8	1.839	1.562	0.273	4.49	0.137	0.407	4.30	0.485
70.7	1.834	1.517	0.254	4.22	0.118	0.351	4.06	0.487
76.6	1.826	1.466	0.242	3.93	0.107	0.318	3.78	0.486
86.2	1.816	1.405	0.231	3.58	0.097	0.288	3.46	0.485
95.6	1.807	1.387	0.219	3.48	0.087	0.259	3.36	0.489

SLOW-COOLED 56/44 P(VDF/TrFE) COPOLYMER IN COOLING RUN

TEMP. (°C)	ρ (g/cm^3)	V_{11} (x10^3 m/s)	V_{66} (x10^3 m/s)	C_{11} (GPa)	C_{66} (GPa)	E (GPa)	B (GPa)	υ
21.7	1.906	1.978	0.601	7.46	0.688	1.994	6.54	0.449
24.9	1.904	1.942	0.575	7.18	0.629	1.827	6.34	0.452
33.7	1.897	1.852	0.511	6.51	0.495	1.444	5.85	0.459
43.6	1.889	1.725	0.394	5.62	0.293	0.863	5.23	0.473
47.4	1.885	1.629	0.341	5.00	0.219	0.647	4.71	0.477
53.5	1.876	1.575	0.304	4.65	0.173	0.512	4.42	0.480
60.5	1.856	1.532	0.273	4.36	0.138	0.409	4.17	0.482
63.3	1.844	1.520	0.269	4.26	0.133	0.395	4.08	0.485
65.7	1.838	1.502	0.258	4.15	0.122	0.362	3.98	0.484
68.2	1.834	1.496	0.251	4.11	0.116	0.345	3.95	0.487
70.4	1.831	1.484	0.239	4.03	0.105	0.312	3.89	0.486
78.4	1.822	1.448	0.232	3.82	0.098	0.291	3.69	0.485
87.7	1.813	1.405	0.225	3.58	0.092	0.274	3.46	0.489
95.1	1.806	1.381	0.217	3.45	0.085	0.253	3.33	0.488

QUENCHED 70/30 P(VDF/TrFE) COPOLYMER IN HEATING RUN

TEMP. (°C)	ρ (g/cm³)	V_{11} (x10³ m/s)	V_{66} (x10³ m/s)	C_{11} (GPa)	C_{66} (GPa)	E (GPa)	B (GPa)	υ
24.4	1.885	2.072	0.893	8.09	1.503	4.167	6.09	0.386
31.7	1.881	2.066	0.849	8.03	1.356	3.792	6.22	0.398
39.2	1.877	2.036	0.795	7.78	1.187	3.347	6.20	0.410
48.8	1.873	1.994	0.741	7.45	1.028	2.919	6.08	0.420
55.7	1.869	1.964	0.700	7.21	0.916	2.615	5.99	0.427
65.9	1.862	1.933	0.639	6.96	0.760	2.187	5.95	0.439
72.5	1.857	1.897	0.600	6.68	0.669	1.933	5.79	0.445
82.3	1.846	1.837	0.571	6.23	0.602	1.742	5.43	0.447
88.0	1.836	1.801	0.530	5.96	0.516	1.499	5.27	0.453
92.2	1.826	1.753	0.504	5.61	0.464	1.350	4.99	0.455
96.7	1.814	1.722	0.469	5.38	0.399	1.165	4.85	0.460
101.2	1.799	1.686	0.436	5.11	0.342	1.001	4.66	0.463
108.9	1.768	1.523	0.252	4.10	0.112	0.333	3.95	0.487
117.9	1.754	1.450	0.151	3.69	0.040	0.120	3.64	0.500
125.4	1.746	1.445	0.147	3.65	0.038	0.114	3.60	0.500

QUENCHED 70/30 P(VDF/TrFE) COPOLYMER IN COOLING RUN

TEMP. (°C)	ρ (g/cm³)	V_{11} (x10³ m/s)	V_{66} (x10³ m/s)	C_{11} (GPa)	C_{66} (GPa)	E (GPa)	B (GPa)	υ
25.5	1.884	2.066	0.863	8.04	1.403	3.913	6.17	0.395
28.7	1.883	2.054	0.836	7.94	1.316	3.687	6.19	0.401
35.3	1.879	2.024	0.788	7.70	1.167	3.292	6.14	0.410
41.0	1.875	1.994	0.727	7.45	0.991	2.821	6.13	0.423
51.5	1.867	1.904	0.612	6.77	0.699	2.017	5.84	0.443
60.5	1.837	1.759	0.483	5.68	0.429	1.252	5.11	0.459
69.2	1.802	1.596	0.347	4.59	0.217	0.640	4.30	0.475
79.3	1.786	1.545	0.307	4.26	0.168	0.497	4.04	0.479
85.0	1.780	1.529	0.299	4.16	0.159	0.471	3.95	0.481
90.7	1.775	1.523	0.286	4.12	0.145	0.430	3.92	0.483
94.6	1.772	1.517	0.286	4.08	0.145	0.430	3.88	0.483
98.8	1.768	1.499	0.279	3.97	0.138	0.409	3.79	0.482
108.0	1.759	1.456	0.219	3.73	0.084	0.250	3.62	0.488
114.9	1.752	1.439	0.168	3.63	0.049	0.146	3.56	0.490
121.3	1.745	1.427	0.144	3.55	0.036	0.108	3.51	0.500

SLOW-COOLED 70/30 P(VDF/TrFE) COPOLYMER IN HEATING RUN								
TEMP. (°C)	ρ (g/cm^3)	V_{11} ($x10^3$ m/s)	V_{66} ($x10^3$ m/s)	C_{11} (GPa)	C_{66} (GPa)	E (GPa)	B (GPa)	υ
22.4	1.897	2.203	0.924	9.21	1.752	4.844	6.87	0.382
31.6	1.892	2.190	0.894	9.07	1.512	4.234	7.06	0.400
39.7	1.887	2.170	0.841	8.89	1.335	3.769	7.11	0.412
49.5	1.882	2.136	0.781	8.58	1.148	3.267	7.05	0.423
58.7	1.876	2.109	0.739	8.34	1.025	2.931	6.98	0.430
70.2	1.868	2.034	0.658	7.73	0.809	2.332	6.65	0.441
80.8	1.856	1.952	0.574	7.07	0.611	1.775	6.26	0.453
90.3	1.831	1.844	0.469	6.23	0.403	1.181	5.69	0.465
95.2	1.809	1.790	0.408	5.80	0.301	0.887	5.40	0.473
97.9	1.797	1.756	0.381	5.54	0.261	0.770	5.19	0.475
100.4	1.788	1.709	0.347	5.22	0.215	0.636	4.94	0.479
103.2	1.778	1.606	0.279	4.59	0.138	0.410	4.40	0.486
108.5	1.762	1.503	0.185	3.98	0.060	0.179	3.90	0.492
117.9	1.750	1.465	0.172	3.76	0.052	0.155	3.69	0.490

SLOW-COOLED 70/30 P(VDF/TrFE) COPOLYMER IN COOLING RUN

TEMP. (°C)	ρ (g/cm^3)	V_{11} (x10^3 m/s)	V_{66} (x10^3 m/s)	C_{11} (GPa)	C_{66} (GPa)	E (GPa)	B (GPa)	υ
23.9	1.896	2.176	0.889	8.98	1.498	4.194	6.98	0.400
31.1	1.892	2.151	0.842	8.75	1.341	3.780	6.96	0.409
39.6	1.886	2.115	0.775	8.44	1.133	3.223	6.93	0.422
50.0	1.878	2.007	0.673	7.56	0.850	2.442	6.43	0.436
58.7	1.828	1.891	0.577	6.54	0.609	1.764	5.73	0.448
67.9	1.796	1.710	0.394	5.25	0.279	0.821	4.88	0.471
81.1	1.781	1.620	0.319	4.67	0.181	0.536	4.43	0.481
91.0	1.771	1.593	0.299	4.50	0.158	0.468	4.28	0.481
94.7	1.768	1.579	0.279	4.41	0.138	0.410	4.22	0.486
99.2	1.763	1.552	0.259	4.25	0.118	0.351	4.09	0.487
101.2	1.762	1.539	0.231	4.17	0.094	0.280	4.05	0.489
108.8	1.754	1.492	0.184	3.91	0.059	0.176	3.83	0.492
116.3	1.747	1.464	0.157	3.74	0.043	0.129	3.69	0.500

APPENDIX E DERIVATION OF EQUATION 4.8

From Snell's law

$$\frac{sin\psi}{v_{liq}} = \frac{sin\theta_r}{v_r} \tag{E.1}$$

one gets

$$v_r = v_{liq}\frac{sin\theta_r}{sin\psi}. \tag{E.2}$$

Also, the difference in transit times (with and without sample), Δt_r, is

$$\Delta t_r = \frac{L}{cos\theta_r}\left[\frac{cos(\theta_r - \psi)}{v_{liq}} - \frac{1}{v_r}\right]. \tag{E.3}$$

Substitution of Equation E.2 into E.3 gives

$$\Delta t_r = \frac{L}{cos\theta_r}\left[\frac{cos(\theta_r - \psi)}{v_{liq}} - \frac{sin\psi}{v_{liq}\,sin\theta_r}\right]$$

$$= \frac{L}{cos\theta_r}\left[\frac{cos\theta_r cos\psi + sin\theta_r sin\psi}{v_{liq}} - \frac{sin\psi}{v_{liq}\,sin\theta_r}\right]$$

Hence,

$$0 = \left[\frac{L\cos\psi}{v_{liq}} - \Delta t_r\right]\cos\theta_r + \frac{L\sin\psi}{v_{liq}}\sin\theta_r - \frac{L\sin\psi}{v_{liq}}\frac{1}{\sin\theta_r}$$

$$= \left[\frac{L\cos\psi}{v_{liq}} - \Delta t_r\right]\cos\theta_r \sin\theta_r + \frac{L\sin\psi}{v_{liq}}\sin^2\theta_r - \frac{L\sin\psi}{v_{liq}}$$

$$= \left[\frac{L\cos\psi}{v_{liq}} - \Delta t_r\right]\cos\theta_r \sin\theta_r - \frac{L\sin\psi}{v_{liq}}\left[1 - \sin^2\theta_r\right]$$

$$= \left[\frac{L\cos\psi}{v_{liq}} - \Delta t_r\right]\cos\theta_r \sin\theta_r - \frac{L\sin\psi}{v_{liq}}\cos^2\theta_r$$

$$= \cos\theta_r\left[\left(\frac{L\cos\psi}{v_{liq}} - \Delta t_r\right)\sin\theta_r - \frac{L\sin\psi}{v_{liq}}\cos\theta_r\right]$$

Since $\cos\theta_r \neq 0$, one has

$$\left(\frac{L\cos\psi}{v_{liq}} - \Delta t_r\right)\sin\theta_r - \frac{L\sin\psi}{v_{liq}}\cos\theta_r = 0$$

or $$\tan\theta_r = \frac{L\sin\psi}{L\cos\psi - \Delta t_r v_{liq}}$$

which gives

$$\theta_r = \tan^{-1}\left(\frac{L\sin\psi}{L\cos\psi - \Delta t_r v_{liq}}\right).$$

Putting this into equation E.2, one obtains

$$v_r = \frac{v_{liq}}{\sin\psi} \sin\left[\tan^{-1}\left(\frac{L\sin\psi}{L\cos\psi - \Delta t_r v_{liq}}\right)\right].$$

APPENDIX F (A) RADIOMETRY SIGNAL PROFILE , AND (B) MATHEMATICALLY SIMULATED RADIOMETRY SIGNAL.